ELECTROCHEMISTRY OF SOME RHODIUM(I) COMPLEXES

Thesis by

Jan Stanley Najdzionek

In Partial Fulfillment of the Requirements

for the Degree of

Doctor of Philosophy

California Institute of Technology

Pasadena, California

1982

(Submitted August 27, 1981)

ABSTRACT

The electrochemistry of $Rh[(C_6H_5)_2P(CH_x)_nP(C_6H_5)_2]_2$ Y where Y = $CF_3SO_3^-$ or ClO_4^-, x = 2 with n = 1, 2, 3, 4 and x = 1 with n = 2 was examined and compared with that of $Co[(C_6H_5)_2P(CH_x)_2P(C_6H_5)_2]_2$ where x = 1 and 2. Cyclic voltammetric (CV), chronoamperometric (CA), polarographic (including D.C., normal and differential pulse) and bulk electrolytic experiments were performed and the results show that all of these Rh(I) phosphine complexes are reduced in a two-electron process.

CV and CA measurements were used to determine the heterogeneous electron transfer rate constants for $Rh[(C_6H_5)_2P(CH_2)_2P(C_6H_5)_2]_2$. The values determined were 0.0092 and 0.0087 cm/sec, respectively, and the results are discussed in relation to the Butler-Volmer formulation of electrode kinetics.

Fluorescence measurements were made on the above rhodium complexes for n = 1, 3 and 4 at room temperature and at 77 K. None emit under ambient conditions in solution but the compound containing ligands with a single methylene unit backbone emitted at 77 K with a lifetime of 20 microseconds. The UV-Visible spectrum of reduced $Rh(DPP)_2^+$, the most stable of the reduced complexes, displayed a very intense absorption at

450 nm which was assumed to be charge-transfer in origin.

The two-electron reduction of Rh_2(2,5-dimethyl-2,5-diisocyanohexane)$_4^{2+}$ produced a unique species in which a CN^- ion has been lost resulting in the formation of a cyclohexylimine ligand which bridges the metal atoms through the imine function. The strain imposed on the TMB ligand backbone forces the rhodium atoms to have the strongest interaction of any of the $Rh(Br)_4^+$ compounds studied [Rh(1)-Rh(2) = 2.970(1) Å]. Linear isocyanide carbon-nitrogen distances range from 1.153(9) to 1.175(9) Å while the imine carbon-nitrogen is extended slightly to 1.254(9) Å.

TABLE OF CONTENTS

I. INTRODUCTION

A. AN HISTORICAL PERSPECTIVE OF RHODIUM ELECTROCHEMISTRY

The amount of electrochemical work dealing with rhodium complexes with pi bonding ligands in nonaqueous solvents is very limited. The first work was reported by Olson and Keim in 1969 (1). They examined $RhCl[C_6H_5)_3P]_3$ and $Rh\ Cl[C_6H_5)_2PCH_3]_4$. Using a toluene-acetonitrile mixture with excess ligand they observed one wave at $E_{1/2}$ = -1.832 V (vs. 0.1 M $AgNO_3/Ag$) with red solution around the electrode. Their logarithmic analysis of the polarographic wave yielded slopes of 84 mV and 99 mV respectively which favor a one-electron reduction, but I values of 3.11 and 4.65 which point more toward a two-electron wave rather than a one-electron wave (I has units of $\mu A\text{-}sec^{-1/2}mg^{-2/3}mM^{-1}$). Upon bulk electrolysis the colored product they obtained was analyzed to be RhL_4 where L is phosphine. The complex was assumed to be a d^9-d^9 dimer. Unfortunately no UV-Visible absorption spectra of the reduced species was reported. Interestingly, no one has reported on any further characterization of these complexes.

In 1962, Pilloni, Valcher, and Martelli (2) examined the reduction

of $RhCl(CO)[P(C_6H_5)_3]_2$ in acetonitrile-toluene and observed a single polarographic wave at $E_{1/2}$ = -1.75 V (vs. SCE) with a limiting current consistent with a two-electron reduction. The shape indicated an irreversible reaction. A scheme was proposed in which the initial reduction product was the two-electron reduced species $[RhCO(PC_6H_5)_3]^-$ which had lost chloride and picked up $P(C_6H_5)_3$. deMontauzon and Poilblanc (3) reexamined the electrochemistry of $RhCl(CO)[P(C_6H_5)_3]_2$ in THF. They also varied the phosphine ligands replacing $P(C_6H_5)_3$ with $P(CH_3)_2(C_6H_5)$, $P(CH_3)_3$, and $P(C_2H_5)_3$. In all cases their experimental results agreed with those reported by Pilloni et al. (2). When they performed the reductive electrolysis without excess phosphine ligand they obtained dimers analogous to those reported by Wilkinson: dimers with Rh-Rh bonds and bridging carbonyls (4). A note of caution should be interjected at this point. deMontauzon and Poilblanc report their potential scan ranges accessible in THF under their experimental conditions. One of the electrolytes they employed was sodium tetraphenyl boron; also some of the cobalt complexes with which they experimented (and later compared to rhodium complexes) used tetraphenyl boron as counter ions. They reported that they could scan to +1.50 V (vs. 0.1 M $Ag/AgNO_3$) on a platinum or gold electrode, whereupon THF began to oxidize. However, Geske (5) much earlier had pointed out that tetraphenyl boron has oxidation electrochemistry of its own in acetonitrile as well as in dimethyl formamide and anhydrous acetic acid. When he performed voltammetry on a platinum electrode he observed a wave at +0.5 V (vs. 0.1 M $AgNO_3/Ag$) which also formed a film greatly reducing the current on subsequent

scans. In the experimental conditions of the Anson lab, millimolar solutions of tetraphenyl boron or 0.1 M tetrabutyl ammonium tetraphenyl boron used as electrolyte formed films which quickly and completely passivated the platinum electrode surface. Therefore the potential scan range possible according to deMontauzon and Poiblanc is quite remarkable.

1973 marked the first examination of a rhodium complex solely with pi backbonding ligands. Pilloni, Vecchi and Martelli (8) examined the reductive electrochemistry of $Rh[(C_6H_5)_2PC_2H_4P(C_6H_5)_2]_2^+$ in acetonitrile with 0.1 M tetrabutyl amonium perchlorate. Their analysis was based primarily on polarographic studies. They obtained a single polarographic wave at $E_{1/2}$ = -1.7 V (vs. SCE), with I_d = 4.3 and a Tomes plot slope of 33 mV (37). The iridium complex yielded nearly identical results: $E_{1/2}$ = -1.70 V, I_d = 4.0 and a Tomes plot slope of 33 mV. A single cyclic voltammogram performed on a dropping mercury electrode showed what they described as "symmetrical reduction and oxidation peaks" which in reality were quite distorted with the anodic current considerably larger than the cathodic current (presumably due to the growth of the mercury drop during the time period of the scan). The peak splitting of the cyclic voltammogram peak was on the order of 60 mV at a scan rate of 250 mV/sec. Bulk electrolysis required two electrons to initially produce a red solution which quickly faded to yellow concurrently with precipitate formation. The precipitate was determined to be the hydride complex. The mechanism they proposed was a two-electron reduction followed by a slow chemical reaction where the rho-

dium anion complex extracted a proton from acetonitrile, from trace amounts of water in the solution, or from the electrolyte tetrabutyl ammonium cation.

The next compound Pilloni and Martelli studied was di-(cis-1,2-bis diphenylphosphinoethylene) rhodium(I) chloride, [$Rh(VPE)_2Cl$], in acetonitrile. They observed one wave at $E_{1/2}$ = -1.60 V (vs. SCE) and noted that the polarographic and cyclic voltammetric patterns were "identical to those found in the reduction of the related complex $Rh(DPE)_2Cl$." Presumably this means that they observed polarograms where the Tomes slope was 30 mV and cyclic voltammograms where the peak splitting was 60 mV at 250 mV/sec. As before, an exhaustive electrolysis required two electrons with a resultant deep red solution which slowly faded with the simultaneous formation of a red-brown solid product. This product was identified as the rhodium hydride complex. The unsaturated phosphine complex reduced to the anion was found to be more stable than the saturated complex, presumably due to the better pi back-bonding electron accepting ability of the unsaturated phosphine.

In 1974, DeArmond, Kew, and Hanck (9) reported the electrochemical response of tris (2,2'-bipyridyl) rhodium(III) chloride trihydrate in acetonitrile. They observed four cathodic waves. The first two were irreversible while the last two [ca. -1.5 V and ca. -1.7 V (vs. SCE)] were reversible on a cyclic voltammetric time scale. The majority of the report was devoted to elucidating the exact nature of the first two waves. These two waves were both one-electron reductions. The second reduction was followed by ligand loss. After the first two reductions

they believed they had a bi-(2,2'-bipyridyl) rhodium(I) complex. This complex subsequently underwent two further reductions to rhodium(0) and rhodium(-1). The peak splittings for the third and fourth waves were 60 mV and 70 mV, respectively, and both appeared to be one-electron in value without any following chemical complications. Unfortunately, since these reductions were not of primary concern, they were not characterized any further.

Makrlik et al. (10) studied the reductive electrochemistry of some rhodium complexes of the form $[Rh(chel)(diene)]^+$ where chel is 2,2' bipyridine or 1,10-phenanthroline and diene is cis,cis-cycloocta,-1,5-diene and norbornadiene. Utilizing polargraphy and cyclic voltammetry, they observed in all cases two reductive waves [-1.2 V and -1.7 V (vs. SCE)] which they characterized as one-electron reductions. With polarography they observed two additional one-electron waves at more negative potentials which were not visible on a cyclic voltammetric time scale. A comparison of the electrochemistry of free bipyridine and the lack of these waves with the phenanthroline complexes indicated that the surplus polarographic waves were due to free bipyridine released when the rhodium complex decomposed. Recently, Fordyce, Pool and Crosby (11) reexamined the electrochemistry of $[M(chel)(diene)]^+$ using cyclic voltammetry and recorded the ESR spectra of the products obtained by bulk electrolysis. They extended the previously studied series by adding 4,7-diphenyl-1,10-phanthroline and 2,2'-bipyrazine. The electrochemistry of the new complexes remained analogous to that of the predecessor complexes.

Recently Eisenberg et al. (15,16) reexamined the electrochemistry of $Rh(DPE)_2^+$ in acetonitrile and benzonitrile with tetrabutyl ammonium salts. They utilized cyclic voltammetry, bulk electrolysis, and chemical reactivity to study the reduction process. They varied the scan rate from 200 mV/sec to 10 mV/sec and observed that CV peak splittings decreased from 65.3 mV to 43.5 mV while the current ratio ip^{red}/ip^{ox} increased from 1.0 to 1.3. They interpreted thesedata as an ECE process: a one-electron reduction to make $Rh(DPE)_2^0$ which then reacted with acetonitrile forming a rhodium hydride and reactive organic radical which was more easily reduced than the starting rhodium complex. Thus they expected a shift in peak splitting from a one-electron to a two-electron process. Bulk electrolysis in acetonitrile yielded a value of n = 2 and a precipitate, $HRh(DPE)_2$. It was determined that the hydride came from the acetonitrile. If dry deuterated acetonitrile was used with a tetrabutyl ammonium anion electrolyte salt only the deuterated hydride was obtained. A bulk electrolysis in benzonitrile required two electrons with the formation of the hydride; however the hydrogen atom source was the tetra n-butyl ammonium moiety, not the aromatic benzonitrile, because tributylamine and 1-butene were isolated. Other molecules were tested to see if they would react with the $Rh(DPE)_2^0$ species. When cyclohexane was added, cyclohexene and bicyclohexyl, which are typical final products of cyclohexyl radical, were observed. When d_9-tert-butylbenzene was added before the electrolysis, isobutylene was produced and $RhD(DPE)_2$ was obtained. Considering the final product and the starting material, the mechanism must involve the neophyl radical

which undergoes rearrangement. With this and some additional evidence the workers concluded that $Rh(DPE)_2^0$ would attack $C(sp^3)$-H bonds but is not strong enough to attack $C(sp^2)$-H bonds.

B. OTHER METALS

Little work has been done on other d^8 complexes with pi back-bonding ligands except for cobalt. Rao, Hughes, and Macero (17) examined the electrochemistry of Co(bipyridine)$_3^{+2}$ in acetonitrile and observed two waves. The first wave was a one-electron reduction at $E_{1/2}$ = -0.938 mV with a Tomes slope equal to 61 mV and a cyclic voltammogram peak separation of 67 mV. The second wave was a two-electron reversible reduction wave from Co(I) to Co(-I), $E_{1/2}$ = -1.580 with a Tomes slope equal to 37 mV and a CV peak separation of 40 mV.

Pilloni, Zotti and Martelli (18) examined the electrochemistry of di(1,2-bis diphenylphosphinoethane) cobalt(I) percholorate in acetonitrile utilizing polarography. In this case they observed two one-electron waves, -1.12 V and -1.60 V (vs. SCE), and I = 2.2. Bulk electrolysis on the plateau of the first wave required one electron and the product Co(DPE)$_2^0$ was identified by comparison with an authentic sample. Electrolysis on the second wave required one electron but the deep purple product was too unstable to isolate directly. The cobalt hydride obtained after the solvent reacted with the cobalt anion was identified. J.A. Sofranko (20), in his thesis, noted the same observations. However he also indicated that during the second bulk electrolysis there was a small catalytic current which did not decay to background levels. It was possible to pass up to n = 60 electrons. This would seem to indicate that some extraordinary complexes and electrochemistry followed the Co(DPE)$_2^-$ decomposition.

The electrochemistry of the triad next to Co, Rh, and Ir, namely Ni, Pd and Pt, with pi back bonding ligands is more limited. A fairly large amount of this work has been devoted to the reduction of mixed ligand pi accepting and pi donating platinum and palladium complexes in nonaqueous and aqueous solutions. Unfortunately, many of these studies (21,22,23,24) are superficial except for two in-depth studies. Hubbard et al. (27,28,29) and Zanello et al. (25,26) studied the reduction of $PtCl_2P[(CH_3)_x(C_6H_5)_{3-x}]_2$ where x = 0, 1, 2, 3, and platinum dichloride isocyanide and phosphine complexes, respectively. In all cases the platinum(II) complex underwent two one-electron reductions with choride loss.

The only study solely concerned with pi backbonding ligands was reported by Martelli, Pilloni, Zotti and Daolio in 1974 (19). Using polarography and electrolysis they studied the reduction of $M(DPE)_2^{2+}$, where M = Ni, Pd, and Pt in acetonitrile. In the case of the nickel complex they observed two one-electron waves at $E_{1/2}$ = -0.23 V, -0.43 V (vs. SCE) with Tomes slopes equal to 60 mV and I_d = 2.3. Exhaustive electrolysis on each plateau required one electron and the final two-electron reduced product was identified by comparison with an authentic sample. In the palladium and platinum cases there was a single two electron reduction with $E_{1/2}$ = -0.59 V and -0.77 V, Tast slopes of 32 mV and 32 mV, and I_d = 4.2 and 4.2 respectively. Bulk electrolysis required two electrons and the products obtained agreed with authentic samples (30).

More recently, Rechberger, Gritzner and Gutmann (31) examined the

oxidative electrochemistry of. M(triphenylphosphine)$_4^0$ where M = Ni, Pt, and Pd in a variety of solvents (DMF, DMSO, acetonitrile and nitromethane). They obtained a variety of results (which varied with the stability of starting materials) and various products in the different solvents. Under the most favorable experimental conditions they observed that all three complexes underwent two one-electron reversible oxidations to d^8 metal complexes. The reversibility of any particular wave depended on the nature of the metal complex and the solvent being used.

C. SUMMARY

An electrochemical study of a series of rhodium complexes was undertaken in an attempt to reconcile the divergent results reported in the literature. An understanding of the electrochemistry of these simple rhodium complexes is important for several reasons. For example Eisenberg et al. (15,16) have suggested the $Rh(DPE)_2^0$ species can catalytically reduce alkyl halides activated C-H bonds in alkanes. On a more esoteric level these complexes in solid state and frozen solution have long lived electronic excited states (32). Should this type of complex be modified to fluoresce in solution at room temperature an understanding of the reductive electrochemistry would aid in electron transfer quenching studies. This is especially appealing if the only electron transfer favored is a two-electron process followed by hydride formation. A major problem with solar water splitting schemes has been the need to move and store two or more electrons simultaneously (35). A thorough understanding of simple rhodium systems is necessary before the photochemistry and electrochemistry of the more complicated rhodium isocyanide complexes (33,34) can be studied.

In order to clarify the situation a series of rhodium and cobalt complexes with bidentate phosphines have been prepared. The rhodium complexes were assumed to be square planar. The ligands are bidentate diphenylphosphines with a carbon-hydrogen backbone connecting them. The length of the backbone was varied from one to four carbons. The cobalt complexes with ethane and ethylene backbone bidentate phosphines were

used as standards because the Co^0 complexes had been obtained chemically and were better understood.

Cyclic voltammetry was performed on the complexes to get an indication of the degree of reversibility of the electrode reaction. This technique also gave diffusion coefficient values. Chronoamperometry was used to measure more accurate diffusion coefficients. Polarography was performed because it was the most commonly used technique reported in the literature. This allowed a direct comparison with previously reported data. Bulk electrolyses were performed because they allowed a direct measurement of n values.

D. NOMENCLATURE

Electrochemistry, like many other disciplines utilizes abbreviations and symbols to facilitate the transfer of information. The abbreviations used in this work have been summarized in the "Major Symbols" and "Standard Abbreviations" sections of Electrochemical Methods by A. J. Bard and L. R. Faulker. Other abbreviations will be given when needed as with others when they differ from the standard list. A few of the most critical abbreviations are listed here:

AN	acetonitrile
CV	cyclic voltammetry
DME	dropping mercury electrode
DPP	differential pulse polarography
EC	heterogeneous electron transfer followed by homogeneous chemical reaction
ECE	heterogeneous electron transfer, homogeneous chemical reaction, heterogeneous electron transfer
HMDE	hanging mercury drop electrode
SCE	saturated calomel electrode
TBABF4	tetra-n-butyl ammonium fluoborate
TBAP	tetra-n-butyl ammonium percholorate
TBATRF	tetra-n-butyl ammonium trifluormethanesulfanate
TBABPH	tetra-n-butyl ammonium tetrphenyl boron
TBAPF6	tetra-n-butyl ammonium hexaflurophosphate

DPM	bis(diphenylphosphino) methane
DPE	bis-1,2-(diphenylphosphino) ethane
VPE	bis-cis-(diphenylphosphino) ethylene
DPP	bis-1,3-(diphenylphosphino) propane
DPB	bis-1,4-(diphenylphosphino) butane

ip^c	C.V. cathodic peak current
ip^a	C.V. anodic peak current
i_l	d.c. polarographic limiting current
I	polarographic diffusion current constant units ($\mu A\text{-}sec^{-1/2}mg^{-2/3}\text{-}mM^{-1}$) have not been included in the text
v	C.V. scan rate

Estimated standard deviations (ESD's) are given in parentheses right adjusted to the least significant digit of the preceding number.

II. EXPERIMENTAL SECTION

A. ELECTROCHEMICAL REAGENTS

Acetonitrile was purchased from Burdick and Jackson and was stored over activated Linde 4A molecular sieves in a dry-box (Vacuum Atmospheres). This acetonitrile was listed as 0.007% or less H_2O and generally did not show an acrylonitrile wave on a cyclic voltammogram using a HMDE. It was used without further purification. Polarographic grade tetra-n-butyl ammonium salts (TBAP, TBABF4 and TBAPF6) were purchased from Southwestern Analytical Co., stored under vacuum over anhydrous calcium sulfate and used as a supporting electrolyte without further purification. Tetra-n-butyl ammonium tetraphenyl boron was made by reacting tetra-n-butyl ammonium bromide (Aldrich) with sodium tetraphenyl boron in triply distilled water. The solid obtained was recrystallized repeatedly from hot acetonitrile until the sodium wave was not visible in a cyclic voltammogram obtained using a HMDE. Tetra-n-butyl ammonium trifluoromethane sulfonate was made by A. Maverick using the method of Brandstrom (55). The TBABF4 was used most often because in solutions it consistently had cleaner backgrounds and lower background

currents. All mercury was purchased from Bethlehem Instrument Co. triply distilled.

B. APPARATUS

Polarograms were obtained with a Princeton Applied Research (PAR) model 174 polarograph analyzer in conjunction with a PAR 174/70 drop timer, and were recorded with a Houston 2000 X-Y recorder. Cyclic volatammograms were obtained by means of a PAR Model 173 potentiostat driven by a PAR 175 signal generator. Voltammograms were recorded on a Houston 200 X-Y recorder, a Hewlett-Packard Model 7004 X-Y recorder and a Hewlett-Packard 7046A X-Y recorder. Scan rates greater than 1 V/sec required the use of a Tektronix 564 storage oscilloscope equipped with two type 3A72 dual trace modules and a Tektronix Oscilloscope C-12 camera for recording permanent copies. Chronoamperometric measurements were obtained with a PAR-173 driven by a PAR-175. The current transient was recorded with a Biomation Model 802 and transferred to paper via a Hewlett-Packard 700A recorder with a 17171A timebase. The system was calibrated by supplying a known square wave into the Biomation and adjusting the H.P. vernier until the wave was exactly reproduced. Bulk electrolysis experiments were carried out with use of a PAR 173 potentiostat and the current was recorded on one of the X-Y recorders mentioned above. The current was integrated by the PAR 179 module on the PAR 173. Chronocoulometric measurements were made with a PDP11/40 minicomputer and its associated conventional electrochemical instrumentation.

Several specially designed electrochemical cells were built. The basic design is shown in Figure 1. This particular cell had several

FIGURE 1

General Purpose Electrochemical Cell

With Auxiliary Electrode and

Reference Electrode Compartments

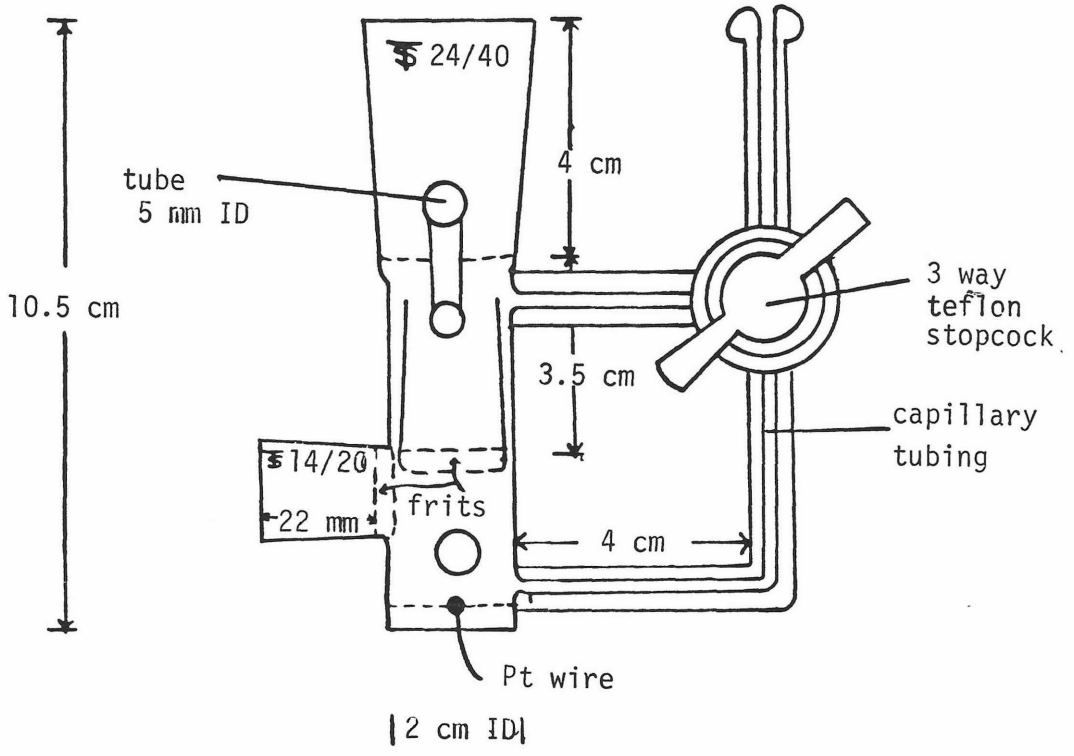
24/40
4 cm
tube
5 mm ID
10.5 cm
3 way
teflon
stopcock
3.5 cm
capillary
tubing
14/20
22 mm
frits
4 cm
Pt wire
2 cm ID

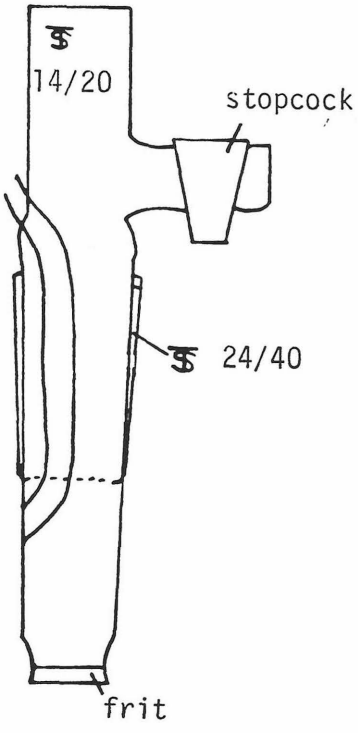
14/20
stopcock
24/40
frit

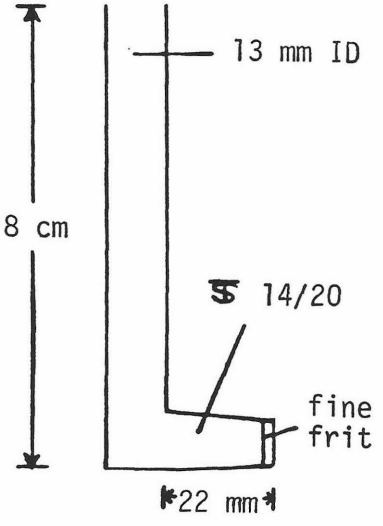
13 mm ID
8 cm
14/20
fine
frit
22 mm

functions. Extra access ports allowed a platinum electrode to enter the cell so CV's could be recorded as electrolysis was being performed and also allowed solution to be withdrawn through a septum without disturbing or disassembling the cell. The tubing passing through the counter electrode compartment allowed a platinum working electrode to be admitted to the cell. A special electrochemical cell with an optical window was used to obtain spectra as the electrochemical experiment was being carried out. A sketch of this cell is shown in Figure 2. This cell had an advantage in that once it was loaded and sealed in the drybox it could be removed and handled at will with little worry of oxygen leakage.

The reference electrode consisted of a silver wire immersed in a solution of 0.1 M $AgNO_3$ in acetonitrile held in a glass tube with a fine frit at the end. The platinum working electrode consisted of a platinum wire (diameter = 0.030 inches) sealed in soft glass and polished to expose a disk-shaped surface flush with the glass surface. The working electrode for the controlled potential electrolyses was a folded gauze electrode supported with a stout platinum wire. The HMDE was of a standard design, manufactured by Metrohm. A five unit drop was used for most cyclic voltammograms and had an area of 0.0235 cm^2. A SMDE PAR 303 was used for the chronocoulometric measurements because of its highly reproducible mercury drops.

The dropping mercury electrode was of standard design. In the present work the mercury flow rate was measured at several heights. The mercury was captured under acetonitrile for 5 minutes, decanted, allowed

FIGURE 2

Electrochemical Cell with Optical Windows

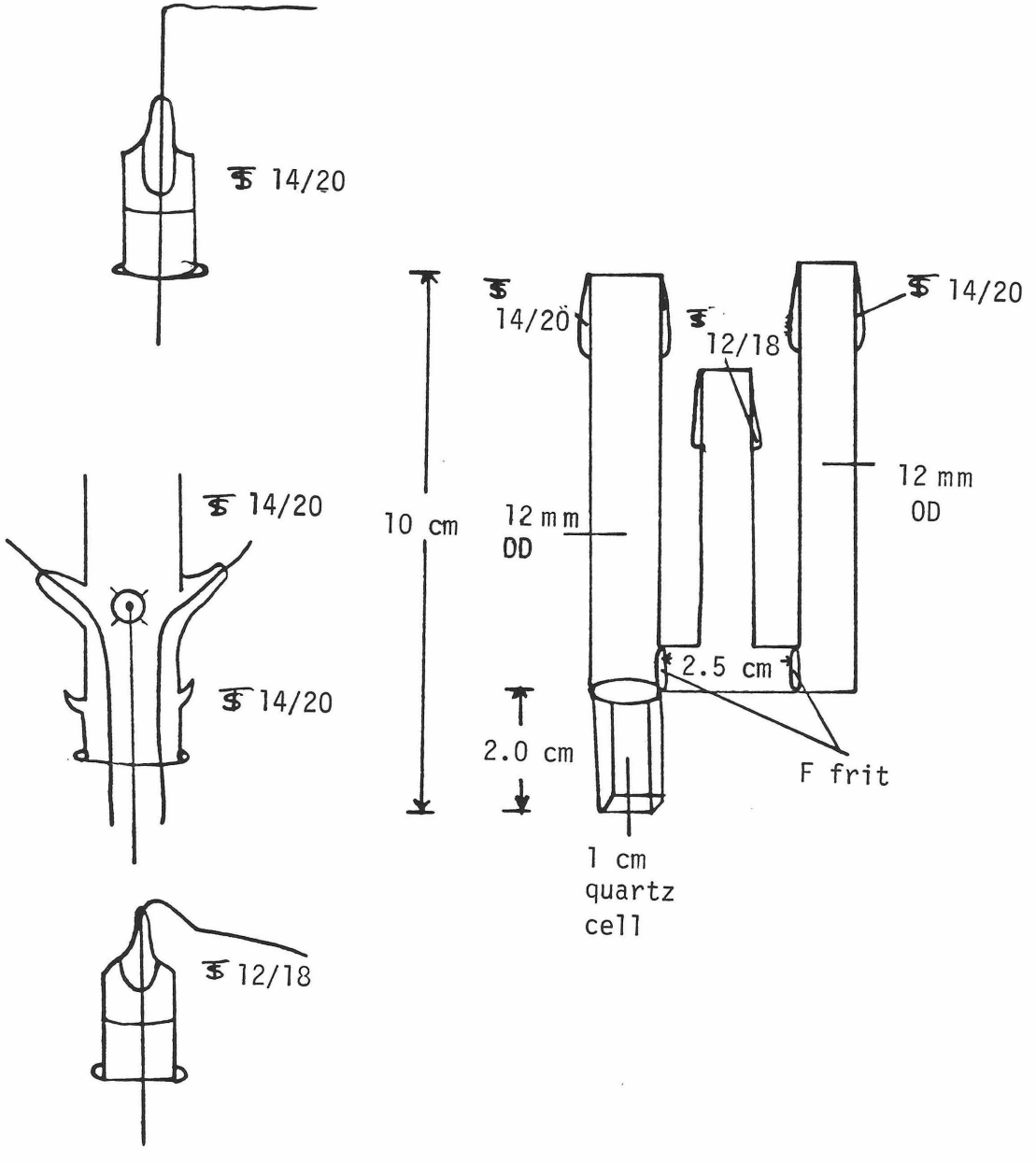
14/20
14/20
14/20
12/18
10 cm
12 mm
OD
14/20
14/20
12/18
12 mm
OD
2.5 cm
2.0 cm
F frit
1 cm
quartz
cell

to dry, and then weighed. The plot of mercury flow rate (m) versus the square root of the mercury column height $(Ht\ Hg)^{1/2}$ gave a straight line that passes through the origin. The mercury flow rates are tabulated in Table 11. Since the surface tension of the mercury is lower in acetonitrile than in water, low mercury heights were used for the experiments. Typically 30 cm of mercury was used with a flow rate of 0.612 mg/sec. At higher column heights of ca. 70 to 100 cm the mercury drop had a marked tendency to fall off before the drop knocker moved especially at more negative potentials. For sample current techniques too frequent an early drop dislodge is disasterous for useful data collection. The tendency for the drop to fall off early at higher column heights or more negative potentials varied among the complexes and is probably related to their interaction with the mercury. Another limit imposed by the lower surface tension was the drop time. Even at 30 cm mercury head height 2 seconds was the maximum allowable drop time. In a typical experiment the drop time was kept at 0.5 sec unless specified otherwise.

Infrared spectra were recorded on a Beckman IR 12 spectrometer. UV-Visible spectra were recorded using either a Hewlett-Packard 8450A or Cary 14 spectrophotometer. The fluorescence spectra were obtained on the instrument built by S. Rice. Since the correction curve was minor at the wavelengths of interest for the rhodium complexes the spectra reported are uncorrected. The fluorometer and fluorescence lifetime equipment have been described elsewhere (12).

Micro analyses were performed by Caltech Micro Analytical Facilities and by Gailbraith Laboratories, Inc.

C. SYNTHESIS

Most of the phosphine starting materials were purchased from Aldrich and used without further purification. VPE was obtained from Pressure Chemical Co. and was used as received. The isocyanide ligand, 1,3-diisocyanopropane (abbrev. bi) and the corresponding rhodium complex, $Rh_2(bi)_2$ were synthesized according to previously established procedures (56). 2,5-dimethy-2,5-diisocyanohexane(TMB) was prepared from the corresponding amine by the method of Ugi *et al.* (57) and was recrystallized from methylene chloride before use. $[Rh(COD)Cl]_2$ was prepared by a standard method from $RhCl_3\ 3H_2O$ which was obtained through a generous loan from Johnson Matthey, Inc. Dr. V. Miskowski is also thanked for a loan of $Co(VPE)_2(ClO_4)_2$, the synthesis of which has been published previously (59).

Standard syringe and Schlenk techniques as outlined by Shriver (63) were used for the synthesis and handling of the rhodium complexes. Optical UV-Visible and infrared absorption data were used to characterize the complexes.

$Rh_2TMB)_4(TRF)$. $[Rh(COD)_2Cl]_2$ (0.50 g, 0.0020 mol) was dissolved in 25 ml of hot degassed acetonitrile and the volume was then reduced under vacuum to 15 ml. AgTRF (0.521 g, 0.0041 mol) dissolved in 5 ml of degassed acetonitrile was added. The white solid, which formed immediately, AgCl, was filtered off and TMB (0.666 g, 0.0041 mol) dissolved in 5 ml of hot degassed acetonitrile was added to the filtrate. The solu-

tion very quickly changed to a deep red color. Approximately 45 ml of freshly opened hydrogen peroxide-free diethyl ether was added resulting in the formation of a red precipitate. The solid was filtered and dried. Small quantities (ca. 100 mg.) were dissolved in 6 ml of hot ethanol under a nitrogen stream and the resulting solution was allowed to cool. After ca. 15 minutes at -20° C a red crystalline solid formed. This solid was then filtered, washed with cold ethanol and allowed to dry giving a 60% yield. Infrared and UV-Visible spectra agreed with the published values (56). Anal. Calculated for $C_{42}H_{64}F_2N_8O_6Rh_2S_2$: C, 43.51; N, 9.48; H, 5.48. Found: C, 43.75, N, 9.69; H, 5.55.

$Co(DPE)_2(ClO_4)_2$. This complex was synthesized by the method of Sacco and Gorieri (36) on the same scale as was reported but with more care in oxygen exculsion. Anal. Calculated for $C_{52}H_{48}Cl_2O_8P_4Co$: C, 59.22; H, 4.59; P, 11.75; Cl, 6.73. Found: C, 59.61; H, 4.88; P, 11.81; Cl, 6.80.

$Rh(DPM)_2TRF$. This complex proved to be the most difficult to synthesize owing to its extreme sensitivity to oxygen and water. Additionally, it is known that a five-coordinate chlorine-containing complex can be formed if the chloride is not removed before the addition of the phosphine (60). It has also been pointed out that rhodium has a propensity to form A-frame complexes in the presence of DPM and chloride ion (61). The complex was synthesized on a vacuum line, entirely sealed-off from the atmosphere. Methylene chloride was dryed over molecular sieves

and was distilled directly into the reaction vessel. Diethyl ether was distilled directly from CaH. $Rh_2(COD)_2Cl_2$ (0.10 g, 0.20 mmol) and AgTRF (0.10 g, 0.40 mmol) were added to a round bottom flask along with a stir bar. DPM (0.35 g, 0.080 mmol) was placed in the sealable sidearm of a two-necked round bottom flask. This flask was then attached to a swivel frit opposite the previous flask and the system was evacuated. Methylene chloride (10 ml) was distilled into the flask containing the rhodium and the mixture was stirred for 30 minutes. The apparatus was inverted and the white solid which had formed, AgCl, was filtered while the filtrate drained into the second flask. The DPM was then added and the solution was stirred at room temperature for an additional 30 minutes. Diethyl ether (15 ml) was added and after 30 minutes the yellow precipitate that had formed was filtered. The solid was dried under vacuum and yielded 280 mg (68%) of a crystalline yellow-orange powder. Anal. Calcd for $C_{51}H_{44}F_3O_3P_4SRh$: C, 60.00; H, 4.35; P, 10.00. Found: C, 58.16; H, 4.31; P, 10.90. UV-Visible spectrum agreed with previously published data (60).

Rh(DPE)$_2$ClO$_4$. Rh(COD)Cl (0.050 g, 0.1 mmol) was dissolved in 5 ml of degassed toluene and a solution of DPE (0.16 g, 0.2 mmol) dissolved in 5 ml of degassed toluene was added with a syringe. The mixture was refluxed under nitrogen for 30 minutes during which time a yellow precipitate formed. After cooling in an ice bath the solution was filtered and the solid washed with toluene and vacuum dried. The ClO_4^- salt was obtained by dissolving the yellow solid in ethanol and

adding excess $LiClO_4$ followed by water until precipitation occurred. The product was collected and air-dried (this compound proved to be the most air-stable of the rhodium complexes). Anal. Calcd for $C_{52}H_{48}ClO_4P_4Rh$: C, 62.50; H, 4.85; P, 12.40. Found: C, 61.56; H, 5.02; P, 12.64. Spectra agreed with those previously published (32).

Rh(VPE)$_2$ClO$_4$. The procedure followed was essentially the same as for $Rh(DPE)_2ClO_4$. First, $Rh(VPE)_2Cl$ was synthesized. A methanol solution of it was combined with $LiClO_4$ and the bright-yellow precipitate that formed immediately was collected, washed with water and dried under vacuum. The yield was 200 mg (95%). This complex was almost as stable, both in solution or as a solid, as $Rh(DPE)_2ClO_4$. The UV-Visible spectrum agreed with the previously reported one (32). Anal. Calcd for $C_{52}H_{44}ClO_4P_4Rh$: C, 62.75; H, 5.11; P, 12.06. Found: C, 62.15; H, 4.75; P, 11.94.

Rh(DPP)$_2$ClO$_4$. The chloride salt was made in exactly the same fashion as the corresponding VPE and DPE complexes. The ClO_4^- salt was obtained through a similar metathesis reaction using $LiClO_4$. Anal. Calcd for $C_{52}H_{52}ClO_4P_4Rh$: C, 63.13; H, 5.17; P, 12.06. Found: C, 62.19; H, 5.13; P, 11.65.

Rh(DPB)$_2$TRF. The DPB complex suffered the same sort of complications as did the DPM complex and so the chloride had to be removed from the starting material to avoid the five-coordinate chloride phos-

phine adduct from forming. . Ag(TRF) (0.11 g, 0.04 mmol) in degassed methanol was syringed against a counter flow of argon into a solution of $Rh_2(COD)_2Cl_2$ (0.10 g, 0.20 mmol) in 2 ml methylene chloride. A white precipitate formed immediately and the mixture was stirred an additional 20 minutes and then filtered under argon. DPB (0.35 g, 0.40 mmol) in methylene chloride was then added to the filtrate and the color of the solution changed form light yellow to deep orange. A mixture of diethyl ether and hexane (1:1) was then added to precipate the solid. An additional 5 ml of diethly ether was added and the mixture was stirred for 15 minutes. The orange crystalline solid obtained was dried under vacuum yielding 350 mg (78%) of product. UV-Visible spectrum agreed with the one previously reported (60). Anal. Calcd for $C_{52}H_{52}ClO_4P_4Rh$: C, 60.87; H, 5.12; P, 9.33. Found: C, 61.12; H, 5.67; P, 9.55.

III. CYCLIC VOLTAMMETRY, CHRONOAMPEROMETRY AND POLAROGRAPHY OF THE COBALT AND RHODIUM COMPLEXES

A. INTRODUCTION

1. Cyclic Voltammetry and Chronoamperometry.

Cyclic voltammetry is a moderately fast electrochemical technique with a time window of 10^{-4} seconds to several seconds. The scan rates (v) employed in this study ranged form 20 mV/sec to 100 V/sec. Cyclic voltammetry is a technique in which the current is monitored as the potential of the working electrode is varied with a triangular waveform. The resulting current shows a peaked behavior with potential. Distortions of these curves have various implications ranging from chemical complications to lack of solution resistance (IR) compensation. Numerous comprehensive reviews of the technique exist (37-43). At slow scan rates an X-Y recorder can be used to record the voltammograms, but at scan rates in excess of 1 V/sec, only the oscilloscope is capable of recording currents and wave shapes accurately. The currents for anodic and cathodic current ratios were calculated by the method outlined by Nicholson (41):

$$i_p^a / i_p^c = (i_{pa})_o / i_{pc} + 0.485\ (i_{sp})_o / i_{pc} + 0.086$$

The current values are diagrammed in Figure 3A (Section B, CV of anthracene). For the reversible cyclics the diffusion coefficients were obtained from the ip^c vs. $v^{1/2}$ plots. This follows from the equation given by Nicholson and Shain (40):

$$i_p^c = (2.69 \times 10^{-5})\ n^{3/2}\ A\ D_o^{1/2}\ C_o\ v^{1/2}$$

where A is the area of the electrode and C_o is the bulk concentration of the species under question.

In cyclic voltammetry the peak current and peak potential, hence the peak splitting, are very sensitive to resistance in the electrochemical cell (45). To minimize this problem the PAR potentiostats have resistance compensation feedback loops. Typically for an experiment the IR compensation was increased until the potentiostat started to oscillate during scans, then the compensation was reduced by fifty percent to collect data. This method works as well as the more difficult method prescribed by Princeton Applied Research in their PAR manual (46).

In a chronoamperometric measurement (37), the potential is stepped from a point where no faradaic current flows to one well past the $E_{1/2}$ value where the currents obey the Cotrell equation:

$$i(t) = n\ FAD_o^{1/2} C_o / \pi^{1/2} t^{1/2}$$

where all symbols have their usual electrochemical meanings. Diffusion coefficients were calculated form the slopes of i(t) verses $t^{-1/2}$ plots. This is a more accurate method for the determination of diffusion coef-

ficients than cyclic voltammetry.

The chronoamperometric results obtained here were measured on a HMDE or platinum electrode. Anthracene was used to calibrate the area of the platinum electrode when mercury proved to be unsatisfactory for some of the complexes. In a typical experiment the current was monitored for 20 ms through 180 ms and 50 ms through 450 ms. This time was long enough to ignore double layer charging but not so long that spherical corrections were needed or convection currents were a problem. Table 9A summarizes the potential step data for all the complexes examined in the study.

2. Polarography.

Since the majority of the previous rhodium electrochemical studies depended on polarographic interpretation it was judged worthwhile to repeat and extend the previous work. Three techniques were employed in this study: d.c. polarography and its variation, sampled d.c. (Tast), normal pulse, and differential pulse polarography. Bard and Faulkner have detailed, accurate descriptions of these techniques in Chapter 5 of their book (37).

Polarography was used to obtain I, the disguised diffusion coefficient. I is related to the diffusion coefficient by:

$$I = i_l/m^{2/3}t^{1/6}C_o = 708\ nD_o^{1/2}$$

where all the symbols have their usual electrochemical significance. In a typical polarographic experiment the potential range was scanned once

at 5 mV/sec with the mercury column height at 30 cm and the drop time at one second. A d.c. polarogram was recorded, then the same scan was repeated on a sampled d.c. setting. A comparison was made and if the two curves were in agreement the mercury column height dependence was studied.

In Tast polarograms reported here the step-like characteristics of the experimental curves have been smoothed in the transcription process. For d.c. and Tast polarography the shape of the current voltage curve can be analyzed to estimate the number of electrons involved in the wave. A plot of E vs. $\log[(i_d-i)/i]$ gives a linear plot, the slope of which is 2.3 RT/nF for a reversible nernstian system (7). The Tomes criterion for reversibility (34) is to evaluate $E_{3/4} - E_{1/4}$. These potentials are where the current is three-fourths and one-fourth of the diffusion currents. For a nernstian wave $E_{3/4} - E_{1/4} = 56.4/n$ mv/sec at 25° C.

The normal pulse and reverse pulse techniques are useful because they give an indication of reversibility of the electrode reaction. The ratios of the plateau current forward scan to the reverse direction scan provide a measure of the electrode reversibility. Oldham and Parry (62) published the equation which would describe the ratios. These values have been calculated (Table 10) for the pulse shape and pulse time of the stock PAR 174.

Differential pulse polarographic peak widths (W_p) can be used to estimate the separation of two consecutive closely spaced electron transfers. Parry and Osteryoung calculated the width at half peak

height for small potential steps for different n value electron transfer processes (51). Richardson and Taube extended this study for two one-electron processes closely spaced and published a working curve for a 10 mV step height (50).

Table 1.

Cyclic Voltammetric Data - p-benzoquinone

V (mV/sec)	E_p^c	ΔE (mV)	i_p^c (μ A)
1000	-0.795	70	45.5
750	-0.860	70	40.0
500	-0.860	65	33.8
350	-0.863	68	26.8
200	-0.863	67	20.0
150	-0.850	65	15.5
100	-0.865	65	15.0
75	-0.868	68	13.5
50	-0.868	73	12.5
35	-0.870	70	9.3
20	-0.870	70	7.9
10	-0.860	65	6.0

Table 2. Cyclic Voltammetric Data - Anthracene

v (mV/sec)	E_p^c (V)	E_p^a (V)	ΔE (mV)	i_p^a/i_p^c	i_p^c (μA)
1000	2.387	2.324	63	.93	47.0
800	2.385	2.321	64	.88	43.0
700	2.386	2.318	68	.94	37.5
600	2.385	2.320	65	.93	35.2
500	2.383	2.325	58	.89	33.8
400	2.380	2.323	57	.91	29.7
300	2.380	2.320	60	.94	25.6
200	2.383	2.320	63	.95	21.2
150	2.383	2.320	63	.96	18.6
100	2.382	2.319	63	.95	15.4
75	2.385	2.320	65	.95	13.5
50	2.385	2.320	65	.96	11.2
30	2.385	2.318	67	.97	8.5
20	2.384	2.316	68	.89	7.6

Table 3. Cyclic Voltammetric Data - $Co(DPE)_2ClO_4$

v (mV/sec)	E_p^c (V)	ΔE (mV)	i_p^c (μ A)	i_p^a/i_p^c
		A. $Co^{II} - Co^{I}$		
500	-0.705	75	7.90	1.04
350	-0.700	70	7.00	0.96
200	-0.705	70	5.30	0.97
150	-0.700	70	4.60	0.94
100	-0.700	70	4.20	1.02
75	-0.700	68	3.54	0.95
50	-0.700	70	2.97	0.86
35	-0.700	65	2.51	0.94
20	-0.700	70	1.98	0.90
		B. $Co^{I} - Co^{0}$		
500	-1.560	65	7.60	0.85
350	-1.558	63	6.70	0.84
200	-1.558	70	5.10	0.89
150	-1.558	65	4.50	0.81
100	-1.555	65	3.90	0.85
75	-1.558	65	3.28	0.99
50	-1.558	65	2.80	0.97
35	-1.558	65	2.30	0.96
20	-1.558	65	1.80	0.91
		C. $Co^{0} - Co^{-I}$		
500	-2.035	65	6.40	1.00
350	-2.035	65	5.70	1.00
200	-2.040	70	4.00	1.02
150	-2.035	68	3.40	1.05
100	-2.040	65	3.60	1.00
75	-2.038	68	3.00	1.00
50	-2.040	65	2.60	1.03
35	-2.040	65	2.30	1.00
20	-2.040	63	1.80	0.82

Table 4. Cyclic Voltammetric Data - $Co(VPE)_2ClO_4$

A. $Co^{II} - Co^{I}$

(mV/sec)	E_p^c (V)	ΔE (mV)	i_p^c (μ A)	i_p^a/i_p^c
1000	0.570	67	9.5	1.03
800	0.575	75	8.5	1.00
600	0.575	72	7.2	0.97
500	0.575	70	6.8	1.00
400	0.575	70	6.0	0.97
300	0.575	65	5.4	0.96
200	0.573	63	4.5	0.91
150	0.573	65	3.9	0.95
100	0.573	63	3.1	1.03
75	0.570	62	2.9	0.96
50	0.573	65	2.5	0.92
30	0.573	65	1.9	0.95
20	0.573	65	1.6	0.94

B. $Co^{I} - Co^{o}$

1000	-1.574	60	10.6	0.77
800	-1.575	65	9.2	0.85
600	-1.575	67	8.2	0.85
500	-1.575	67	7.5	0.86
400	-1.573	63	6.6	0.82
300	-1.573	65	5.8	0.84
200	-1.573	66	4.9	0.86
150	-1.576	65	4.2	0.98
100	-1.575	66	3.5	1.03
75	-1.572	61	3.0	0.87
50	-1.575	64	2.6	0.85
30	-1.573	63	2.1	0.81

C. $Co^0 - Co^{-1}$

v (mV/sec)	E_p^c (V)	ΔE (mV)	i_p^c (μ A)	i_p^a/i_p^c
1000	1.895	65	8.5	1.26
800	1.895	65	7.2	1.28
600	1.897	67	6.5	1.31
500	1.897	67	5.8	1.29
400	1.897	64	5.1	1.32
300	1.897	64	4.5	1.32
200	1.897	64	3.8	1.33
150	1.897	64	3.1	1.32
100	1.898	65	2.6	1.32
75	1.894	64	2.4	1.22
50	1.897	65	1.9	1.31
30	1.895	58	1.4	1.36
20	1.898	64	1.3	1.19

D. With Anthracene
(1.3 mM)

500	2.370	62	23.2	1.00
200	2.375	67	15.0	0.93
100	2.375	67	11.1	0.95
50	2.374	69	7.8	0.92

Table 5. Cyclic Voltammetric Data - $Rh(DPM)_2^+$

v (mV/sec)	E_p^c (V)	ΔE (mV)	i_p^c (μ A)	i_p^a/i_p^c
500	2.071	56	59.0	0.54
200	2.065	45	44.2	0.44
150	2.064	44	36.8	0.42
100	2.059	45	28.8	0.15
75			25.0	
50			18.8	

Table 6. Cyclic Voltammetric Data - $Rh(VPE)_2Clo_4$

v (mV/sec)	ΔE (mV)	E_p^c (V)	i_p^c (μA)	i_p^a/i_p^c
1000	36	1.973	43.5	0.90
800	33	1.973	37.5	0.89
700	36	1.973	31.3	0.94
600	35	1.975	31.2	0.89
500	33	1.970	27.0	0.93
400	38	1.972	25.2	0.90
300	37	1.974	21.8	0.92
200	40	1.972	18.4	0.82
150	39	1.973	15.0	0.96
100	40	1.972	12.8	0.93
75	38	1.970	10.5	0.91
50	38	1.968	8.8	0.86

Table 7. Cyclic Voltammetric Data - $Rh(DPE)_2ClO_4$

A. $Rh(DPE)_2ClO_4$

v (mV/sec)	ΔE (mV)	E_p^c (V)	i_p^c (μA)	i_p^a/i_p^c
50000	200		170.0	
20000	150		105.0	
10000	130		80.0	
5000	95		55.0	
2000	80		38.0	
1000	85	2.125	25.8	0.95
800	77	2.117	23.8	1.00
700	78	2.120	21.5	1.10
600	77	2.122	20.3	1.10
500	76	2.123	19.5	1.10
400	76	2.116	14.8	0.99
300	62	2.116	15.3	1.00
200	53	2.107	13.0	1.00
150	50	2.103	11.0	1.00
100	49	2.102	9.0	1.00
75	49	2.103	8.0	1.00
50	45	2.100	6.8	0.98
30	41	2.098	5.5	0.92

B. Anthracene

v (mV/sec)	ΔE (mV)	E_p^c (V)	i_p^c (μA)	i_p^a/i_p^c
50000	80		500.0	
20000	70		340.0	
10000	65		250.0	
5000	60		175.0	
2000	55		110.0	
1000	60	2.375	70.0	0.92
800	59	2.372	61.0	1.00
700	68	2.383	57.0	1.00
600	60	2.377	53.0	1.00
500	63	2.380	49.0	1.00
400	63	2.380	41.0	1.00
300	63	2.380	37.0	1.00
200	62	2.382	31.0	0.98
150	63	2.382	27.0	1.00
100	64	2.383	22.0	0.97
75	67	2.384	18.8	1.10
50	65	2.385	15.4	1.00
30	68	2.385	12.3	1.00

Table 8. Cyclic Voltammetric Data - $Rh(DPP)_2ClO_4$

v (mV/sec)	E_p^c (V)	ΔE (mV)	i_p^c (μ A)	i_p^a/i_p^c
1000	1.765	60	36.0	0.95
800	1.760	53	33.0	0.96
700	1.760	53	29.0	0.88
600	1.757	51	26.0	0.99
500	1.758	53	25.0	0.99
350	1.757	54	21.0	0.99
200	1.760	53	16.0	0.96
150	1.760	54	15.0	0.96
100	1.760	50	11.3	0.96
75	1.763	56	9.8	0.95
50	1.760	53	8.1	0.90
20	1.765	53	5.8	1.02
		with Anthracene		
1000	2.180	75	35.0	1.19
800	2.180	65	33.0	1.13
700	2.185	70	28.0	1.06
600	2.185	70	27.0	1.09
500	2.180	65	24.0	1.12
350	2.180	65	21.0	1.09
200	2.180	65	18.3	1.08
150	2.185	70	15.5	1.07
100	2.180	65	11.4	1.07
75	2.183	69	10.2	1.03
50	2.185	72	8.6	0.99
20	2.190	85	7.1	0.72

Table 9A

Cyclic Voltammetric and Chronoamperametric D_o

Master Table

Compound	CV D_o (cm^2/sec)	Chronoamperametric D_o (cm^2/sec)
Anthracene		
1.7 mM	2.9×10^{-5}	2.8×10^{-5}
1.5 mM	3.0×10^{-5}	2.8×10^{-5}
1.3 mM	3.0×10^{-5}	2.6×10^{-5}
$Co(DPE)_2^+$		
$Co^{II} - Co^{I}$	8.7×10^{-6}	1.25×10^{-5}
$Co^{I} - Co^{o}$	8.7×10^{-6} *8.8×10^{-6}	*1.4×10^{-5}
$Co^{I} - Co^{-I}$		*1.5×10^{-5}
$Co(VPE)_2^{2+}$		
$Co^{II} - Co^{I}$	9.3×10^{-6}	1.3×10^{-5}
$Co^{I} - Co^{II}$	9.7×10^{-6}	1.4×10^{-5}
$Co^{I} - Co^{o}$	1.07×10^{-6}	
$Rh(DPM)_2^+$	not useful	9.4×10^{-6} 9.7×10^{-6}
$Rh(VPE)_2^+$	7.0×10^{-6}	9.49×10^{-6}
$Rh(DPE)_2^+$		
	6.0×10^{-6}	$9.7(3) \times 10^{-6}$
	8.1×10^{-6}	
$Rh(DPP)_2^+$	*2 e^- 4.9×10^{-6} *2X 1e^- 9.8×10^{-6}	9.5×10^{-6}
$Rh(DPB)_2^+$		#1.1×10^{-5} 7.3×10^{-6}

* after bulk electrolysis

on Pt electrode

Table 9B

CV Master Table

Compound	i vs. $v^{1/2}$	ΔE (mV)	$E_{1/2}$ (V)	D_o (cm^2/sec)	Anthracene D_o (cm^2/sec)
Anthracene	linear	60-80	-2.352(2)		3.0×10^{-5}
$Co(DPE)_2^{2+}$					
$Co^{II} - Co^{I}$	1	60-70	-0.665	8.7×10^{-6}	
$Co^{I} - Co^{o}$	1	60-70	-1.525	8.8×10^{-6}	
$Co^{o} - Co^{-I}$	1	60-70	-2.005		
$Co(VPE)_2^{2+}$					
$Co^{II} - Co^{I}$	1	60-70	-0.575	-6.1×10^{-6}	2.9×10^{-5}
$Co^{I} - Co^{o}$	1	60-70	-1.545	1.07×10^{-5}	
$Co - Co^{-I}$	1	60-70	-1.870		
$Rh(DPM)_2^{+}$	1	45	-2.020		
$Rh(VPE)_2^{+}$	1	33-40	-1.950	6.4×10^{-6}	2.2×10^{-5}
$Rh(DPE)_2^{+}$	not linear	40-120	-2.070	8.0×10^{-6}	2.8×10^{-5}
$Rh(DPP)_2^{+}$	1	50-60	-1.935	*4.9×10^{-6}	2.2×10^{-5}
				**3.9×10^{-5}	
				***9.8×10^{-6}	
$Rh(DPB)_2^{+}$			-1.865(10)		
			-2.090(20)		

* 1 e^-

** 2 e^-

*** 2X 1e^-

Table 9C

Polarographic Master Table

Complex	$-E_{1/2}$ (V)	I †	$E_{3/4} - E_{1/4}$ (mV) or *Tomes plot	NP(i_f/i_r) (sec) 0.5	1.0	2.0	DP (W_p) (mV) 5	10	25
Anthracene	2.340	3.2	*55	1.8			130		
$Co(VPE)^{2+}$									
2-1	0.565	2.19	60	1.0					130
1-0	1.620		55	1.0					120
1--1	1.955		55	1.0					130
			#(1.0, 1.1, 1.08)	#(1.0, 1.1, 1.2)			#(1.0, 1.1, 1.2)		
$Co(DPE)_2^{2+}$									
2-1	0.660	2.2	60	1.0(1)					110
1-0	1.525		70	0.95					130
0-1	2.010		60	0.95					120
			#(1.0, 1.05, 1.1)	#(1.0, 1.05, 1.10)			#(1.0, 1.05, 1.4)		
$Rh(DPM)_2^{+}$	2.025	3.5	*38.1	1.24	1.97				75
$Rh(DPE)_2^{+}$	2.045	4.1	30(3)					70	90
$Rh(VPE)_2^{+}$	1.875	4.2	*28.5	1.34			63	55	63
$Rh(DPP)_2^{+}$	1.935	3.8	40	1.14	1.05		90	95	90
$Rh(DPB)_2^{+}$	-1.900	2.0	90						
	-2.075	4.1	30						

† $\mu A\ sec^{-1/2}\ mg^{-2/3}\ mM^{-1}$

ratio of currents ($i^{2/1}$: $i^{1/0}$: $i^{0/1}$)

Table 10

A. Pulse Polarography i_1^a / i_1^c

droptime (sec)	reversible	irreversible
0.5	0.95	2.1
1.0	0.98	2.9
2.0	0.99	4.2
5.0	1.00	6.7

B. Differential Pulse Polarography

Peak Width At Half Peak Height

n	$E_{1/2}$ (mV)
1	90.4
2	45.2
3	30.1

Table 11. Hg Flow Rate

Ht. (cm)	mg/sec
30	0.612
40	0.839
50	1.077
60	1.310
70	1.516
80	1.749
90	1.979
100	2.213

B. p-BENZOQUINONE AND ANTHRACENE

1. Cyclic Voltammetry and Chronoamperometry.

The electrochemistry of anthracene and p-benzoquinone (38) has been well established allowing their use as standards or "known" complexes for reductions. In addition to their well-understood electrochemistry, these two compounds were chosen because they are free of electrochemical waves in the area of the inorganic complexes. The compounds were used to adjust the IR compensation of the potentiostat circuits and to estimate the correction factors for cyclic voltammetric peak splittings. First, measurements were performed on the desired complexes with IR compensation, then the organic compounds were added to see how the CV peak splittings compared. The amount of added organic reagent was such that the new current peaks were of comparable size with those of the inorganic complexes. Unless otherwise noted, the size and position of the inorganic waves were unaffected by the organic additions.

In acetonitrile, p-benzoquinone is reported to undergo two one electron reductions. Using cyclic voltammetry, the two waves appear at -0.83 V and ca. -1.75 V (vs. 0.1 M $AgNO_3$/Ag) (Figure 4A). In agreement with the literature (39) the first reduction to the semiquinone is reversible while the second reduction shows quasi-reversible characteristics. This result is visible in the cyclic voltammograms shown in Figure 4A. The difference in potentials for the current peaks do not increase as the scan rate increases for the first wave, but do for the second one. The peak currents and peak splittings for the first wave

FIGURE 3

A. Cyclic Votammogram of 1.3 mM Anthracene

   v = 400 mV/sec

   with definitions

B. Plot of i_p^c vs. $v^{1/2}$ for Anthracene

C. Chronoamperametric data for 1.5 mM Anthracene

   i vs. t raw data

D. i vs. $t^{1/2}$ plot for 1.5 mM Anthracene

E. Tast Polarogram of 1.7 mM Anthracene at 30 cm Hg

   D.T. = 0.5 sec

F. Plot of i vs. $(Ht.\ Hg)^{1/2}$ for 1.7 mM Anthracene

   V vs. 0.1 m $AgNO_3/Ag$

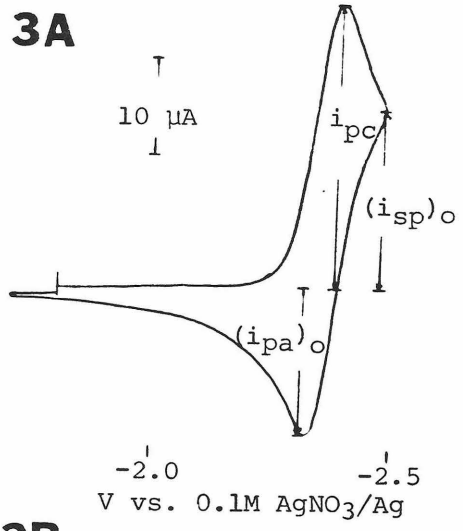
3A
10 μA
i_{pc}
$(i_{sp})_o$
$(i_{pa})_o$
-2.0
-2.5
V vs. 0.1M $AgNO_3$/Ag

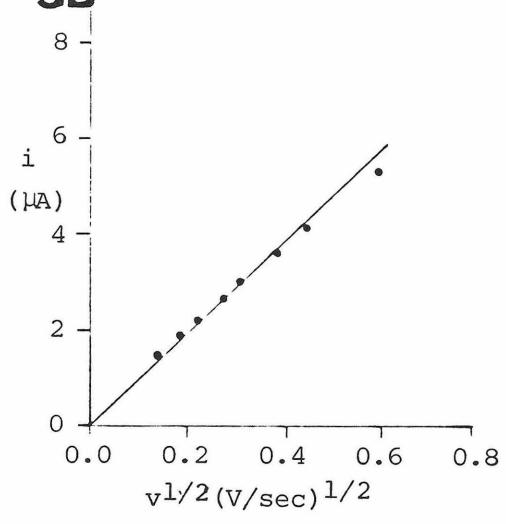
3B
i
(μA)
8
6
4
2
0
0.0
0.2
0.4
0.6
0.8
$v^{1/2}$ $(V/sec)^{1/2}$

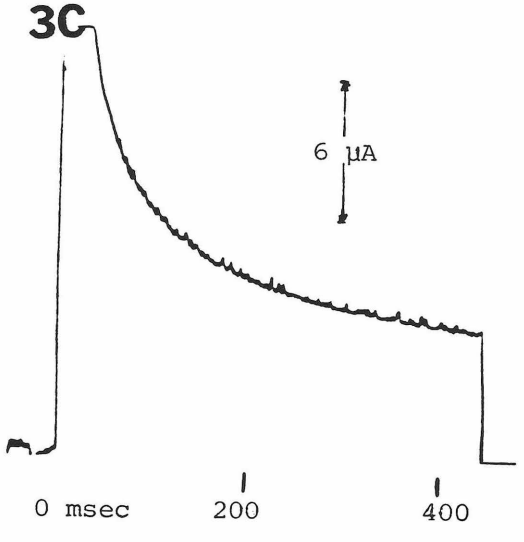
3C
6 μA
0 msec
200
400

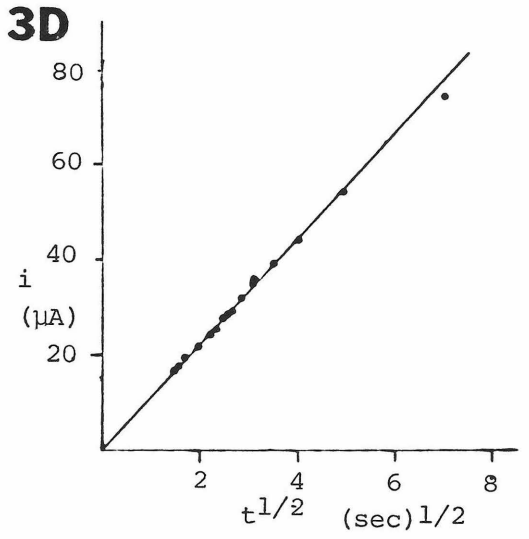
3D
80
60
40
20
i
(μA)
2
4
6
8
$t^{1/2}$ $(sec)^{1/2}$

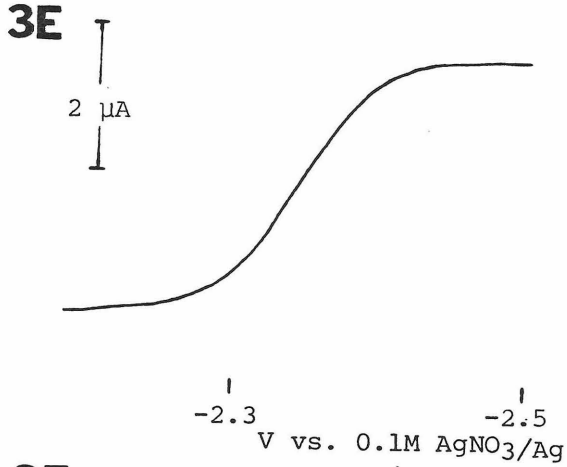
3E
2 μA
-2.3
-2.5
V vs. 0.1M $AgNO_3$/Ag

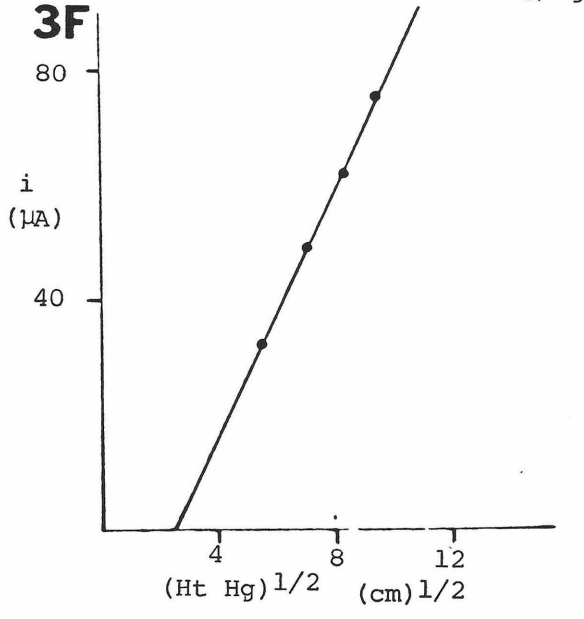
3F
80
40
i
(μA)
4
8
12
$(Ht\ Hg)^{1/2}$ $(cm)^{1/2}$

FIGURE 4

A. Cyclic Voltammogram of a 2.0 mM solution of p-benzoquinone

   a. v = 500 mV/sec

   b. v = 200 mV/sec

   c. v = 100 mV/sec

   d. v = 50 mV/sec

B. Plot of i_p^c vs. $v^{1/2}$ for p-benzoquinone

4A

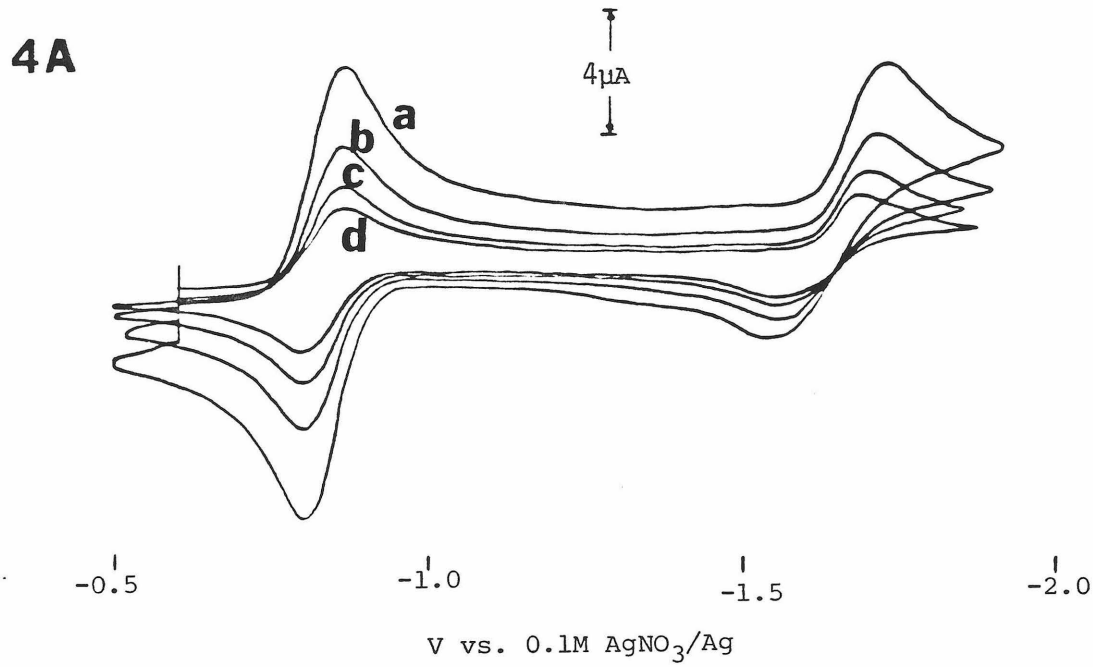
4μA
a
b
c
d
-0.5
-1.0
-1.5
-2.0
V vs. 0.1M $AgNO_3$/Ag

4B

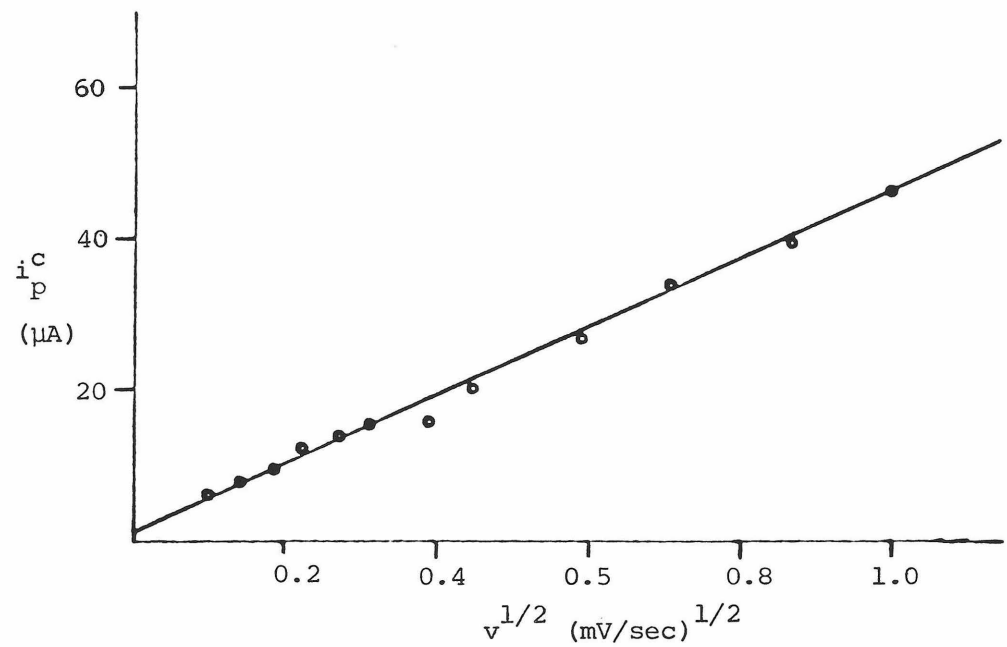
60
40
20
i_p^c
(μA)
0.2
0.4
0.5
0.8
1.0
$v^{1/2}$ $(mV/sec)^{1/2}$

are given in Table 1. Very noticeable is the fact that even with IR compensation, the peak splitting never reaches 60 mV but is always greater and varies a little from scan to scan. This indicated a small amount of uncompensated resistance was inherent in the electrochemical set up. A graph of peak current plotted against the square root of the scan rate (ip^c vs. $v^{1/2}$ plot) is linear (Figure 4B) as expected for the reversible reduction (46).

Anthracene undergoes two one-electron reductions (41,42). The first wave is of primary interest (Figure 3A). It occurs at more negative potentials than observed for all the inorganic complexes and hence does not interfere with the other waves. Tabulated in Table 2 are the current peak potentials, the peak splittings and the anodic and cathodic peak ratios. The peak splittings are generally greater than 60 mV but the scatter is not greater than 10 mV. The value of the ip^a/ip^c ratio is slightly smaller than one, indicating that some reduced material is being lost. However no real trend is evident with scan rate suggesting that the cause lies with factors other than trace water present in the acetonitrile (41). A graph of peak current versus the square root of scan rate (Figure 3B) is a straight line with a slope that gives a diffusion coefficient of 3.0×10^{-5} cm^2/sec. This measurement was repeated two additional times with 1.5 mM and 1.7 mM solutions giving D_o values of 3.0×10^{-5} and 2.9×10^{-5} cm^2/sec respectively. These values are tabulated on the CV and chronoamperometry master table (Table 9A). It is obvious that the CV values of D_o are reproducible and comparable even if consistently larger than the potential step measurements of

D_o. No literature value of D_o for anthracene exists under the exact conditions used in this study (0.2 M $TBABF_4$ in acetonitrile). The most similar conditions were 0.1 M TBA iodide in acetonitrile. In this case I_d was 3.14 which corresponded to a D_o value of 2.0×10^{-5} cm^2/sec. In cases where anthracene was added to solutions of the inorganic complex the cyclic voltammetric diffusion coefficients for anthracene ranged from 2.2×10^{-5} cm^2/sec to 2.9×10^{-5} cm^2/sec. The range may be due to loss of anthracene by evaporation into the dry box or into the vacuum of the antechamber.

Several solutions of anthracene in various concentrations were used to test the precision of the chronoamperometric method and the capability of the equipment. A typical raw data output for a 1.5 M anthracene in acetonitrile solution with 0.2 M $TBABF_4$ is shown in Figure 3C. The curve spans 0 to 450 milliseconds. Figure 3D displays the same data but now the two axes are current and the inverse of the square root of time. The plot is a straight line which passes through the origin. The slope of this line gives a diffusion coefficient of 2.8×10^{-5} cm^2/sec. Table 9 contains a summary of the anthracene chronoamperometric data.

2. Polarography.

A 1.7 mM anthracene solution was studied by all three electrochemical methods mentioned previously. Figure 3E shows the polarogram obtained by Tast polarography. The plot of i_d vs. $(Ht\ Hg)^{1/2}$ gave a straight line (Figure 3F) indicating a diffusion controlled process.

The $E_{3/4} - E_{1/4}$ value was 55 mV, typical for a one-electron nernstian process. The I value obtained from the polarogram was 3.2 which compares favorably with the value 3.14 reported previously. The previous measurement was in a slightly different system: acetonitrile with 0.1 M TBA Iodine. The $I_d = 3.2$ value corresponds to a diffusion coefficient of 2.0×10^{-5} cm^2/sec. The CV value was $D_o = 2.9 \times 10^{-5}$ cm^2/sec while the potential step value was 2.8×10^{-5} cm^2/sec The normal pulse polarogram scanned -2.1 V to -2.5 V with a drop time of 0.5 sec. The previous scan covered the potential range from -2.5 V to -2.1 V. The reverse scan showed a maximum which made the exact current measurement more difficult and much less accurate. Nevertheless a value was estimated and the forward to reverse current ratio was found to be about 1.8. This is considerably larger than expected from the cyclic voltammetric results, indicating that the anthracene radical anion is unstable; this was later supported by bulk electrolysis. A differential pulse polarogram was recorded with a drop time of 0.5 sec and a modulation amplitude of 25 mV. A single peak was found with a peak width at half amplitude equal to 130 mV which is slightly larger than that expected for a one electron wave.

C. $Co(DPE)_2^{2+}$

1. Cyclic Voltammetry and Chronoamperometry.

A 0.64 mM solution of $Co(DPE)_2^{2+}$ exhibited three waves on both a HMDE and a platinum electrode. The waves occurred at -0.705 V, -1.560 V and -2.035 V (vs. 0.1 M $AgNO_3$/Ag) (Table 3, Figure 5A). The waves were well shaped although at slow scan rates some small "bumps" appeared at -0.9 V along with what appeared to be a more misshapen background. This could be an indication of some solvent decomposition or more likely it is a manifestation of the interaction of Co(-I) with mercury which will be discussed later. The peak splittings for all three waves were on the order of 65 mV. This indicates that three one-electron reductions occurred. The current ratios were all close to one; however, the lower values may be symptomatic of mis-measured currents (for example it is difficult to draw a baseline when more than one wave is being considered). No trend was seen with scan rate, suggesting no complication to the simple electron transfer. A plot of i vs. $v^{1/2}$ for the three waves gave straight lines whose slopes are similar. Two of these are shown in Figure 5B. The slopes from these plots give values of $D_o = 8.7 \times 10^{-6}$ cm^2/sec and 8.8×10^{-6} cm^2/sec.

Chronoamperometric measurements were made by stepping the potential from -0.5 V to -1.14 V. The D_o obtained for the cobalt(II) by this process was 1.25×10^{-5} cm^2/sec. After bulk electrolysis had been performed (discussed later) the solution contained the one-electron reduced species $Co(DPE)_2^{+}$. A potential step from -1.3 V to -1.8 V caused

FIGURE 5

A. Cyclic Voltammogram of 0.64 mM $Co(DPE)_2^{2+}$

   v = 500 mV/sec

B. Plot of i vs. $v^{1/2}$ for 0.64 mM $Co(DPE)_2^{2+}$

C. Tast Polarogram of 1.48 mM $Co(DPE)_2^{2+}$ at 30 cm Hg Ht.

5A

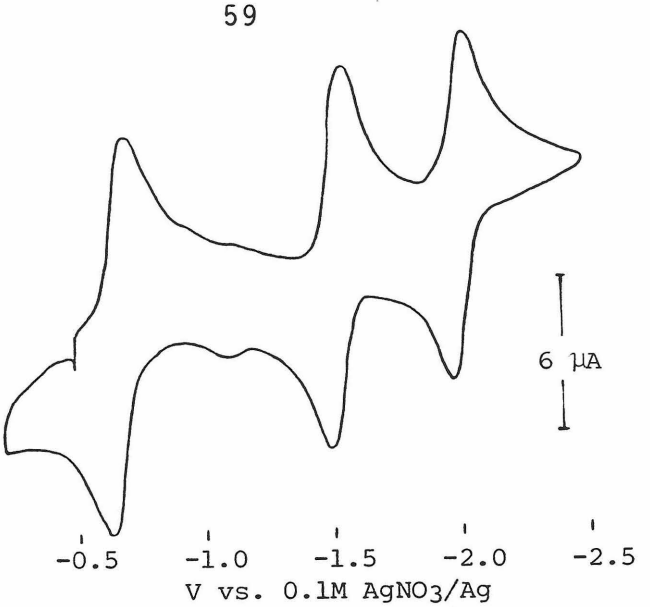
6 μA
-0.5
-1.0
-1.5
-2.0
-2.5
V vs. 0.1M AgNO3/Ag

5B

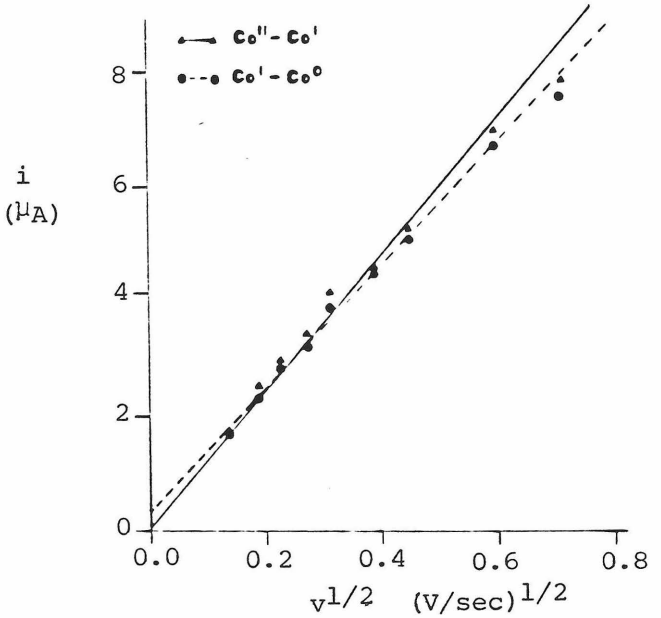
Co''-Co'
Co'-Co°
i (μA)
8
6
4
2
0
0.0
0.2
0.4
0.6
0.8
v1/2 (V/sec)1/2

5C

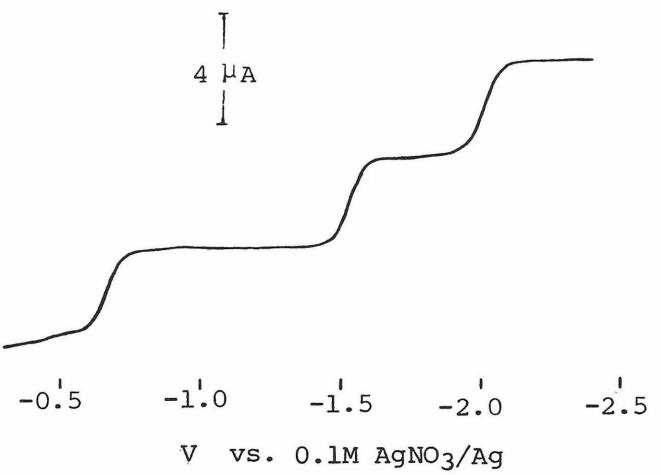
4 μA
-0.5
-1.0
-1.5
-2.0
-2.5
V vs. 0.1M AgNO3/Ag

the reduction of Co(I) to Co(0) and the diffusion coefficient obtained was 1.4×10^{-5} cm^2/sec. It was also possible to step over two waves by stepping from -1.3 V to -2.3 V. This corresponded to Co(I) being reduced to Co(-I). The current decay obeyed the Cottrell equation and the diffusion coefficient was found to be 1.5×10^{-5} cm^2/sec for n = 2.

2. Polarography.

A solution of $Co(DPE)_2^{2+}$ exhibited three polarographic waves (Figure 5C). The $E_{1/2}$ values were -.660 V, -1.525 V and -2.010 V (vs. 0.1 M $AgNO_3/Ag$). The separations of these waves are in agreement with the previously published values which measured potential relative to a SCE reference electrode (18). At 30 cm Hg and at higher mercury column heights the ratio approached 1.0: 1.0: 1.0. The I value is 2.2 which agrees exactly with the previously reported value (18). The Tomes criterion for reversibility gave values of 60 mV, 70 mV, and 60 mV respectively for the three waves. The forward to reverse current ratios were 1.11(5), 1.0(5) and 0.95(5) respectively. The fact that there were three waves allowed for some scan range variations. Scans were performed over the first and second wave and back and also over the second and third wave and back. These two scans had similar currents and in both cases the forward to reverse current ratios were 1.0.

A differential pulse polarogram which spanned all three waves was recorded. With a modulation amplitude of 25 mV the peak widths at one half height were 110 mV, 130 mV, and 120 mV respectively. The current magnitude ratio was 1 : 1.05 : 1.4. The normal and differential pulse

results, especially for the first and second reductions, agree with anthracene for a one-electron reduction. Under the experimental conditions the actual peak width at one-half height for the differential pulse polarograms appears to be ca. 120 mV for a one-electron process rather than the theoretical 90 mV value.

D. $Co(VPE)_2^{2+}$

1. Cyclic Voltammetry and Chronoamperometry.

Acetonitrile solutions of $Co(VPE)_2^{2+}$ exhibited three waves (Figure 6A) that were very similar to those found for $Co(DPE)_2^{+}$. The tabulated values (Table 4) of peak splittings for the three waves are in agreement with a one-electron nernstian process. The ΔE_p for anthracene is similar to that of the cobalt complexes. Plots of ip^c vs. $v^{1/2}$ for the three waves (Figure 6B) are all straight lines. The slope of the Co(II) - Co(I) plot gives a D_o value of 9.3×10^{-6} cm^2/sec.

A potential step from -1.4 V to -1.7 V stepped over the Co(II) to Co(I) wave. The D_o value calculated from the i vs. $t^{-1/2}$ plot was $D_o = 1.3 \times 10^{-5}$ cm^2/sec. Again a one-electron reduction was performed to bring the cobalt complex into an oxidation state comparable to that of the rhodium complexes. A step from -1.4 V to -1.7 V stepped the potential over the Co(I) to Co(0) wave. The D_o value obtained was $D_o = 1.4 \times 10^{-5}$ cm^2/sec value.

2. Polarography.

The $Co(VPE)_2^{2+}$ results were very similar to the $Co(DPE)_2^{2+}$ results. Three waves were visible in the Tast polarogram (Figure 6C), $E_{1/2}$ = -0.565 V, -1.620 V and 1.955 V (vs. 0.1 M $AgNO_3/Ag$). The three waves were roughly the same size with the current ratios remaining approximately 1.00 : 1.10 : 1.08 for all mercury column heights accessible. The I value obtained was 2.19 which compares favorably with the value

FIGURE 6

A. Plot of i vs. $v^{1/2}$ for 0.83 mM $Co(VPE)_2^+$

v = 400 mV/sec

B. Plot of i_p^c vs. $v^{1/2}$ for $Co(VPE)_2^+$

C. Tast Polarogram of 1.42 mM $Co(VPE)_2^{2+}$ at 40 cm Hg Ht.

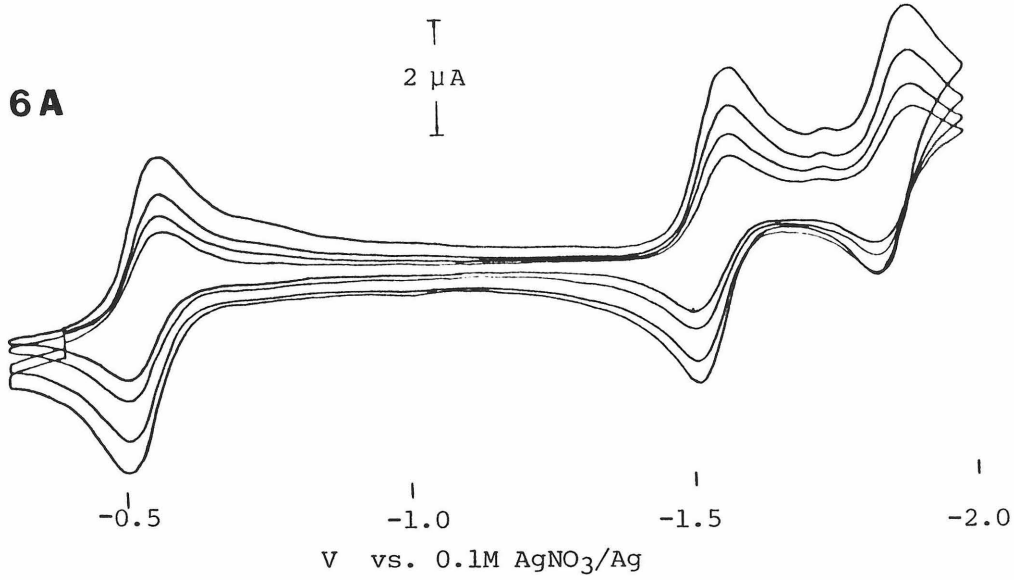
6A
2 μA
-0.5
-1.0
-1.5
-2.0
V vs. 0.1M AgNO3/Ag

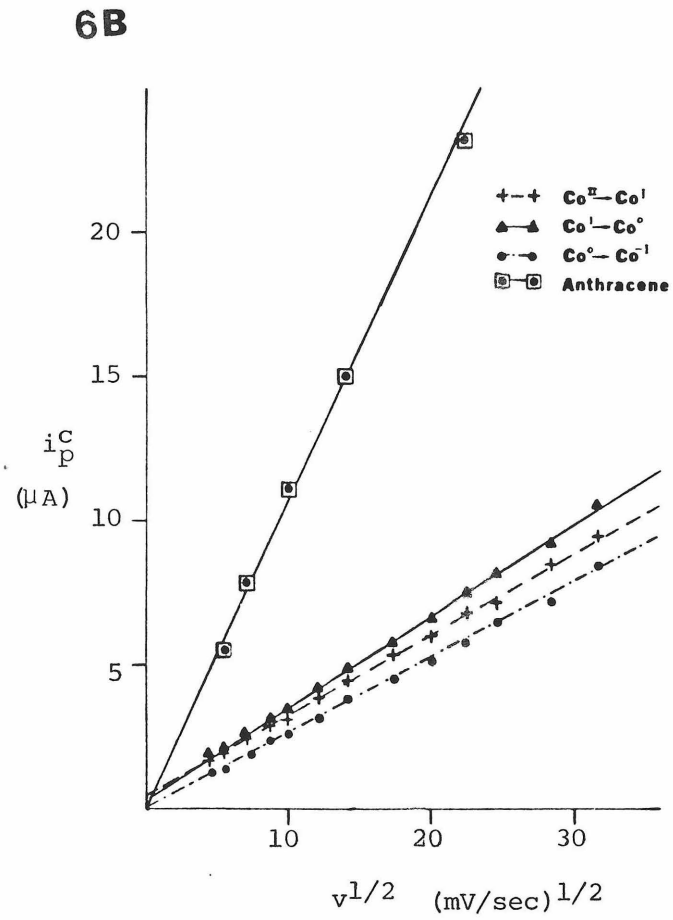
6B
Co^II—Co^I
Co^I—Co^0
Co^0—Co^-I
Anthracene
20
15
10
5
ip^c (μA)
10
20
30
v^1/2 (mV/sec)^1/2

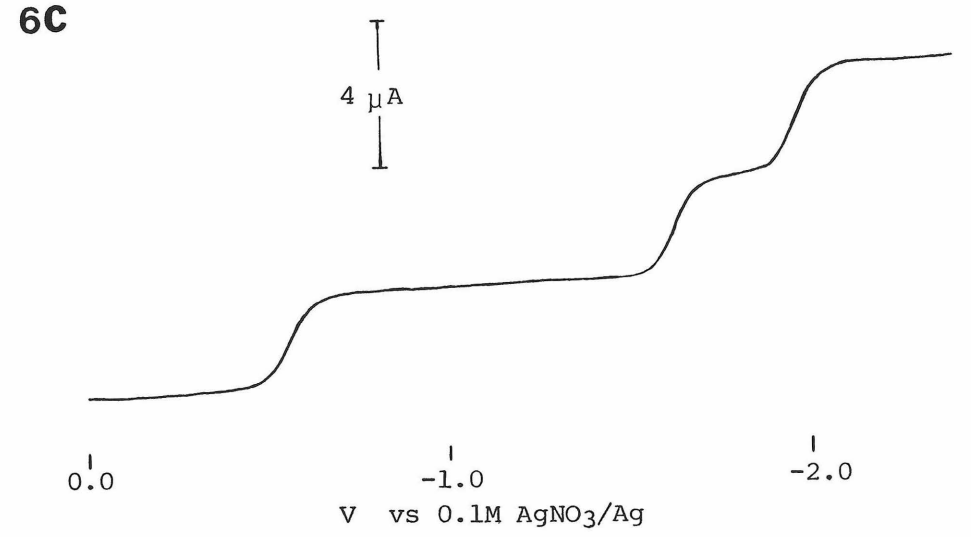
6C
4 μA
0.0
-1.0
-2.0
V vs 0.1M AgNO3/Ag

obtained with $Co(DPE)_2^{2+}$. The Tomes criterion for reversibility was 60 mV: 55 mV: 55 mV respectively for each of the waves. The N.P. polarograph current ratio for the three waves was 1.0: 1.1: 1.2. The waves were then scanned in the reverse direction one at a time over each wave. The ratios of forward currents to reverse currents was 1.00: 1.01: 1.00. A differential pulse polarogram exhibited three waves. The ratios of the current values for the three waves was 1.0: 1.1: 1.2. The modulation amplitude during the scan was 25 mV. These polarographic results are similar to those found for $Co(DPE)_2^{2+}$. The sizes and position of the various waves are very similar. This suggests that $Co(VPE)_2^{2+}$ undergoes the same electrochemical steps as $Co(DPE)_2^{2+}$: three consecutive, reversible one-electron reductions.

E. $Rh(DPM)_2^+$

1. Cyclic Voltammetry and Chronoamperometry.

Solutions of $Rh(DPM)_2^+$ exhibited one cathodic wave at -2.060 V (vs. 0.1 M $AgNO_3/Ag$). At high scan rates this wave had an anodic component (Figure 7A) with ip^a/ip^c = 0.54 at 350 mV/sec which decreased as the scan rate decreased. At 100 mV/sec the anodic component was barely visible and at slower scan rates the waves took the appearance of an irreversible wave. A small irreversible anodic wave was visible at -0.9 V. As the scan rate was increased the cathodic wave ip^a/ip^c current ratio increased and the small anodic wave became smaller. The peak splitting increased from 45 mV at the slowest scan rate accessible to 56 mV at 350 mV/sec (Table 5). The peak splitting at low scan rate suggests that a two-electron reduction is occurring followed by a fast chemical reaction. A small cathodic shift was observed for the reduction wave as the scan rate increased. Unfortunately the waves were not reproducible enough to distinguish between a first order and second order following chemical reaction (40,47). A graph of ip^c vs. $v^{1/2}$ presents a straight line. However since the reduction is not a simple electron transfer the slope of the line does not transform into D_o in a straightforward fashion, and so D_o was not calculated by CV.

If the cathodic scan was allowed to proceed negative of -2.3 V (Figure 8A) a large spike became visible and on the return scan a large spike was seen. In contrast to adsorbed electroactive material these features became more prominent at slow scan rates. The features reap-

FIGURE 7

A. Cyclic Voltammogram of 2.55 mM $Rh(DPM)_2^+$

   a. v = 350 mV/sec

   b. v = 200 mV/sec

   c. v = 150 mV/sec

   d. v = 100 mV/sec

B. i vs. $t^{1/2}$ plot for 2.55 mM $Rh(DPM)_2^+$

   Chronoamperometry on a HMDE

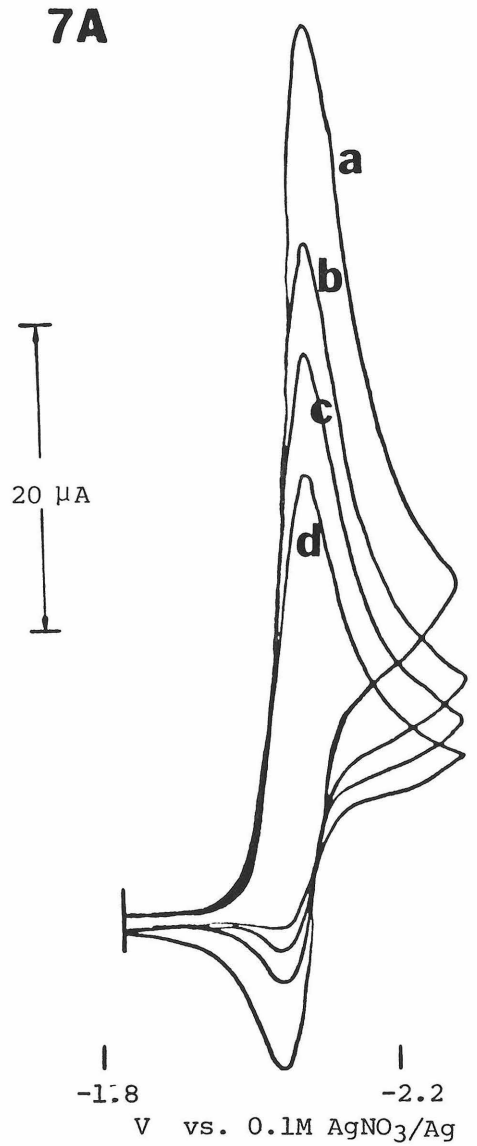
7A
a
b
c
d
20 µA
-1.8
-2.2
V vs. 0.1M AgNO3/Ag

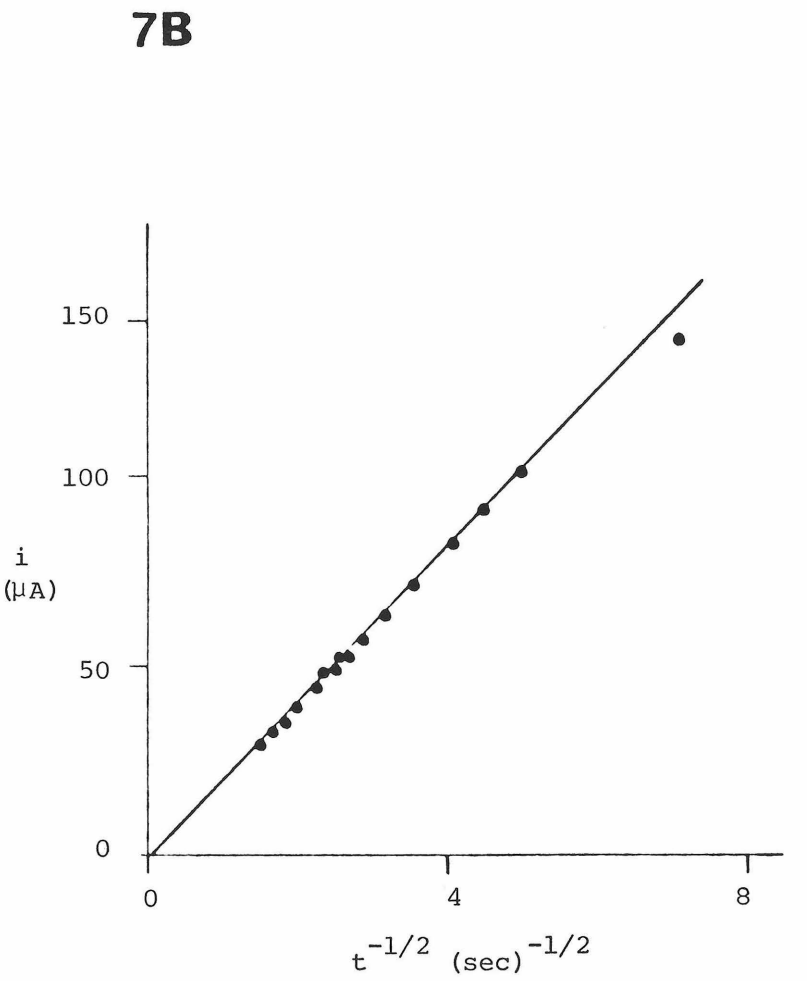
7B
150
100
50
0
i
(µA)
0
4
8
t-1/2 (sec)-1/2

FIGURE 8

A. Cyclic Voltammogram of 2.5 mM $Rh(DPM)_2^+$

scanning past -2.30 V on a HMDE

Upper curve v = 200 mV/sec

Lower curve v = 20 mV/sec

B. Chronoamperametric data for $Rh(DPM)_2^+$

Upper curve -1.9 V to -2.3 V step

Lower curve -1.9 V to -2.35 V step

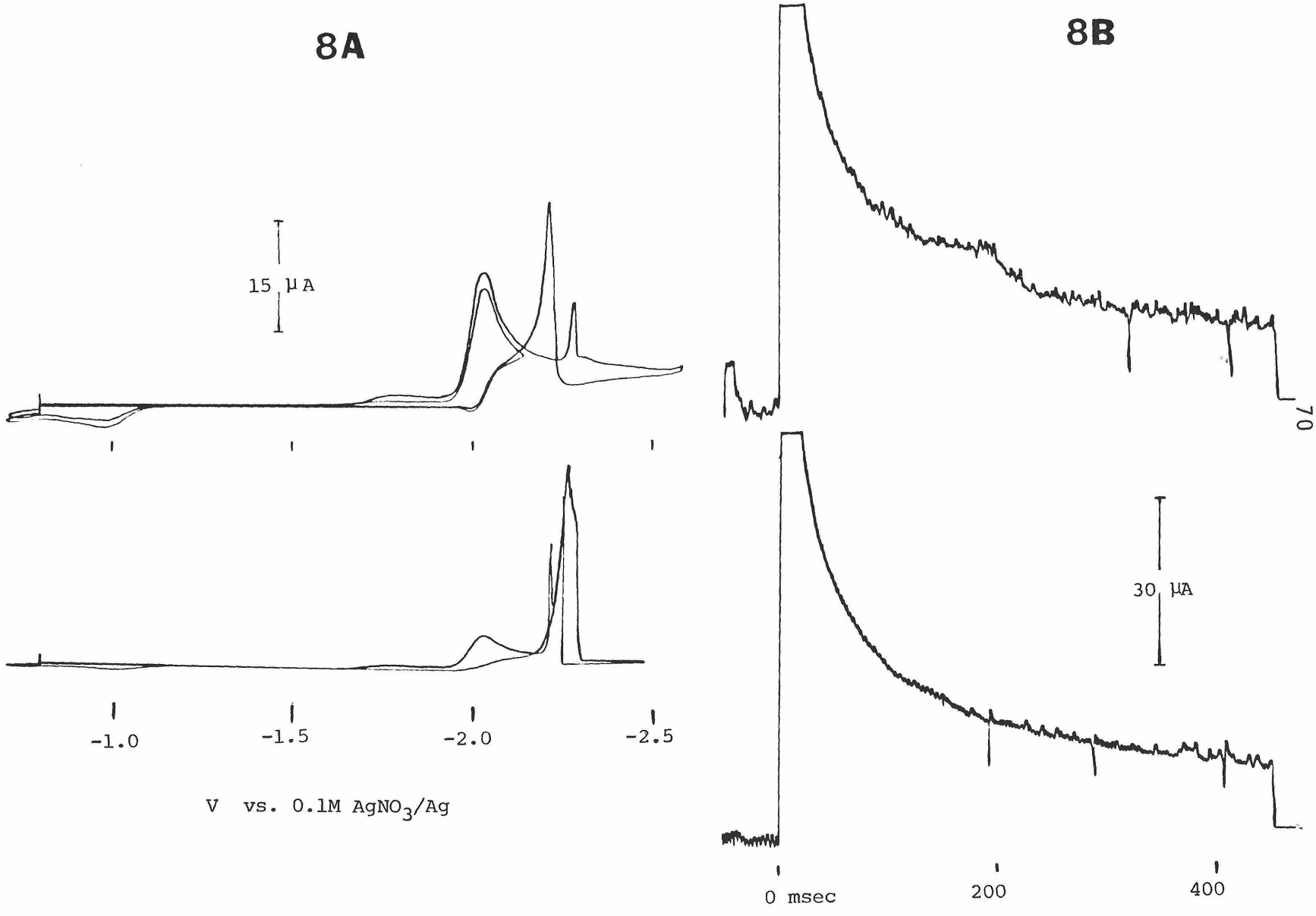
8A
15 μA
-1.0
-1.5
-2.0
-2.5
V vs. 0.1M $AgNO_3$/Ag
8B
70
30 μA
0 msec
200
400

peared in Normal Pulse (N.P.) polarography and potential step measurements when the potential step was increased past -2.3 V. One possible explanation is a rapid change in the mercury surface tension caused by interaction of the $Rh(DPM)_2^+$ with the mercury leading to a stirring of the solution. This stirring action will bring fresh $Rh(DPM)_2^+$ from the bulk solution giving a reduction spike and a second one on the reverse anodic scan.

Measurements of D_o by chronoamperometry for $Rh(DPM)_2^+$ were more critical because the cyclic voltammetric method could not be used. The time window of the chronoamperometric potential step was shorter than that for the cyclic voltammetric scans. Since the following chemical reaction is slow, the chronoamperometric technique could "beat out" the following chemical reaction in the same fashion that very fast cyclic voltammograms will. If the following chemical reaction was an attack of the reduced species on the starting material and the reaction was fast, the chronoamperometric current would decrease faster than expected for a simple electron transfer. Figure 7B displays the plot of i vs. $t^{1/2}$ for a potential step from -1.9 V to -2.30 V. The plot is a straight line that passes through the origin. The diffusion coefficient obtained from this plot was 9.14×10^{-6} cm^2/sec. The diffusion coefficient using the same solution but with a platinum electrode was 9.7×10^{-6} cm^2/sec. The diffusion coefficient using the same solution but with a platinum electrode was 9.7×10^{-6} cm^2/sec. These values were calculated assuming a two-electron process. The numbers are similar to the D_o values obtained for the cobalt and other rhodium complexes. Figure 8B shows the raw

current-time data for the step from -1.9 V to -2.3 V. This corresponds to a step 250 mV past the cyclic voltammetric peak. Steps to -2.20 V and -2.30 V gave virtually identical current decay curves. Interestingly if the step is -1.9 V to -2.35 V the current-time curve has a reproducible "bump" at ca. 175 ms (Figure 8B). The potential dependence of this bump is probably related to the spike and wrong wave of the cyclic voltammograms. The time dependence of the bump supports the idea that the phenomenon is some active process such as mercury surface tension changes rather than a reactant adorption spike.

2. Polarography.

A d.c. polarogram of $Rh(DPM)_2^+$ (Figure 9A) contained one single well defined wave with $E_{1/2}$ = 2.045 V. A plot of i vs. (Ht. Hg)$^{1/2}$ (Figure 9B) gave a straight line indicating a diffusion controlled process. A logarithmic analysis was performed on the wave obtained at 30 cm Hg. A straight line resulted (Figure 9C). The slope of the Tomes plot was 38.1 mV. For a reversible process the slope should equal 59.1 mV when n = 1 or 30 mV when n = 2. For an irreversible process the slope is equal to $(54.2/n_{alpha})$ mV. If n = 2 and alpha is assumed to be 0.5 (not always a proper assumption) the slope is 27 mV. Normal pulse polarograms were recorded with 0.5 sec and 1.0 sec drop times. The forward to reverse current ratios were 1.24 and 1.97 respectively indicating that the reduction is not totally irreversible. The differential pulse polarograms with a pulse height of 25 mV revealed a single peak, with peak width at half peak height equal to 75 mV. Though this value

FIGURE 9

A. Tast Polarogram of 2.55 mM $Rh(DPM)_2^+$ at 30 cm Hg Ht.

B. Plot of i vs. $(Ht.\ Hg)^{1/2}$ for 2.55 mM $Rh(DPM)_2^+$

C. Tomes Plot of 2.55 mM $Rh(DPM)_2^+$ at 30 cm Hg Ht.

D. Normal Tast Polarogram for 2.55 mM $Rh(DPM)_2^+$ at 30 cm Hg Ht.

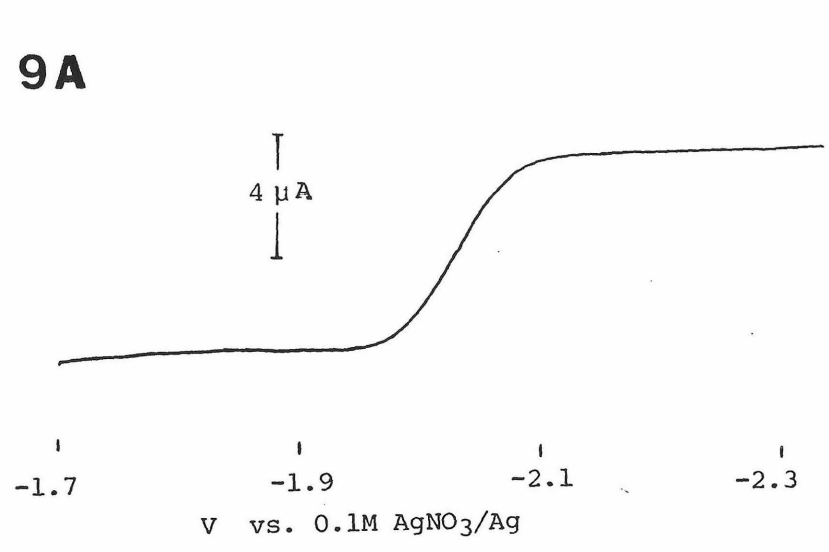
9A
4 μA
-1.7
-1.9
-2.1
-2.3
V vs. 0.1M AgNO3/Ag

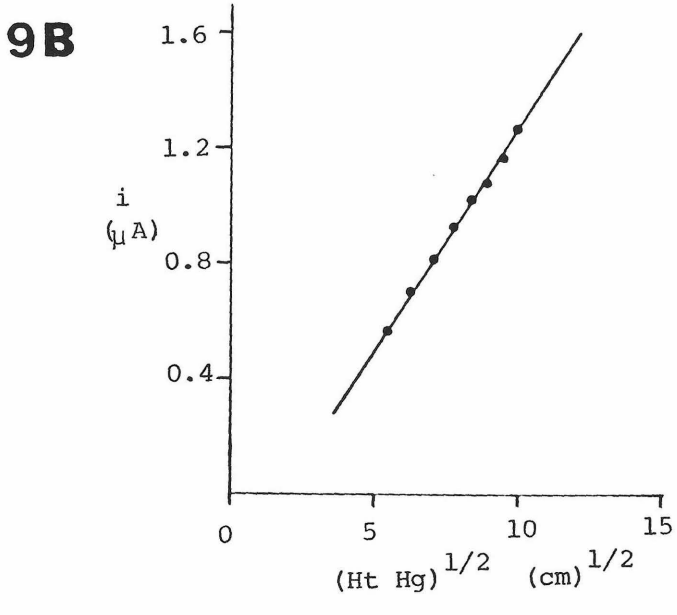
9B
1.6
1.2
i
(μA)
0.8
0.4
0
5
10
15
(Ht Hg)1/2 (cm)1/2

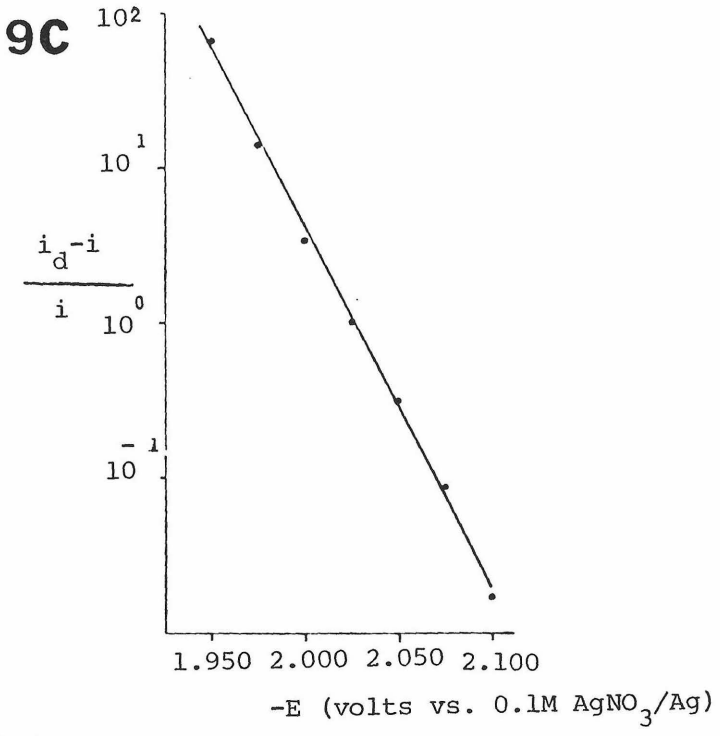
9C
10²
10¹
id-i
i
10⁰
10⁻¹
1.950 2.000 2.050 2.100
-E (volts vs. 0.1M AgNO3/Ag)

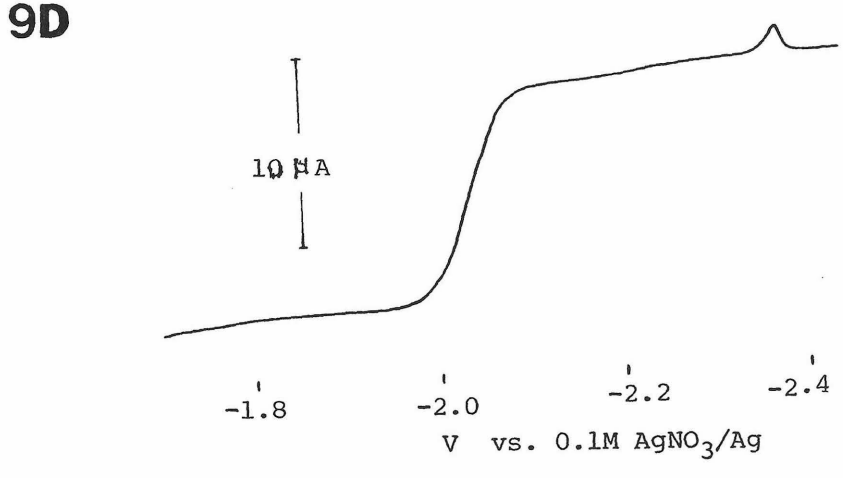
9D
10 μA
-1.8
-2.0
-2.2
-2.4
V vs. 0.1M AgNO3/Ag

is larger than the value expected for a theoretical two-electron wave, it is much smaller than the values of 120 mV obtained for the real one-electron waves.

The normal pulse polarogram (Figure 9D) at more negative potentials (-2.375 V) exhibited a small bump which resembled a differential pulse peak. The differential pulse polarograms showed no such features. The extraneous peak is probably related to the distorted chronoamperometric current transient. This feature had previously appeared in the cyclic voltammograms and was attributed to stirring caused by mercury surface tension changes.

F.-$Rh(VPE)_2^+$

1. Cyclic Voltammetry and Chronoamperometry.

Millimolar solutions of $Rh(VPE)_2^+$ exhibited a single well developed cathodic wave at $E_{1/2}$ = -1.952 V (vs. 0.1 M $AgNO_3$/Ag). Figure 10A allows a comparison between the wave for the rhodium complex and the wave for anthracene. The anthracene wave has a peak splitting of 60 - 75 mV while the wave for the inorganic complex has a peak splitting of 33 - 40 mV (Table 6). This result is in strong contrast with the value of 60 mV reported by Pilloni et al. (19). Only at very high scan rates of v = 5 V/sec does the peak splitting begin to increase, possibly due to electrode kinetic effects. Plots of ip^c vs. $v^{1/2}$ for several experiments gave straight lines which passed through the origin (Figure 10B). The average of several experiments yielded D_o = 6.2 x 10^{-6} cm^2/sec.

The chronoamperometric data for $Rh(VPE)_2^+$ were straightforward and facile to analyze. The potential was stepped over the wave from -1.8 V to -2.2 V. The current was then replotted against $t^{-1/2}$, giving a straight line that passed through the origin. The D_o determined from the slope of the plot was 9.49 x 10^{-6} cm^2/sec. This compares favorably with the cyclic voltammetric values. In both cases the assumption was a two-electron reduction process.

2. Polarography.

The polarographic results for $Rh(VPE)_2^+$ were in many ways very

FIGURE 10

A. Cyclic Voltammogram of 1.53 mM $Rh(VPE)_2^+$

   v = 400 mV/sec

B. Plot of ip^c vs. $v^{1/2}$

   Anthracene and $Rh(VPE)_2^+$

C. Tast Polarogram of 1.7 mM $Rh(VPE)_2^+$ at 30 cm Hg Ht.

D. Tomes Plot of 1.7 mM $Rh(VPE)_2^+$ at 30 cm Hg Ht.

10A

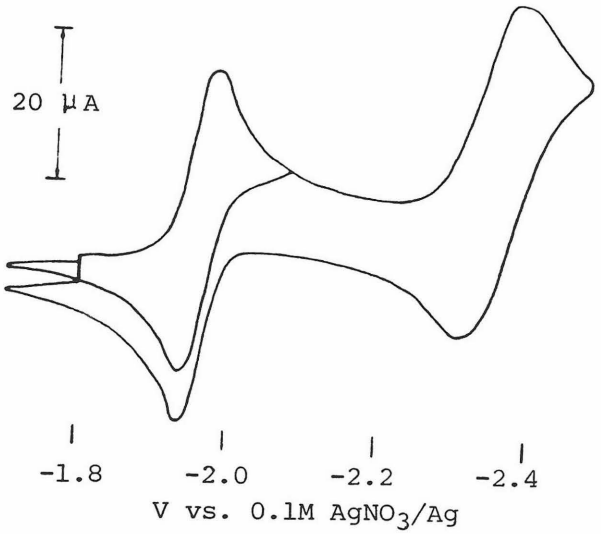

10B

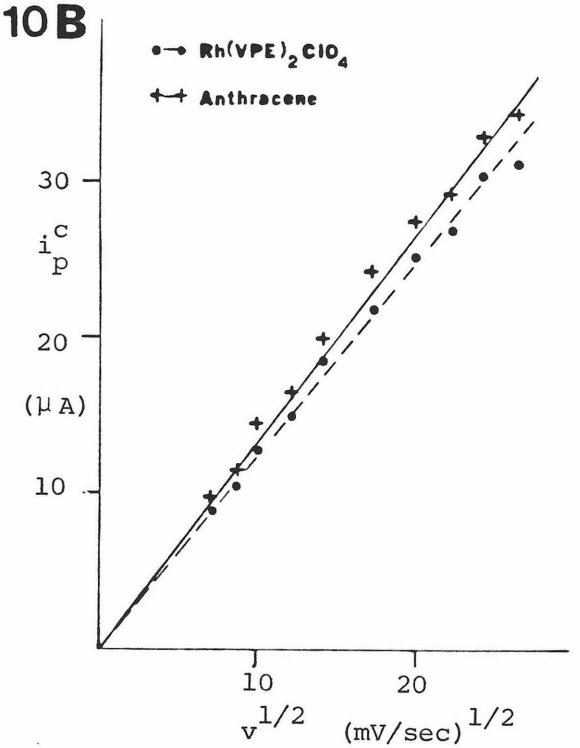

10C

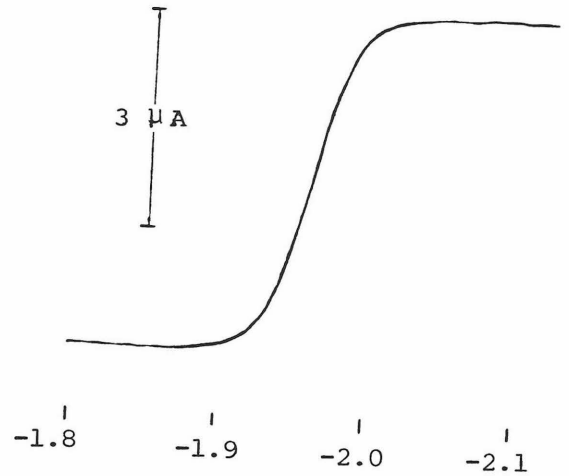

10D

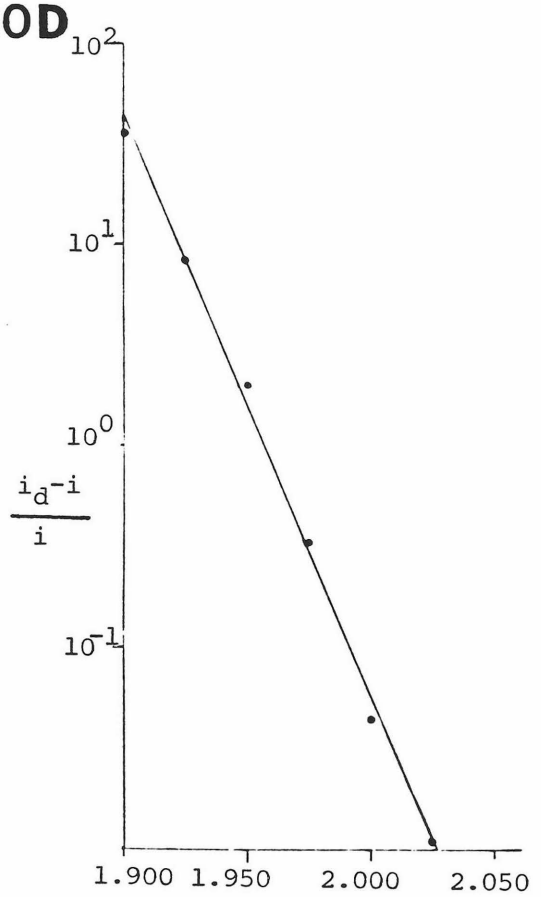

similar to those obtained for $Rh(DPE)_2^+$. There was a single polarographic wave, $E_{1/2}$ = -1.950 V (vs. 0.1 M $AgNO_3$/Ag) (Figure 10C). The current dependence with $(Ht.\ Hg)^{1/2}$ was linear for this wave. The I value obtained was 4.2 which compares well with that obtained for $Rh(DPE)_2^+$. A Tomes plot of the wave (Figure 10D) gave a slope of 28.5 mV. Normal pulse polarograms were recorded at 0.5 sec and 1.0 sec drop times. The ratios of the forward to reverse currents were 1.17 and 1.24, respectively, suggesting a high degree of reversibility to the process. Differential pulse polarography was performed with three different step heights (5, 10, and 25 mV) and the E_w were 63 mV, 55 mV, and 63 mV respectively. These values are approaching the theoretical value of 45 mV and are much less than 120 mV values recorded earlier for the one-electron processes. These polarographic results are in agreement with previously published work and strongly support a reversible two-electron reduction.

G. $Rh(DPE)_2^+$

1. Cyclic Voltammetry and Chronoamperometry.

Millimolar solutions of the phosophine complexes showed one well developed cathodic wave on a HMDE. The wave was much more drawn out on a platinum working electrode with a large cathodic-anodic peak separation. Figure 11A shows a cyclic voltammogram with a HMDE of $Rh(DPE)_2^+$ and anthracene. There is one symmetric, well-shaped wave with a peak splitting of 60 mV; this is in contrast with the published results of Pilloni and Martelli (8) who reported an asymmetric wave with a peak splitting of 130 mV at a scan rate of 250 mV/sec. Table 7 summarizes the HMDE cyclic voltammetric data. In agreement with Eisenberg et al. (15) the peak splitting does increase from 40 mV at low scan rates to higher values at higher scan rates. However in the present study the peak splitting increased well past the maximum value reported by Eisenberg's group up to 200 mV at 50 V/sec. The peak splitting for anthracene in these solutions does not vary greatly suggesting that uncompensated resistance is not causing the peak splitting. Figure 11B shows a graph of ip^c vs. $v^{1/2}$ for both anthracene and $Rh(DPE)_2^+$. In the anthracene case there is a straight line that passes through zero. The line for $Rh(DPE)_2^+$ passes through the origin, however at higher scan rates it curves. This curvature is quite reproducible with $Rh(DPE)_2^+$ alone, with p-benzonquinone added or with anthracene added. There are several possible causes for this nonlinearity. One possibility, adsorption of the product, was dismissed by chronocoulometric studies which indicated

FIGURE 11

A. Cyclic Voltammogram of 0.6 mM $Rh(DPE)_2^+$ and 1.8 mM Anthracene
   v = 150 mV/sec

B. Plot of i_p^c vs. $v^{1/2}$ for $Rh(DPE)_2^+$ and Anthracene

C. Tast Polarogram for 1.0 mM $Rh(DPE)_2^+$

D. i vs. $(Ht.\ Hg)^{1/2}$ for $Rh(DPE)_2^+$

11 A

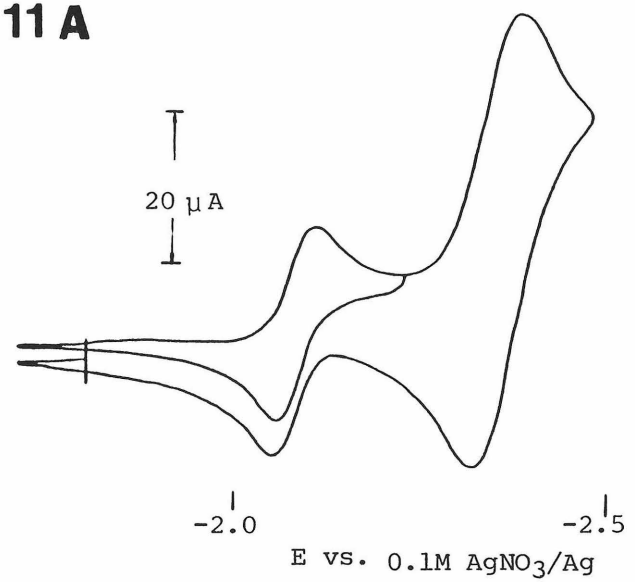

11B

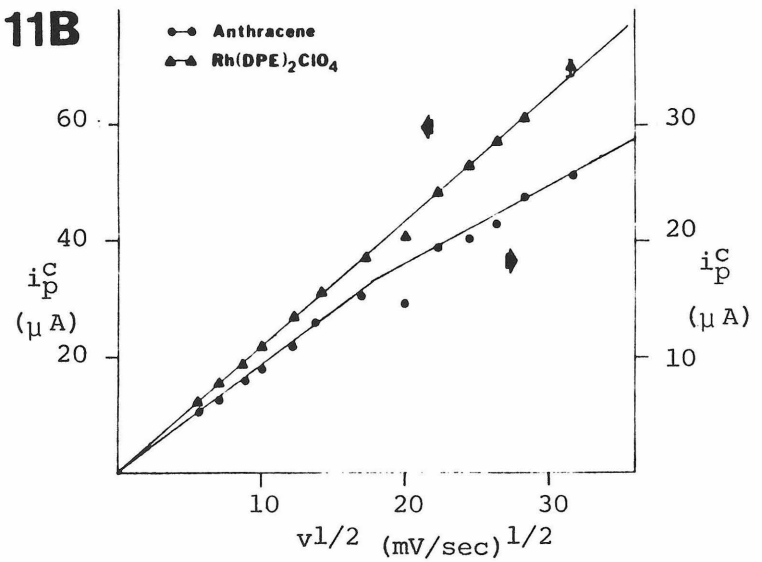

11C

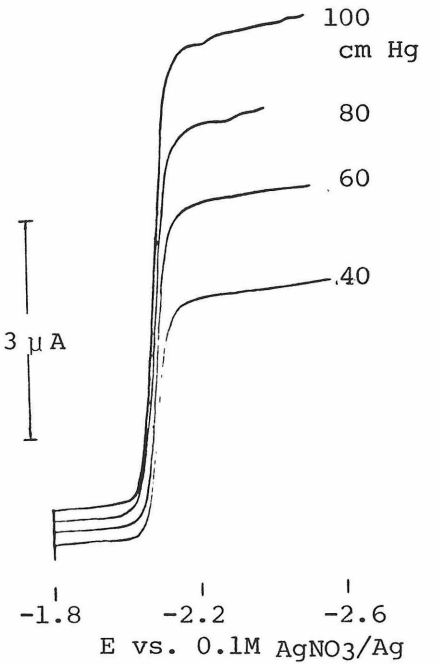

11D

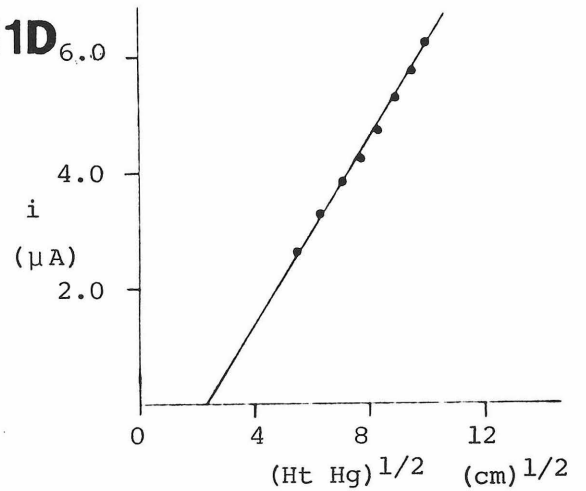

little or no adsorption. The other possibility which agrees with the cyclic voltammetric peak splittings is a two electron-reduction with slow electrode kinetics (a low k_s value). When k_s is low enough the wave makes a transition from purely reversible diffusion control to totally irreversible kinetic control and here the line bends over in the intermediate quasi-reversible area (44). The slope obtained from the line close to the origin gave a D_o value of 6.2×10^{-6} cm^2/sec while the anthracene gave the expected value of 3.1×10^{-5} cm^2/sec. Other values obtained at different concentrations were 8.1×10^{-6} and 6.2×10^{-6} cm^2/sec (Table 9A). However even this number for $Rh(DPE)_2^+$ may not be valid because with the low k_s value measured, ip^c vs. $v^{1/2}$ should show nonlinearity at scan rates lower than are experimentally possible (48).

Since the cyclic voltammetric study indicated that the reduction of $Rh(DPE)_2^+$ was quasi-reversible care had to be taken with the chronoamperometric measurement. The potential had to be stepped well past $E_{1/2}$, so that diffusion rather than electrode kinetics was the limiting factor controlling concentration of the reducible material at the electrode surface. For $Rh(DPE)_2^+$ this was accomplished by stepping 200 mV to 250 mV past the Ep^c. The i vs. $t^{-1/2}$ plot gave a straight line that passed through the origin. The D_o value obtained from the slope was 9.7(3) x 10^{-6} cm^2/sec.

2. Polarography.

A d.c. polarogram revealed a single well developed wave, $E_{1/2}$ = -2.070. This value agrees with the $E_{1/2}$ value obtained from cyclic

voltammetry. This wave gives an I value of 4.1 which compares favorably with the reported I value of 4.3. The recorded Tast polarograms are displayed in Figure 11C. A plot of i vs. (Ht. Hg)$^{1/2}$ shows a very slight curvature but this may be within the limits of experimental error (Figure 11D). The Tomes criterion for reversibility was 30(3) mV. This also is in agreement with the previously published polarography where a logarithmic analysis had been performed on the wave shape to get a slope of 33 mV. In both cases the value is slightly larger than expected for the type of analysis employed. Two differential pulse polarograms were recorded. The peak widths at half height were 70 mV for 10 mV pulse amplitude and 90 mV for 25 mV pulse amplitude. These values are larger than expected even for actual two electron waves seen previously. However differential pulse polarography is a much faster technique than d.c. polarography and at the step times involved heterogeneous electron transfer kinetics is involved and the peak is broadened. This effect is also visible in staircase voltammetry where the peak splitting is much larger than the peak splitting at comparable cyclic voltammetric scan rates.

H. $Rh(DPP)_2^+$

1. Cyclic Voltammetry and Chronoamperometry.

A 0.88 mM $Rh(DPP)_2^+$ solution was examined with 1.1 mM added anthracene. The rhodium phosphine exhibited a single well developed wave $E_{1/2}$ = -1.785 V (vs. 0.1 M $AgNO_3$/Ag) (Figure 12A). In this case the CV wave was much broader and more similar in shape ($E_p - E_{p1/2}$) to anthracene than either $Rh(VPE)_2^+$ or $Rh(DPE)_2^+$ at slow scan rates. Table 8 allows a further comparison between the phosphine complex and anthracene. In both cases the ratio ip^a/ip^c is nearly 1.0. The anodic-cathodic peak splitting for the anthracene ranges from 60 - 75 mV as it should for a one-electron reduction. The rhodium values, however, are visibly and consistently smaller than the anthracene values. At the same time the values are larger than those found for $Rh(VPE)_2^+$ where a simple two-electron transfer is suspected. A plot of ip^c vs. $v^{1/2}$ (Figure 12B) consists of a straight line which passes through the origin. The slope of this line gives a D_o value of 4.2×10^{-6} cm^2/sec while anthracene yielded $D_o = 2.2 \times 10^{-5}$ cm^2/sec assuming two electrons for the rhodium and one for the anthracene. The experiment was repeated giving a D_o = 4.9×10^{-6} cm^2/sec to 3.9×10^{-5} cm^2/sec, which is considerably too large for this complex. The drastic shift in D_o is due to the fact that n appears as $n^{3/2}$ in the Randes-Sevcik equation. This large ΔE_p and the low D_o for a two-electron process suggest that the electron process may be more aptly described as two one-electron reductions which are close together. The waves are so close together that they are not resolved

FIGURE 12

A. Cyclic Voltammogram of 0.88 mM $Rh(DPP)_2^+$ and 1.1 mM nAnthracene
v = 300 mV/sec

B. Plot of ip^c vs. $v^{1/2}$ for $Rh(DPP)_2^+$

C. Tast Polarogram of 0.86 mM $Rh(DPP)_2^+$

12A

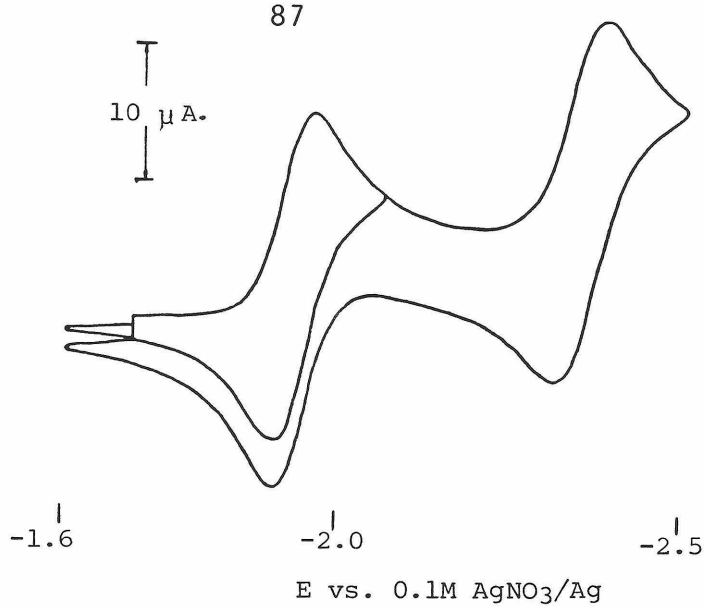
10 μA.
-1.6
-2.0
-2.5
E vs. 0.1M AgNO3/Ag

12B

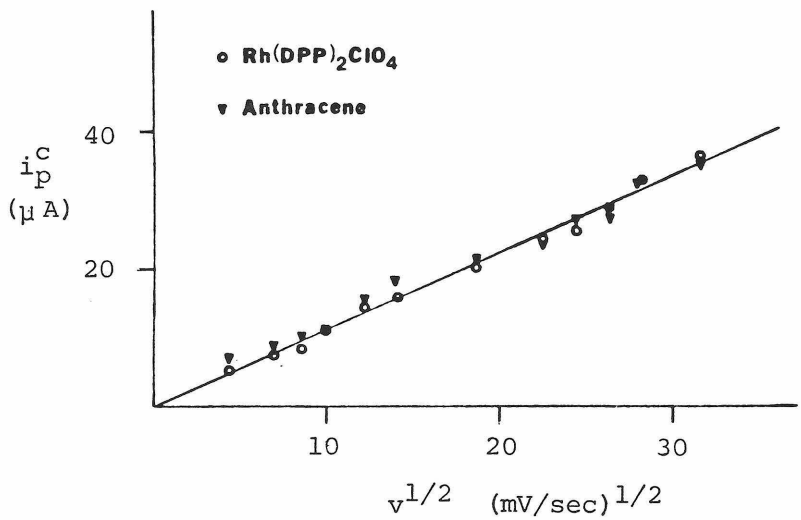
o Rh(DPP)2ClO4
▾ Anthracene
40
20
ip c
(μA)
10
20
30
v1/2 (mV/sec)1/2

12C

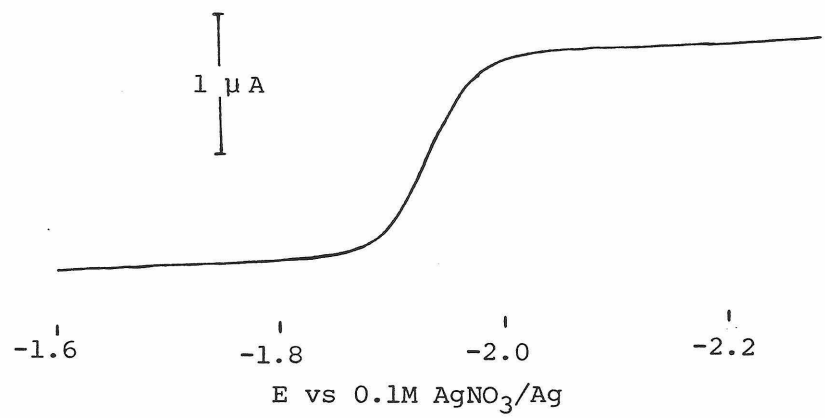
1 μA
-1.6
-1.8
-2.0
-2.2
E vs 0.1M AgNO3/Ag

into individual waves. Polycyn and Shain mentioned that in these situations current values will be obtained that are in-between one-electron currents and two-electron currents (49). Recently, Richardson and Taube expanded Polycyn and Shain's calculations and published working curves (50). In one case they plotted the separation of the two $E_{1/2}$ values as a function of anodic-cathodic peak splitting. When the peak splitting is 30 mV as in the case of $Rh(VPE)_2^+$, the $E_{1/2}$ of the second wave is anodic of the first wave by 180 mV. In other words, the second electron is easier to add to the molecule than the first. In the present case the peak splitting is most probably in the range of 45 - 50 mV. The corresponding value from the curve is +10 mV to +30 mV indicating the second reduction potential is cathodic of the first. Both sets of workers indicate that during the collapse of two one-electron waves into a single two-electron wave the current function is very complicated. In the Polycyn and Shain paper when $E_{1/2}^1 - E_{1/2}^2$ is 0 mV the accompanying diagram shows a peak current which is approximately twice a one-electron wave. In the more precise Richardson and Taube tabulation when $E_{1/2}$ is 30 mV to 40 mV the current expected will be approximately twice a one-electron current. Although this is a crude method the D_o obtained by treating the wave in this fashion (two one-electron waves) gives D_o = 9.8×10^{-6} cm^2/sec. This value more closely agrees with diffusion coefficients obtained for the other complexes.

For a 0.86 mM $Rh(DPP)_2^+$ solution the potential was stepped from -0.8 V to -2.2 V. The chronoamperometric curve looked normal and the i vs. $t^{-1/2}$ plot consists of a straight line. The slope from the plot

converted into a D_o value of 9.5 x 10^{-6} cm^2/sec. This value is closer to the 2 x 1-electron value of a D_o by cyclic voltammetry than the one-electron or two-electron values. This lends credence to the current approximations and formal potential separations developed for the cyclic voltammetric results.

2. Polarography

A 0.86 mM solution of $Rh(DPP)_2^+$ gave a single wave with $E_{1/2}$ = -1.935 V (vs. 0.1 M $AgNO_3$/Ag) (Figure 12C). This wave has an I value of 3.8. The $E_{3/4} - E_{1/4}$ value is 40 mV. The plot of i vs. $(Ht. Hg)^{1/2}$ is a straight line indicative of a diffusion controlled process. The forward and reverse normal pulse polarograms with drop times of 0.5 seconds and 1.0 seconds were recorded. The ratios of the current were 1.14 and 1.05 respectively. The differential pulse polarograms were measured with 5 mV, 10mV, and 25 mV modulation amplitudes. The peak widths at half current maximum were found to be 90 mV, 95 mV, and 90 mV. Using the working curve published by Richardson and Taube (50), the second reduction is estimated to be 10 mV to 20 mV more negative than the first reduction. This value is comparable to that obtained by cyclic voltammetry.

I. $Rh(DPB)_2^+$

1. Cyclic Voltammetry and Chronoamperometry.

$Rh(DPB)_2^+$ solutions proved to be the only ones which could not be studied effectively with a HMDE but necessitated the use of a platinum working electrode. This is evident in Figure 13A. The first wave is due to the rhodium complex and the one at more cathodic potentials is due to the anthracene. A scan with a fresh mercury drop will never be reproduced with the same shape on that drop again. The complex also influences the shape of the anthracene wave as in Figure 13A. Bulk electrolysis evidence (see Chapter V) suggests that the distortion is due to passivating film formation on the mercury which breaks down once the potential becomes negative enough.

On a platinum electrode (Figure 13B) two waves are visible at Ep^c = -1.94 V and Ep^c = ca. -2.020 V (vs. 0.1 M $AgNO_3$/Ag). The first wave appears to be reversible with a peak splitting of ca. 90 mV. There is no peak potential shift with increasing scan rates. The second peak is irreversible and shows no anodic components even at high scan rates. It is impossible to tell if the second reduction peak shifts with scan range changes because the second peak is irreproducible from scan to scan. Due to the unusual shapes of the waves no attempt was made to measure a diffusion coefficient from cyclic voltammetric data.

Since the cyclic voltammograms for $Rh(DPB)_2^+$ were irreversible and showed a strong mercury interaction, chronoamperometric methods with a platinum electrode were the sole recourse. The two waves for $Rh(DPB)_2^+$

FIGURE 13

A. Cyclic Voltammogram of

0.52 mM $Rh(DPB)_2^+$ and 1.6 mM Anthracene

HMDE: 200 mV/sec

B. Cyclic Voltammogram of 1.4 mM $Rh(DPB)_2^+$

Platinum Electrode Area = 0.00375 cm^2

v = 350 mV/sec

C. Tast Polarogram of 1.4 mM $Rh(DPB)_2^+$ at 80 cm Hg Ht.

13A

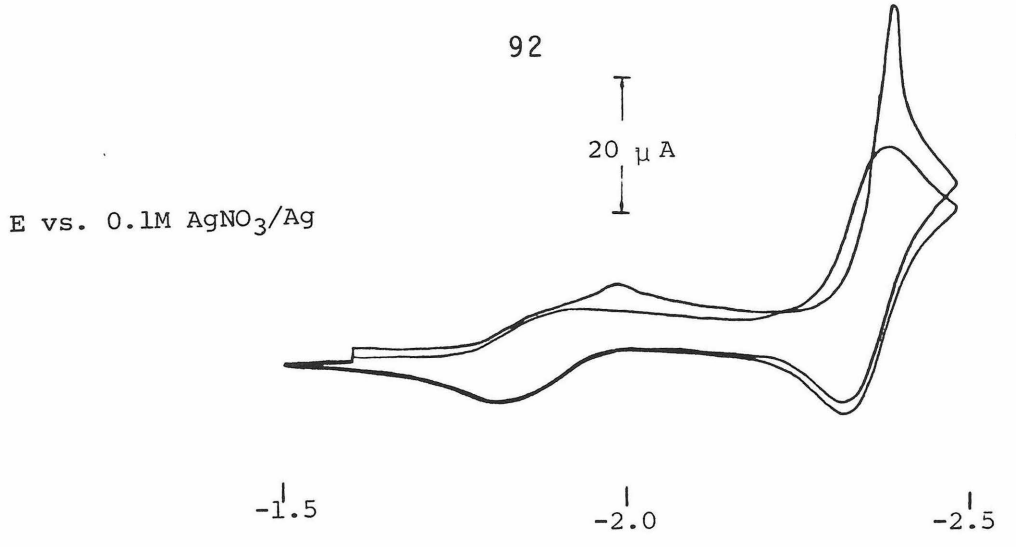

13B

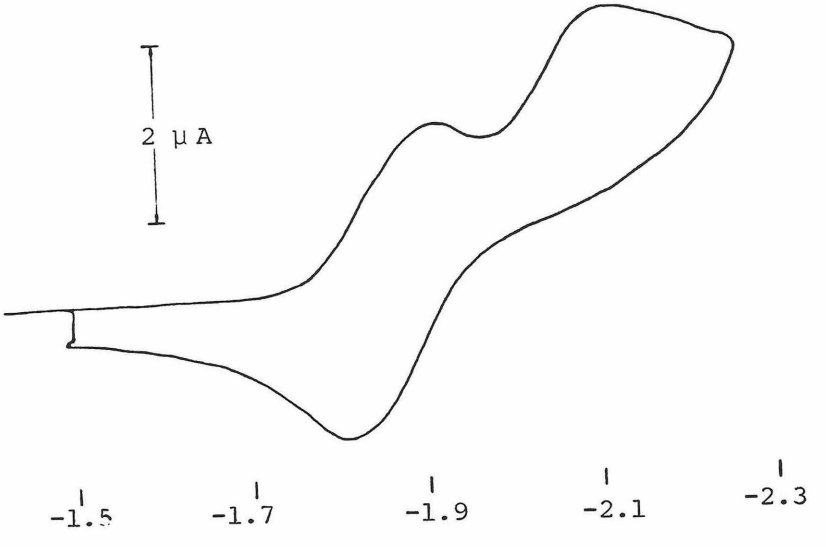

13C

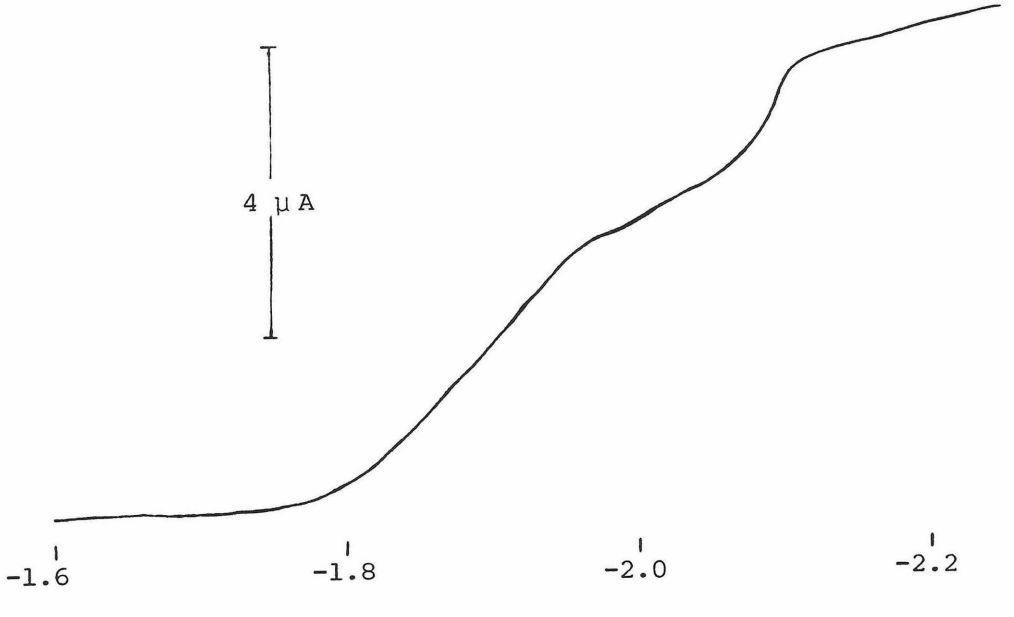

were juxtaposed too close to be able to step between them and get one electron diffusion current values. The potential was stepped over both waves from -1.7 V to -2.350 V. The chronoamperometric curve looked normal and the i vs. $t^{-1/2}$ plot consisted of a straight line passing through the origin. The slope of the plotted data gave a D_o value of 1.1 x 10^{-5} cm^2/sec, assuming a two-electron reduction. Interestingly, when a HMDE was used the chronoamperometric curve looked normal. Unlike the cyclic voltammograms a second scan on the same mercury drop looked the same as the first though the current was slightly lower. The i vs. $t^{-1/2}$ plot of the HMDE data consists of a straight line that passes through the origin. The slope of this plot gave a D_o value of 7.0 x 10^{-6} c m ^{2}/sec.

2. Polarography.

The polarograms obtained with $Rh(DPB)_2^+$ were little more useful than the data collected by cyclic voltammetry on the HMDE. The polarograms exhibited two very broad and distorted waves $E_{1/2}$ = ca. -1.900 V and $E_{1/2}$ = ca. -2.075 V (Figure 13C). The I value estimated for the first wave was 2.0 while the value for both waves was 4.1. The plots of current vs. square root of mercury column height gave straight lines. The waves were very broad and gave $E_{3/4}$ - $E_{1/4}$ values of 90 and ca. 40 - 50 mV. The forward normal pulse polarogram displayed three closely spaced waves, while the reverse scan displayed two broad waves. The current ratio i_f/i_r was approximately 1.5 - 2.0 for a two second drop time. The scan just over the first two waves had a single wave on the

return scan. In this case the cathodic to anodic scan current ratio was also approximately 2.0. The differential pulse polarogram had what was either a very broad peak (half width ca. 200 mV) with two shoulders or three broad overlapping peaks.

These polarographic results are difficult to interpret because they are so complex. Certainly an important factor must be the large interaction $Rh(DPB)_2^+$ must have with mercury. The d.c. polarographic data and I value do suggest that a two-electron process is occurring but the exact nature of the process is not obvious.

J. A COMPARISON OF CYCLIC VOLTAMMETRIC, CHRONOAMPEROMETRIC AND POLAROGRAPHIC RESULTS

The chronoamperometric data has been summarized in Table 9A. Since the cobalt and rhodium complexes have similar ligands and charges it was expected that their diffusion coefficients would be similar. The values for the cobalt complexes were evaluated from the Cottrell equation assuming a one-electron process. The n values for the rhodium complexes were then estimated by choosing the integer value (1 or 2) that gave D_o values for the rhodium complexes close to the D_o value of the cobalt complexes. The cobalt complexes had D_o values that ranged from 1.2×10^{-5} cm^2/sec to 1.4×10^{-5} cm^2/sec. The substitution of DPE for VPE made little difference. The rhodium complexes had diffusion coefficients which ranged from 9.1×10^{-6} cm^2/sec for $Rh(DPM)_2^+$ to 1.1×10^{-5} cm^2/sec for $Rh(DPB)_2^+$ These D_o values for the rhodium complexes had been calculated assuming a two-electron process. If they had been calculated assuming a single-electron process they would have been unreasonably large.

The polarographic I values are summarized in Table 9C. The I values of the cobalt complexes were 2.2, typical for a single electron reduction. The rhodium values ranged from 3.5 to 4.2, typical values for a two-electron reduction (34). The polarographic I value for the first $Rh(DPB)_2^+$ wave was 2.0 and the value for both waves was 4.1.

The cyclic voltammetric peak splittings proved to be good indicators of the n values for the electrode process. These values have been summarized on Table 9B. The values measured were all larger than the theoretical values but they were internally consistent. The cobalt complexes exhibited normal looking single-electron waves. The peak

splittings were of the same magnitude as those of anthracene. The rhodium complexes exhibited smaller peak splittings in accordance with a two-electron transfer. The $Rh(VPE)_2^+$ values ranged from 30 to 40 mV. The 29 mV Tomes plot slope for the $Rh(VPE)_2^+$ polarographic wave supports a two electron process. The $Rh(DPM)_2^+$ peak splittings at high scan rates where an anodic component was detectable were about 45 mV. This is considerably less than the CV peak splitting values for the cobalt complexes but more than the $Rh(VPE)_2^+$ peak splitting values. However, at the high scan rates necessary to detect the anodic current several factors may be contributing to the peak splitting (uncompensated resistance, slow electrode kinetics). The $Rh(DPP)_2^+$ peak splittings values are decidedly larger than the $Rh(VPE)_2^+$ values, but both of these values are considerably smaller than the cobalt or anthracene values. This has been explained by fitting the cyclic voltammetric value and the differential pulse peak width value to the working curve given by Richardson and Taube (50). For $Rh(VPE)_2^+$ the potential for the second electrochemical charge transfer is anodic to the first (causing the current characteristics of a two-electron wave), whereas for $Rh(DPP)_2^+$ it is cathodic to the first by 10 - 30 mV. This 10 - 30 mV spacing is too close to resolve the electron transfers into separate waves which appear as a single broad wave. With $Rh(DPB)_2^+$ this separation of the two electrochemical charge transfer potentials has increased to the point where the cyclic voltammogram has two resolvable one-electron waves.

The differential pulse peak widths also helped assign the n values of the electrode processes. However, the experimentally measured values

were larger than the theoretical values. Information can be gained from the relative values. The W_p values measured for anthracene ranged from 110 to 130 mV for the one electron process. The W_p values for the rhodium complexes ranged from 55 mV for $Rh(VPE)_2^+$ to 95 mV for $Rh(DPP)_2^+$. The W_p values for the $Rh(DPB)_2^+$ complex were not valid because of the large distortions caused by rhodium complex-mercury interaction. With the exception of $Rh(DPB)_2^+$ the W_p values for the rhodium complexes are clearly smaller than the W_p values for the cobalt complexes indicating an electrode process that was greater than a single-electron process.

The $Rh(DPE)_2^+$ complex is more comprehensible when examined as part of the cobalt and rhodium series. The polarographic and chronoamperometric D_o values place the complex in the middle of the series as a two-electron reduction. The $Rh(DPE)_2^+$ cyclic voltammetric peak splitting behavior is very similar to the quasi-reversible behavior seen for the second reduction of p-benzoquinone. Pilloni and Martelli (18) did not note this behavior. Sofranko et al. (15) observed the peak splittings but misinterpreted their meaning. Although not included in the text of this work, cyclic voltammetry and chronoamperometry were also used to measure the heterogeneous electron rate of $Rh(DPE)_2^+$. Appendix I contains a simplified discussion of electrode kinetics and the experimental details of the measurements. Using cyclic voltammetry the heterogeneous electron transfer rate constant k° for $Rh(DPE)_2^+$ was measured to be 0.0092 cm/sec. The value obtained by chronoamperometry was 0.0087(5) cm/sec.

IV. BULK ELECTROLYSIS

A. INTRODUCTION

Bulk electrolysis is a technique where each electroactive species in solution is brought to the electrode at a potential where electron transfer can occur. As the name implies this is a bulk technique rather than a sampling of the diffusion layer around the electrode. The bulk concentration during an electrolysis is given by $C(t) = C_o(0)\exp(-p)$ where p is related to various physical properties of the cell: electrode shape, electrode dimensions, cell design, and stirring rate. The current is given by a related equation $i(t) = i(0)\exp(-pt)$. For a simple electron transfer uncomplicated by chemical reaction a plot of the logarithm of the current vs. time should give a straight line. The integration of the current is carried out electronically and gives the number of coulombs passed. The number of coulombs passed coupled with the knowledge of the concentration allows the determination of the n value for the process. If chemical complications interfere the current time behavior may be modified. A summary of the technique and the various complications have been published by Bard and Santhanam (52).

In a typical experiment 10 ml of a 0.3 mM to 5 mM solution of complex was reduced in the cell shown in Figure 1. A potential was applied approximately 150 mV to 200 mV past the polarographic wave or cyclic voltammetric peak. The working electrode was typically mercury with a teflon stir bar on top.

B. ANTHRACENE

A 1.5 mM solution of anthracene was reduced at -2.5 V. After 1.0(1) equivalent of electrons had passed the current had leveled off at a value higher than background. The background at -2.5 V was considerably larger than the background at -2.1 or -2.2 V. This suggests that some impurity exists in the solution. The plot of log i vs. t gave a straight line (Figure 14A). After electrolysis a dark blue solution remained which slowly faded to yellow. A cyclic voltammogram soon after the end of the electrolysis showed only approximately 40% of the original wave. The level of current after passing one electron was higher than the background current.

Several facts must be considered. There could be some impurities in the solvent with which the radical reacted. The background at -2.5 V was considerably higher than that found at -2.0 V or -2.2 V suggesting a reducible material might exist in the solvent. At the completion of the experiment the stir bar had turned black possibly because it was attacked by the radical. However these results do not differ significantly from those of Santhanam and Bard who studied the reduction in dimethylformamide solution. They obtained a steady state situation and n values greater than 1.0 under several conditions (53). The anthracene radical is a very reactive species. However an irreversible, following chemical reaction does not change the ln (current) vs. time plot and a catalytic following reaction merely causes a higher final base line. These anthracene results indicate a single one-electron reduction to a

FIGURE 14

A. Plot of ln i vs. t for 1.5 mM anthracene electrolysis

B. Plot of ln i vs. t for 0.64 mM $Co(DPE)_2^+$

First reduction at -1.20 V

C. Plot of ln i vs. t for $Co(DPE)_2^{2+}$

Second Reduction

D. Cyclic Voltammogram of $Co(DPE)_2^0$ after second reduction

HMDE: 50 mV/sec

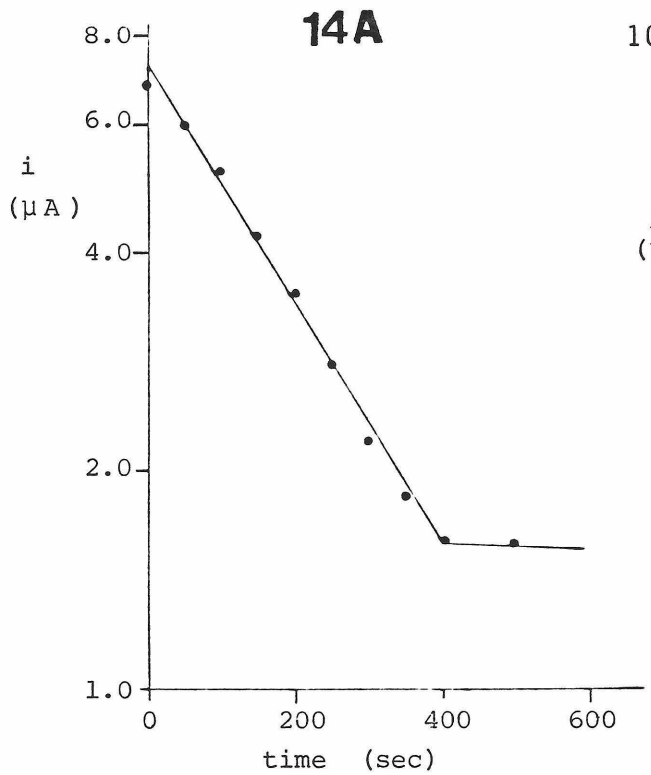
14A
8.0
6.0
i
(μA)
4.0
2.0
1.0
0
200
400
600
time (sec)

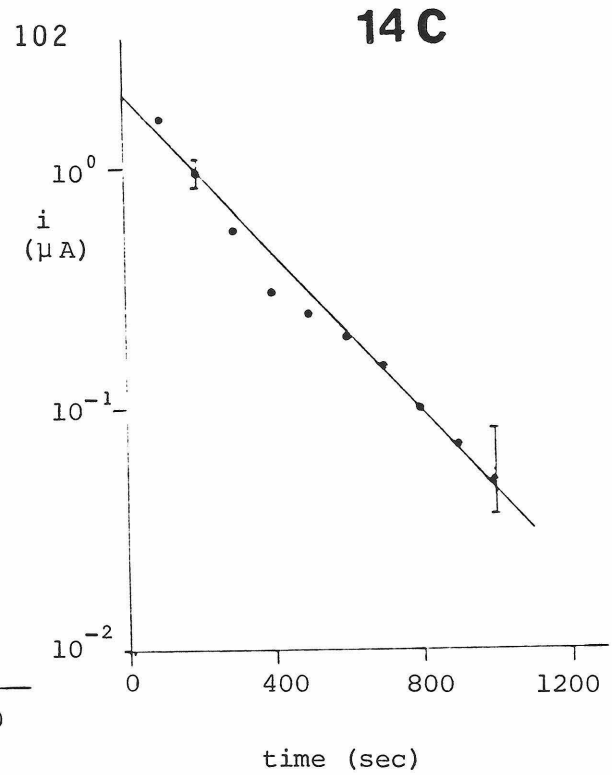
14C
102
10^0
i
(μA)
10^{-1}
10^{-2}
0
400
800
1200
time (sec)

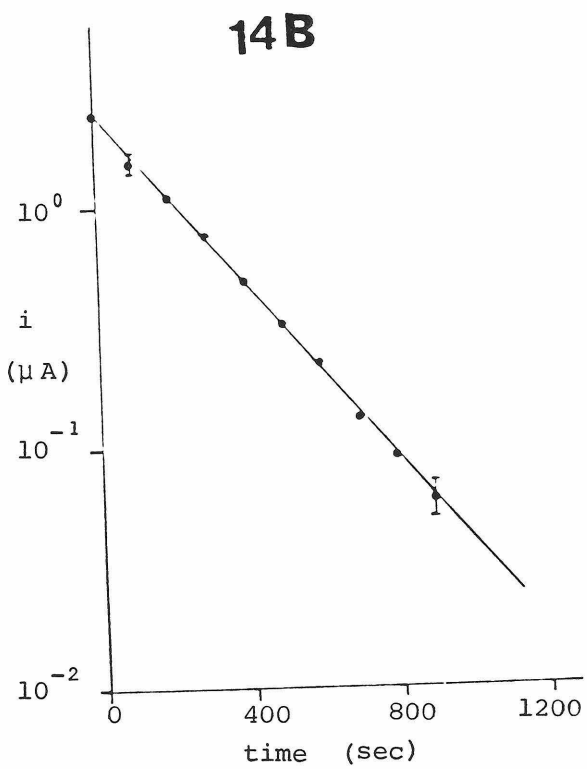
14B
10^0
i
(μA)
10^{-1}
10^{-2}
0
400
800
1200
time (sec)

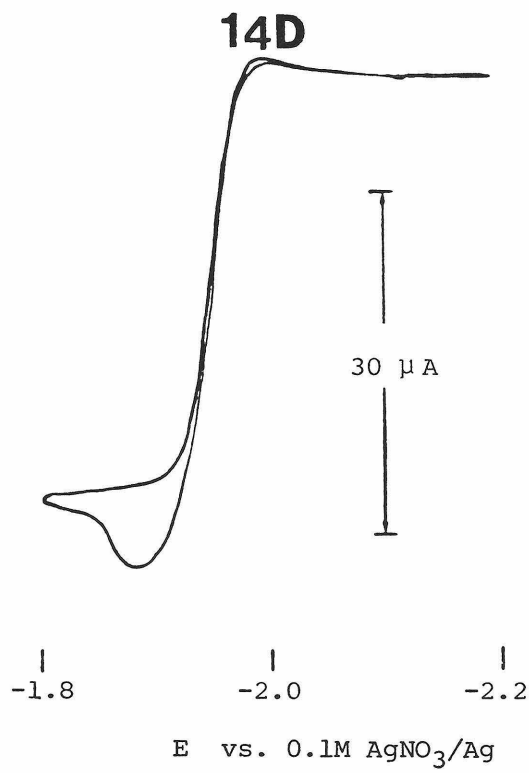
14D
30 μA
-1.8
-2.0
-2.2
E vs. 0.1M $AgNO_3$/Ag

radical anion which then slowly decomposes. The cyclic voltammetry agrees with the slow decomposition because the cathodic current ratios are close to 1.0 even at slow scan rates.

C. $Co(DPE)_2^{2+}$

A 0.64 mM solution of $Co(DPE)_2^{2+}$ was electrolysed at -1.2 V after preliminary cyclic voltammetric and chronoamperometric measurements. The plot of ln i vs. t is a straight line over 97% of the electrolysis time (Figure 14B). The reduction required 1.0(1) electrons to produce the dark colored solution. This solution was very stable and has in the past been made chemically. This was the starting oxidation state of materials used by Pilloni et al. (19). From this point potential step measurements and cyclic voltammetric measurements were made. A chronoamperometric measurement over the Co(I) - Co(0) wave gave D_o = 8.8 x 10^{-6} cm^2/sec while the cyclic voltammetric slope gave D_o = 1.4 x 10^{-5} cm^2/sec. The second reduction to $Co(DPE)_2^0$ required 1.0(1) electrons. The ln i vs. t plot was fairly linear but not as linear as for the first reduction (Figure 14C). No further chronoamperometric or cyclic voltammetric measurements were obtained because of the unusual complex mercury interaction (Figure 14D) in the cyclic voltammogram. The CV scan was from -2.2 V, scanning over the Co(0) - Co(I) wave. The unusual shape does not change with scan rate. The third reduction consumes ca. 1.0(1) electrons and the ln i vs. t plot is linear. After electrolysis the Co(-I) solution was removed from the cell and stored in a sealed vial in the dry box. Over a period of days the dark color was replaced by a bronze colored solution and a precipitate. The solution was filtered and the reddish-brown crystals obtained were washed with acetonitrile and dried. The crystals were found to be insoluble in acetonitrile,

toluene and benzene. A KBr pellet was prepared in the box pressed under vacuum and an I.R. spectrum was recorded. The spectrum agreed with that published by Sacco and Ugo for $HCo(DPE)_2$ (54). The Co-H stretch was at 1884 cm^{-1}. The electrolysis results agreed well with the results obtained by Sofranko (20). However, for the third reduction he observed that the current never reached background levels. He could pass up to n = 60 electrons concomitant with the solution undergoing several color changes. In light of this study a likely explanation is available: since the ultimate product is $HCo(DPE)_2$ there must be some solvent or electrolyte species being broken down to provide the proton. This breakdown will undoubtedly release bizzare reactive species which can react with $Co(DPE)_2^{-1}$ to give the low catalytic current.

D. $Co(VPE)_2^+$

A 0.66 mM solution of $Co(VPE)_2^{2+}$ was studied. The first reduction to $Co(VPE)_2^+$ was accomplished by setting the potential to -1.4 V and electrolyzing for ca. 10 minutes. The reduction required 1.0(1) electrons per cobalt unit. The ln i vs. t plot was a straight line (Figure 15A) for 95% of the reduction time. Once the stable dark-colored $Co(VPE)_2^+$ solution had been formed cyclic voltammetric and chronoamperometric measurements were made. The chronoamperometric value for D_o for the Co(I) - Co(0) transition was found to be 1.4×10^{-5} cm^2/sec while the CV value was found to be 1.07×10^{-5} cm^2/sec. The solution was then reduced one last time. The ln i vs. t plot (Figure 15B), though not as linear as for the first reduction, is reasonably so. The reduction required one electron to completion.

FIGURE 15

A. Plot of ln i vs. t for 0.64 mM $Co(VPE)_2^+$

First Reduction

B. Plot of ln i vs. t for $Co(VPE)_2^+$

Second Reduction

C. Plot of ln i vs. t for 2.55 mM $Rh(DPM)_2^+$

Bulk electrolysis

D. Cyclic Voltammogram of $Rh(DPM)_2^+$ after reduction

v = 200 mV/sec

15A

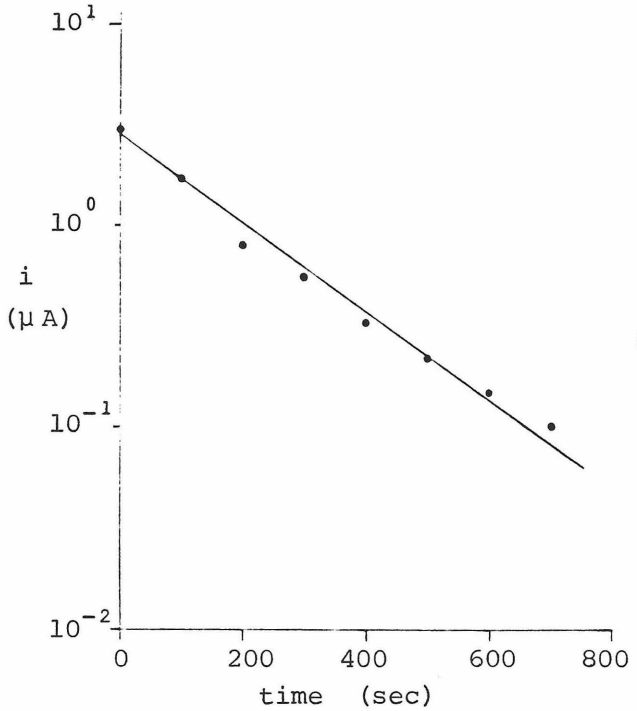

15B

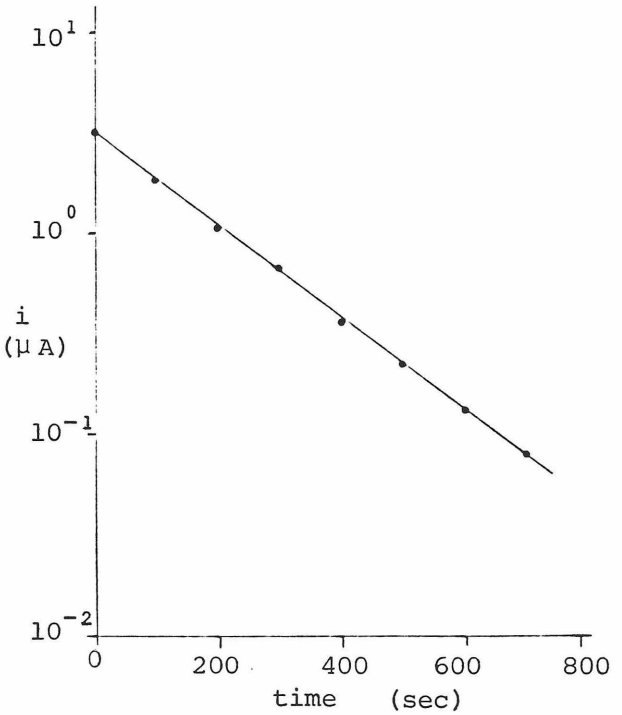

15C

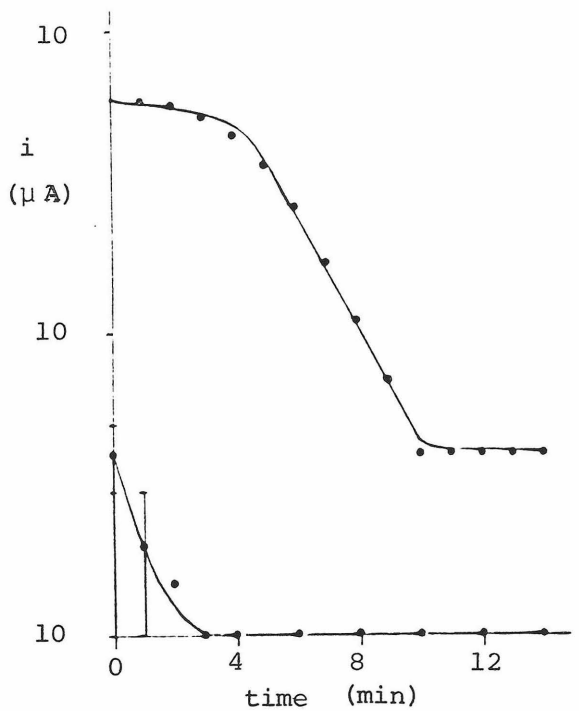

15D

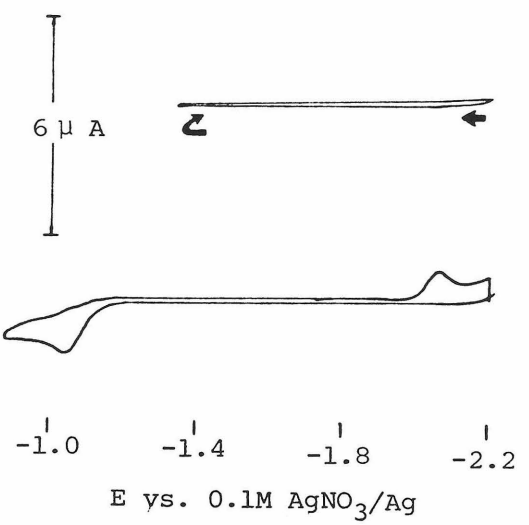

E. $Rh(DPM)_2^+$

A 2.55 mM solution of $Rh(DPM)_2^+$ was reduced at 2.2 V (vs. 0.1 M $AgNO_3/Ag$). In this case the ln i vs. t plot was not linear but was "S"-shaped (Figure 15C). At ca. 0.8 equivalents, the current began to drop such that ln i vs. t was linear. At about one equivalent the current leveled to a point considerably higher than the background. At this point a dark, red-brown precipitate formed. A cyclic voltammogram recorded at this point (Figure 15D) displayed none of the original cathodic wave. However, an irreversible anodic wave was visible. This wave was at the same potential as the small anodic "bump" found earlier in the initial irreversible cyclic voltammograms of the starting complex. By scanning over this wave and back, some of the original reduction wave returned. Scanning further past the anodic wave increased the size of the anodic wave. The fact that one electron was consumed by two rhodium atoms suggests that a rhodium dimer of some sort was formed. The cyclic voltammetric data indicate an initial two-electron reduction to a $Rh(DPM)_2^-$ species. This species may then attack the starting material leading to a Rh^0 - Rh^0 dimer. This would account for the net one-electron reduction. This dimer then oxidizes at -1.050 V regenerating the starting material. The solid was soluble in benzene and toluene, but insoluble in acetonitrile. The infrared spectrum was virtually identical with the starting material and no Rh-H was seen. The material was dissolved in toluene and acetonitrile was added until precipitation occurred. The precipitate was then filtered and allowed to dry. A

sample for NMR was also prepared using d_6-benzene. In contrast with the simple NMR for the starting material with two aromatic peaks and a methylene signal at 3.6 delta, the reduced species had four aromatic peaks, two methylene peaks at 3.3 and 3.8 delta, and also four new misshapen peaks between 0 and 1 (delta = .1, .2, .4, .8). No hydride resonances were found at negative values of delta. The splitting of the methylene peaks and the extra peaks suggest that the product is not a simple Rh^0 - Rh^0 dimer. The characterization of this product was not pursued further.

F. $Rh(DPE)_2^+$

A 0.90 mM solution of $Rh(DPE)_2^+$ was reduced at -2.2 V. The plot of ln i vs. t is linear for 90% of two equivalents at which point the rate of electrolysis decreases more slowly (Figure 16A). After approximately 1.0(1) electrons had passed the current leveled off to a value slightly above the background current. After some time a precipitate formed. This is in contrast with the results of Sofranko, et al. (16) who reported that the current decay plot was linear for one equivalent but the current slowly decayed to background levels as a second equivalent was passed into the solution. They attributed this to a facile one-electron reduction of all the rhodium ions in solution to $Rh(DPE)_2^0$ which then slowly reacted with solvent to form a rhodium hydride. The organic radical formed was then reduced at the electrode. The rate, and hence current, were thus controlled by the rate of rhodium decomposition (20). Pilloni and other workers (18,19,23) performed low temperature electrolysis which required two electrons and gave a red solutions (8). In the reduced solutions the anodic wave height was within 85% of the height of the initial anodic wave. Upon warming the solution the color lightened and a yellow precipitate identified as $HRh(DPE)_2$ formed. In the present study, immediately after the room temperature electrolysis was completed, a cyclic voltammogram showed 57% of the original current was present but the red color faded quickly and the wave disappeared. The yellow product which precipitated was identified by its infrared spectrum (Rh-H stretch 1800 cm^{-1}) in agreement with the previous studies (8,15,16,20).

FIGURE 16

A. Plot of ln i vs. t for 0.9 mM $Rh(DPE)_2^+$
Bulk Electrolysis

B. Plot of ln i vs. t for 0.76 mM $Rh(DPP)_2^+$
Bulk Electrolysis

C. Plot of ln i vs. t for 1.25 mM $Rh(DPB)_2^+$
Platinum Electrode

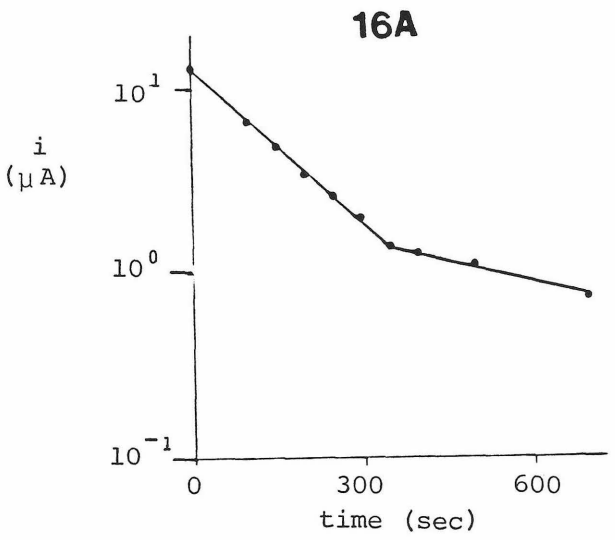
16A
i
(μA)
10^1
10^0
10^-1
0
300
600
time (sec)

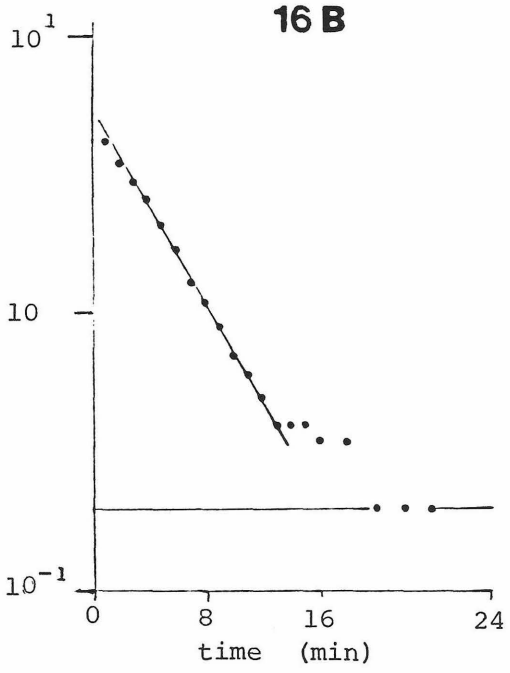
16 B
10^1
10
10^-1
0
8
16
24
time (min)

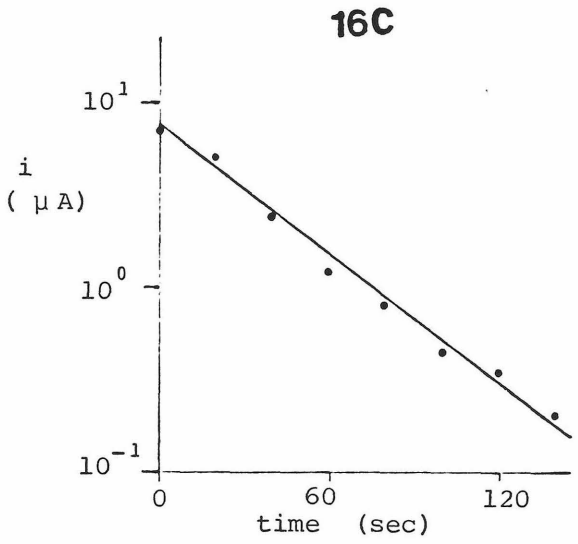
16C
i
(μA)
10^1
10^0
10^-1
0
60
120
time (sec)

G. $Rh(VPE)_2^+$

The exhaustive electrolysis of 10 ml of 1.16 mM $Rh(VPE)_2^+$ required two equivalents of electrons per rhodium and the solution changed from yellow to red. The ln i vs. t plot consisted of a straight line down to background current levels. Immediately at the conclusion of the electrolysis the cyclic voltammetric peak current response was 70% of the initial value. After 45 minutes with the red color fading continuously, the current had decreased to 29% of the initial value. The spent, now yellow solution was allowed to slowly evaporate for several days as reddish-brown crystals formed in the more concentrated solution. An infrared spectrum identified the product as the hydride complex, $HRh(VPE)_2$ (Rh-H = 1895 cm^{-1}) (8).

H. $Rh(DPP)_2^+$

The reduced solutions of $Rh(DPP)_2^-$ proved to be the most stable relative to the other complexes but they were still quite unstable. Figure 16B displays the ln i vs. t plot for a 10 ml solution of 0.86 mM $Rh(DPP)_2^+$ reduced at -2.2 V. The plot is linear for 90% of the reduction process then current decreases less quickly than expected until it reaches background levels. The resultant red solution was stable for several minutes before fading to yellow. Immediately after electrolysis in some of the solutions a cyclic voltammogram revealed up to 80% of the original wave. Due to its longer stability, solutions of this complex were later reduced electrochemically and U.V.-Visible spectra were recorded.

I. $Rh(DPB)_2^+$

A 1.44 mM solution was reduced at -2.3 V with a mercury working electrode. The two polarographic waves were too close together to allow for a one-electron reduction study on the reversible wave. For the reduction with the mercury electrode the ln i vs. t plot was initially a straight line for ca. one-half equivalent at which point it leveled off to a flat current plateau above the background. By this time, the mercury pool which had been serving as the working electrode, transformed from a pool of mercury into a mass of globules or balls of mercury. This indicates a strong interaction of the rhodium complex with the mercury. This agrees with the cyclic voltammetric studies and polarography, both of which indicated a high degree of interaction. As the mercury was being broken up the newly-formed coated balls did not conduct as well and the surface area of the electrode was altered. As the area of the electrode was lowered and the electrode was covered successively with layers of insulators, the current level dropped until it hit the plateau value observed.

The electrolysis was repeated with a platinum working electrode and a 1.25 mM solution of $Rh(DPB)_2^+$. The current density was much higher and the reduction proceeded quickly. The plot of ln i vs. t (Figure 16C) was linear. The value of n was 2.0(1) electrons when the current had reached background levels. The final red solution slowly faded but no precipitate formed nor did any form as the solution evaporated. Product analysis was not continued for the same reason as given for

$Rh(DPP)_2^+$. After the solution had been evaporated to dryness an I.R. spectrum provided no further information about the product. The I.R. spectrum was dominated by the electrolyte absorptions which were more numerous and intense than the rhodium product.

V. SPECTROSCOPY

A. FLUORESCENCE

Geoffroy (71) had previously described the fluorescence of $Rh(DPE)_2^+$ and $Rh(VPE)_2^+$ in great detail. To briefly summarize his results, he observed that excitation in the lowest energy band led to emission red-shifted by approximately 4000 cm^{-1} from the absorption peak. $Rh(VPE)_2Cl$ luminesced at room temperature [600 nm, peak width (W_p) = 105 nm] and at 77 K with lifetimes of 22.3 microseconds and 27.5 microseconds, respectively. $Rh(DPE)_2Cl$ did not luminesce at room temperature but did so at 77 K [in diethyl ether-isopentane-ethanol (EPA), 613 nm, W_p = 85 nm]. Neither complex luminesced at room temperature in solution. In his Caltech thesis (71) Geoffroy reported a brief study of $Rh(DPP)_2^+$. He noted that at low temperature in EPA a weak fluorescence was visible (645 nm; W_p = 110 nm). At 77 K the peak sharpened and the luminescence became more intense. He attributed the layer shift and wider peak width to a more flexible carbon backbone on the phosphines.

Having synthesized the next two species in the series started by Geoffroy it seemed worthwhile to perform a cursory examination of the

fluorescence spectroscopy of these compounds.

Solutions of $Rh(DPM)_2^+$ and $Rh(DPP)_2^+$ in degassed acetonitrile did not emit at room temperature. At 77 K the frozen solution of $Rh(DPM)_2^+$ emitted at 640 nm. No emission was detectable from the frozen solution of $Rh(DPB)_2^+$. With these data in hand it was decided to further examine only solid samples.

A very weak luminescence was detected at room temperature for $Rh(DPM)_2TRF$, the peak maximum occurring at 690(5) nm. At 77 K the peak sharpened and became much more intense (maximum at 688 nm, W_p = 115 nm). The solid $Rh(DPB)_2^+$ did not emit at room temperature or at liquid nitrogen temperature. From this experiment it is impossible to conclude that the lack of emission from $Rh(DPB)_2^+$ is related to the C-H atom backbone chain length. The emission maximum for $Rh(DPM)_2^+$ was further red-shifted from those of $Rh(DPE)_2^+$ or $Rh(VPE)_2^+$ also suggesting something more complicated than the carbon backbone length is playing a significant role.

The lifetimes of the emissions from $Rh(DPM)_2TRF$ and $Rh(VPE)_2ClO_4$ in the solid state were measured at room temperature and at liquid nitrogen temperature. The emission lifetime of $Rh(VPE)_2ClO_4$ was only measured at room temperature. The increase in emission intensity for this complex at low temperature was negated by the increased scatter by the dewar flask and the increased noise from the bubbling liquid nitrogen. The lifetimes were found to be as follows: $Rh(DPM)_2^+$, 1.8 and 20 microseconds; $Rh(VPE)_2^+$, 14.1 and 21.5 microseconds; $Rh(DPP)_2^+$, 3.5 microseconds. The first of the two values indicated is at room temperature. $Rh(DPM)_2^+$ showed a marked increase in emission lifetime upon cooling.

No apparent correlation could be found between luminescence wavelength/lifetime results and the electrochemical results mentioned earlier (not that one was expected, however).

B. U.V.-VISIBLE SPECTRUM OF $Rh(DPP)_2^-$

All of the rhodium(I) complexes examined were yellow-orange in color initially but upon reduction all turned red-brown. Typically this color quickly faded. Solutions of $Rh(DPE)_2^-$ proved to be the most unstable while those of $Rh(DPP)_2^-$ were the most stable.

To obtain the spectrum a 0.47 mM solution of $Rh(DPP)_2ClO_4$ (in preelectrolyzed actonitrile with 0.2 M TBABF4) was reduced at -2.2 V. The reduction required two electrons reaching background levels within a total time of about 9 minutes. The ln i vs. t plot was linear almost to completion deviating only as background current level was approached. A cyclic voltammogram recorded immediately after the electrolysis indicated that over 75% of the initial material was still present. Upon completion an aliquot was removed from the electrochemical cell by syringe and transferred to a degassed 1 mm cuvette. The spectrum is shown in Figure 17. The starting material, $Rh(DPP)_2^+$, displayed two bands at 280 nm and 405 nm. Upon reduction these two features disappeared and the new spectrum was dominated by the large, broad absorption centered at 450 nm. The extinction coefficient was estimated to be 1.1 x 10^5. This large value suggests that the new band corresponds to an allowed transition.

The disappearance of the band upon electrolysis at 400 nm is not surprising since it was the lowest energy allowed transition. In the reduced complex the orbital to which this transition occurred must now be filled. Attempts to obtain intermediate spectra before the

FIGURE 17

U.V.-Visible Spectrum of $Rh(DPP)_2^+$

a. Before electrolysis

b. After electrolysis

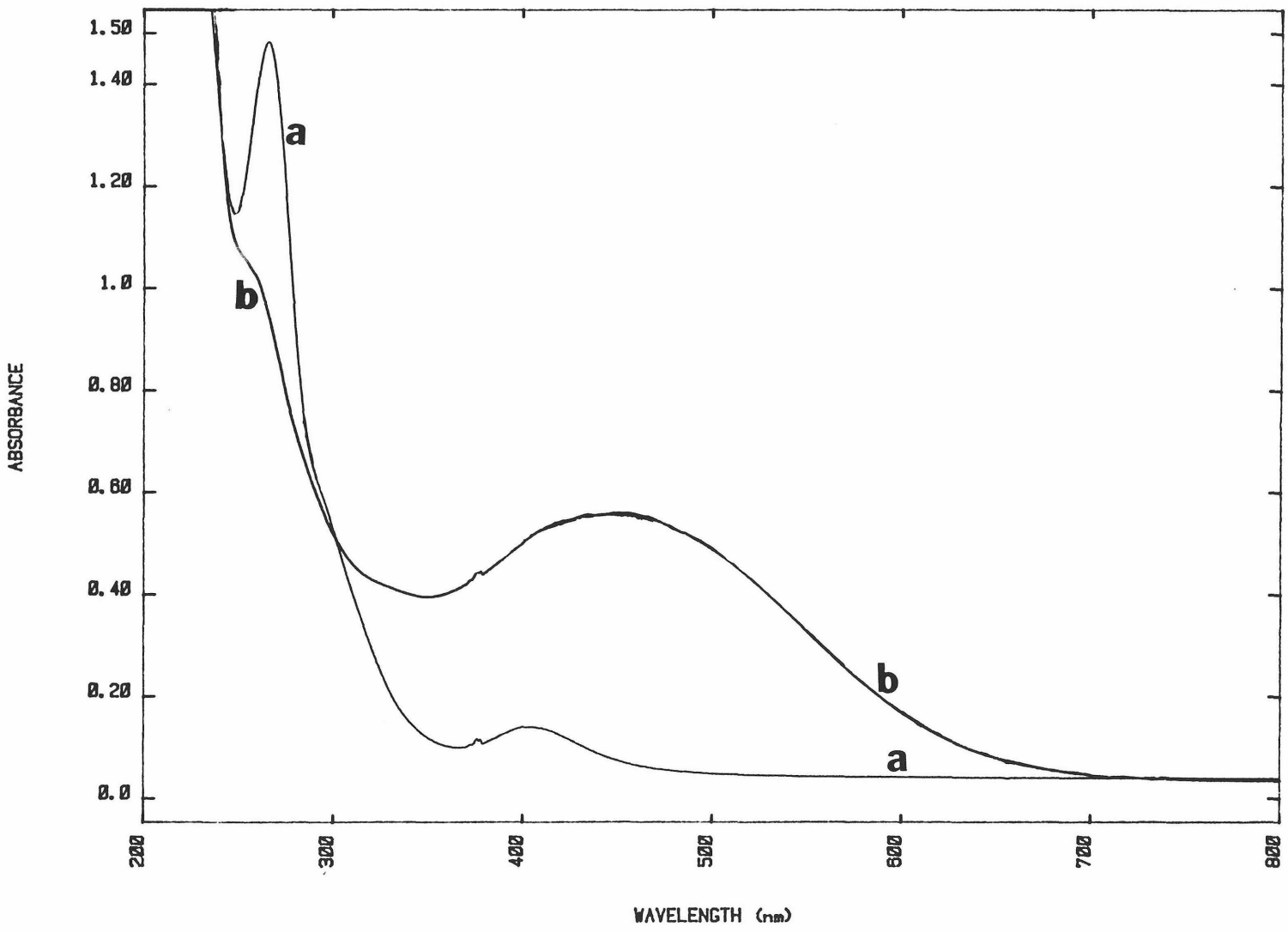
ABSORBANCE
1.50
1.40
1.20
1.0
0.80
0.60
0.40
0.20
0.0
200
300
400
500
600
700
800
WAVELENGTH (nm)
a
b
b
a

completion of the electrochemical process were unsuccessful due to the time involved for the extra manipulations and the increased chance of admitting oxygen into the system. The spectrum is unique in that Pd(0) and Pt(0) phosphine complexes are yellow in color and do not exhibit broad low energy bands (74-78).

VI. SUMMARY

All the experimental results support an initial two-electron reduction of the rhodium complexes with a subsequent chemical reaction leading to the formation of hydrides. The bulk electrolysis experiments for all the rhodium complexes (with the exception of $Rh(DPM)_2^+$) required two electrons and proceeded such that linear ln i vs. t plots resulted. The unusual behavior noted by Sofranko (20) which led him to propose a $Rh(DPE)_2^0$ species was not evident. The results of bulk electrolysis experiments with $Rh(DPM)_2^+$ can be explained by assuming a two-electron reduction followed by a chemical reaction which involves dimerization with starting material. The irreversible cyclic voltammetric results are in agreement with this scheme. The final product does not appear to be a hydride because the other rhodium hydrides are electro-inert in the potential range where the $Rh(DPM)_2^+$ reduction product wave occurs. Also, NMR and IR evidence rules out the possibility that the product is a hydride.

The mechanism by which the rhodium anion formed in the electrolysis undergoes chemical reaction is not known. The reaction must be slow, because cyclic voltammograms for all the complexes except $Rh(DPM)_2^+$

and $Rh(DPB)_2^+$ exhibit forward to reverse current peak ratios near one. However, if the two extra electrons added to the complexes are to any extent localized on the phosphines then some of the radical products observed by Eisenberg et al. (15,16) may be formed by a phosphine decay process. Reduced trivalent phosphine compounds have been found to decompose by a process that releases free radicals (79). However the phosphines studied were not complexed to metals.

The overall process for the rhodium complexes is clear: a two-electron reduction followed by a chemical reaction typically forming a hydride. The previous work had disagreed as to whether the first step was a one- or a two-electron reduction process centered on $Rh(DPE)_2^+$. This species is not well suited for these studies because of slow heterogeneous electron tranfer. When the $Rh(DPE)_2^+$ was examined in the context of the series of rhodium complexes, it was found to initially undergo a two-electron reduction.

Although the E° values for the rhodium complexes follow no trend, the nature of the reduction process does change. $Rh(VPE)_2^+$ shows a two-electron wave, $Rh(DPP)_2^+$ shows two juxtaposed one-electron waves while $Rh(DPB)_2^+$ exhibits two one-electron waves.

VII. $Rh_2(TMB)_4^{2+}$

A. INTRODUCTION

The reductive electrochemistry of $Rh_2(TMB)_4^{2+}$ has been of interest since Milder et al. (33) observed that the photo-excited state could be quenched by electron transfer quenching reagents. It was therefore felt that it would the worthwhile to study the electrochemical characteristics of the reduced species. The $Rh_2(TMB)_4^{2+}$ species was preferred over the other rhodium bridged species for a variety of reasons. It is by far the easiest to synthesize, store, and handle. It can be obtained by recrystallization as the most pure of all the complexes. $Rh_2(TMB)_4^{2+}$ is the most soluble of the bridged rhodium isocyanide complexes. In addition it was hoped to avoid the oligomerimization type of chemical complication evident with $Rh_2(bi)_4^{2+}$ in aqueous solution (84).

B. CYCLIC VOLTAMMETRY

Cyclic voltammograms were recorded for $Rh_2(TMB)_4(PF_6)_2$ and $Rh_2(TMB)_4(TRF)_2$ in acetonitrile and DMF using TBATRF, $TBAPR_6$ OR $TBABF_4$. In all the combinations tried the electrochemistry remained unchanged: one reduction wave over the scannable potential range. This wave was measured at E_p = 1.55 V (vs. SCE) or E_p = 1.970 V (vs. 0.1 M $AgNO_3$/Ag). Figure 18 was obtained with 0.3 mM solution $Rh_2(TMB)_4(TRF)_2$ in 0.1 M $TBABF_4$ in acetonitrile using a platinum electrode. The figure only displays the potentials of interest. Upon scanning past the wave and back no additional waves appeared. As can be seen in Figure 18 the cathodic current is larger than the anodic counterpart. As the scan rate increased the ratio ip^a/ip^c approached unity but never reached it. Generally the closest approach was 0.6, even at scan rates up to 200 V/sec. As the scan rate increased the anodic wave broadened and this may be why the current ratio never reached unity. The size of the anodic wave depended on the switching potential. As the switching potential became more cathodic the amount of anodic wave decreased. This was qualitatively observed and no rate constants were evaluated because of the complicating wave distortion visible in Figure 18. As the scan rate increased the cathodic wave shifted to more negative potentials (ca. 30 mV per factor of 10 ln scan rate). Consequently the peak splitting was observed to increase from 70 mV at 50 mV/sec to 130 mV at 1000 mV/sec. At higher scan rates the splitting continued to increase. A plot of i_p vs. $v^{1/2}$ is a straight line that passes through

FIGURE 18

C.V. of 0.3 mM $Rh_2(TMB)_4^{2+}$

Pt electrode area = 0.00375 cm^2

v vs. SCE

a. 350 mV/sec

b. 200 mV/sec

c. 150 mV/sec

d. 100 mV/sec

e. 50 mV/sec

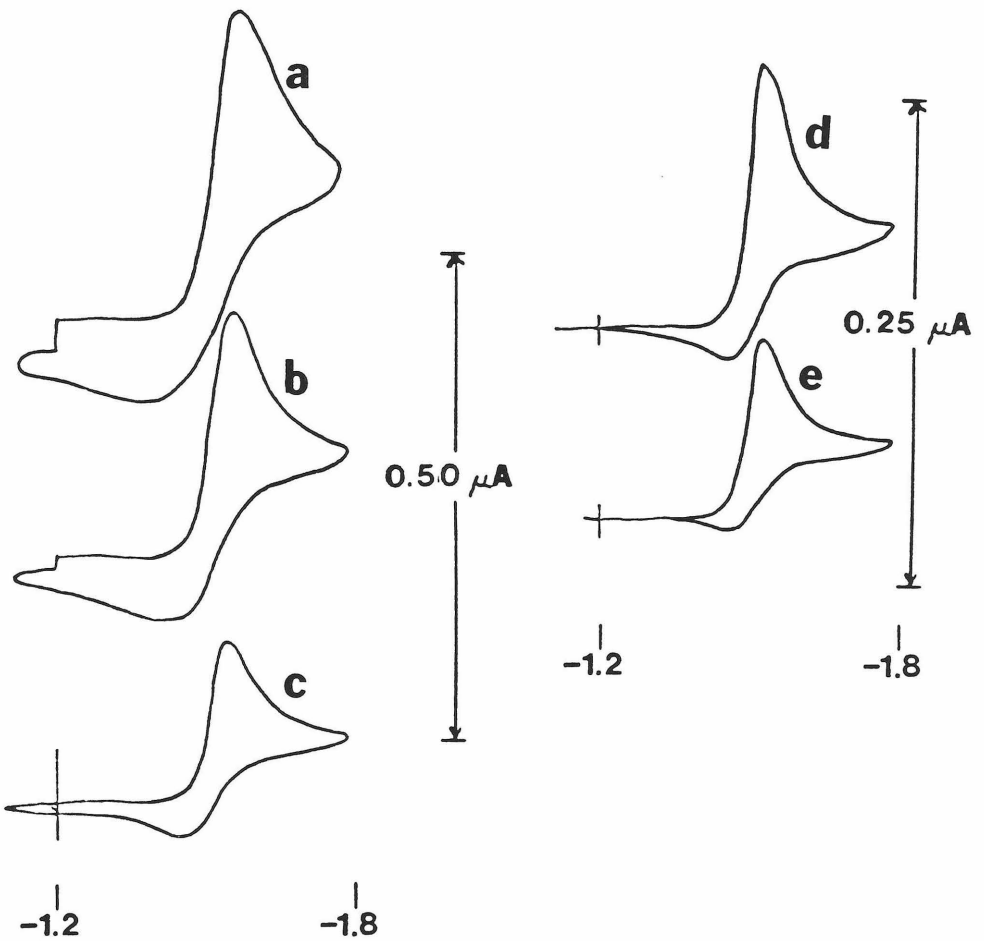
a
b
c
d
e
0.50 μA
0.25 μA
-1.2
-1.8
-1.2
-1.8

the origin. Care had to be taken to wipe the electrode before each scan because the electrodes became passivated with time even though no film was visible on the electrode surface. The calculation of D_o from the slope of the i_p vs. $v^{1/2}$ plot was not attempted because of the irreversible nature of the cyclic voltammograms.

A chronoamperometric measurement was made on a 0.91 mM solution of $Rh_2(TMB)_4(TRF)_2$ is acetonitrile with 0.2 M $TBABF_4$. The D_o values obtained were 6.7×10^{-5} cm^2/sec if n = 1 and 9.9×10^{-6} to 1.6×10^{-5} cm^2/sec if n = 2. The main problem with the experiment was formation of passivating films. The electrochemically active area of the electrode changed after each cleaning but new values were assumed to be close to the value obtained by calibration with anthracene. The D_o value obtained by assuming a one-electron process was inconceivably large when compared with the rhodium phosphine values. The value assuming n = 2 was also large but reasonable though a value smaller than that obtained for phosphine monomers would be expected because of the larger size of the molecule.

Cyclic voltammograms recorded using a HMDE revealed several additional features not found with platinum though the basic irreversibility of the wave remained the same. In a cyclic voltammogram of a solution of 0.25 mM $Rh_2(TMB)_4^{2+}$ with 0.1 M TBATRF a shoulder appeared on the reduction wave cathodic of the main peak as the scan rate increased. This peak shifted cathodically and grew in magnitude until the previous main peak became a shoulder on the peak. These are the characteristics one would expect for an electroactive species which is specifically

adsorbed to the electrode surface (86).

Aside from this adsorption behavior, when the potential was scanned over a reduction wave and then scanned anodic to 0.0 V (vs. SCE) no new waves appeared. In particular no wave appeared where one would be expected for cyanide assisted mercury oxidation, ca. 0.0 V (vs. 0.1 M $AgNO_3$/Ag) (83).

The CV results have suggested an electron transfer followed by an irreversible chemical reaction. The chronoamperometric and polarographic results suggest a two-electron wave. When it is possible to observe an anodic wave the CV peak splitting is too large for a one- (or two-) electron nernstian process. It probably indicates slow electrode kinetics. The amount of anodic return wave at a particular scan rate and turning potential showed some concentration effects. A 0.25 mM solution approached reversibility more than a 1.3 mM solution which showed more than an 8 mM solution, however the effect was not large. In any case one would expect this type of result for a reaction in which a reduced complex reacts with starting material to give an electroinactive species.

C. POLAROGRAPHY

The polarographic results obtained were not very useful. A d.c. polarogram shown in Figure 19 displays the one observed wave. This wave had a maximum which made the calculation of a diffusion plateau difficult. The I value was estimated to be 3.2 - 3.8 which is in agreement with a two-electron wave. Normal pulse data were useless as a criterion of reversibility because of the large polarographic maxima observed in both directions. This same rhodium-mercury interaction that appeared in the CV, d.c. and N.P. polarographic techniques also manifested itself in the D.P. polarogram as a broad shoulder on the main wave.

FIGURE 19

Tast Polarogram

1.0 mM $Rh_2(TMB)_4^{2+}$

41 cm Hg Ht.

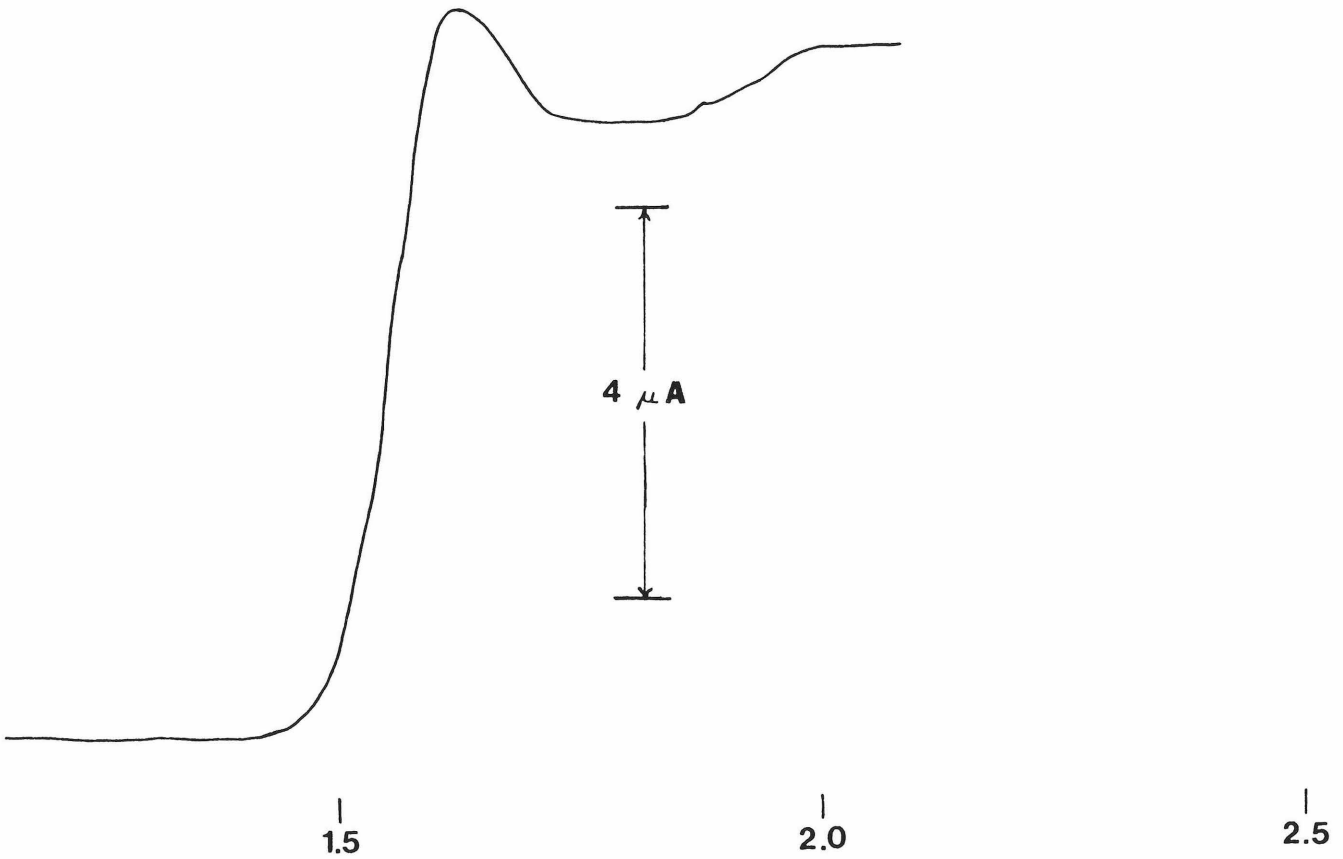
4 μA
1.5
2.0
2.5

D. BULK ELECTROLYSIS

Bulk electrolysis of pink $Rh_2(TMB)_4^{2+}$ solutions 200 mV past the CV reduction peak potential resulted in purple or blue solutions depending on the duration of the electrolysis. Initially the current decayed exponentially giving a linear ln i vs. t plot. However after approximately one Faraday per mole of complex had passed the current quickly decayed to a level above background. At this point a purple solution resulted and a CN revealed that the original wave had disappeared.

Several items concerning this initial reduction product were observed although the exact nature of the species could not be determined. No E.S.R. signal could be detected in the frozen solution at 77 K indicating no unpaired electrons. The cyclic voltammogram recorded after the electrolysis revealed a single, anodic, totally irreversible wave at -0.4 V (vs. 0.1 M $AgNO_3/Ag$).

If the purple solution is reoxidized at the anodic wave the solution changes back to pink but new absorption bands have appeared in the UV region. A CV voltammogram of the new pink solution showed only a fraction of the original reduction wave; in addition the background became larger with several low current, irreversible, broad anodic and cathodic waves. If the purple solution was exposed to oxygen the pink color quickly returned but extra bands appeared in the UV region of the absorption spectrum.

The purple color itself was due to the large band present in the starting material at 515 nm shifting to 550 nm. The purple solution

fluoresced at 640 nm. In comparison, the starting material fluoresced at 620 nm. This shift in emission wave length paralleled the shift observed in the visible absorption spectra. The uncorrected fluorescence spectrum is shown in Figure 20 along with the uncorrected spectrum of $Rh_2(TMB)_4^{2+}$ under identical though more dilute conditions. A 0.9 mM solution of $Rh_2(TMB)_4^{2+}$ in 0.2 M $TBABF_4$ was reduced in the general purpose bulk electrolysis cell. Aliquots of solution were removed before, during, and after the electrolysis to one equivalent. The spectra obtained was recorded in a 1 mm cell and are shown in Figure 21. The upper spectrum with a band at ca. 500 nm is the original spectrum and the lower curve is the final spectrum. As the absorption band shifted during electrolysis the size of the cathodic wave decreased.

FIGURE 20

Fluorescence Spectra $Rh_2(TMB)_4^{2+}$

a. After electrolysis

b. Before electrolysis - diluted

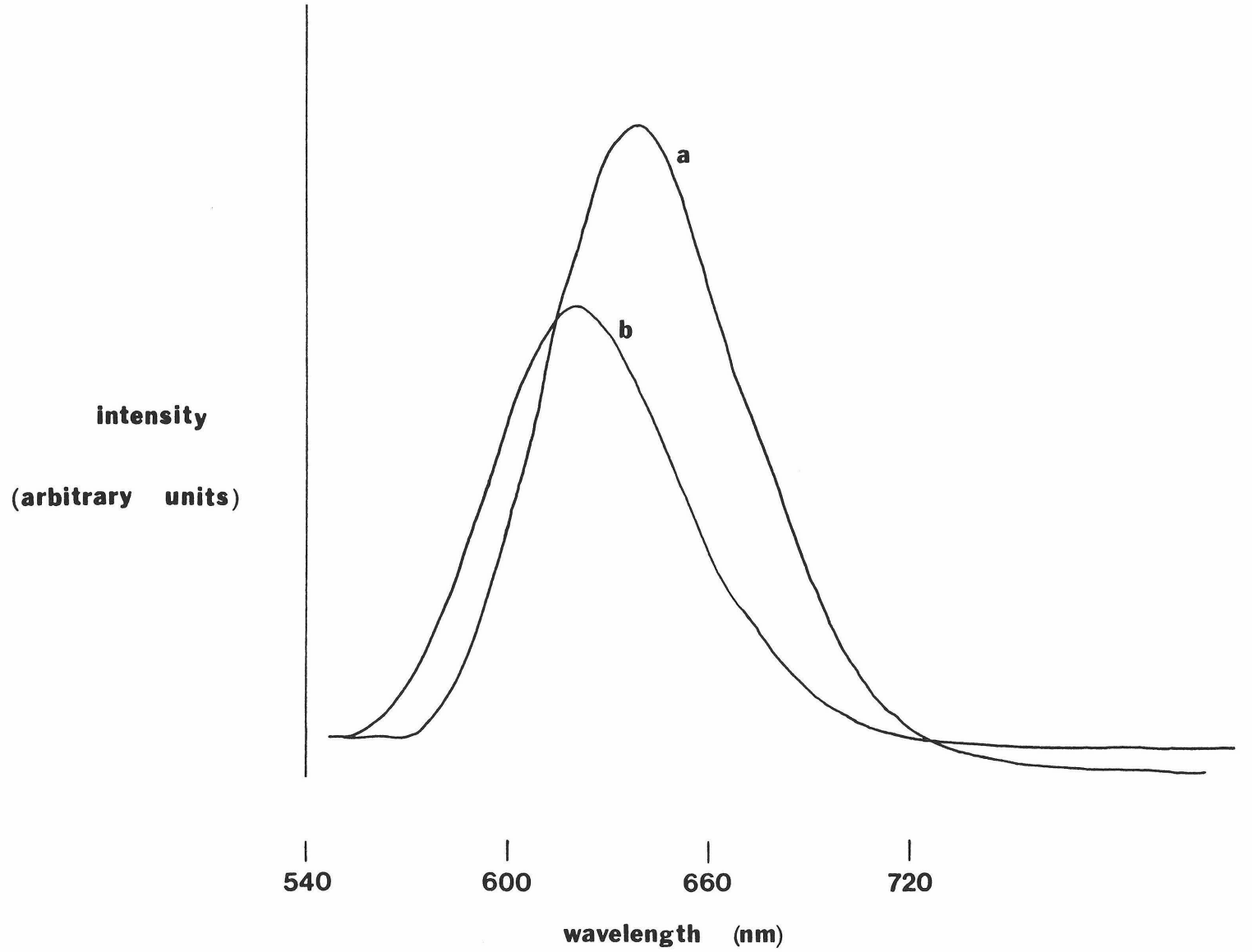
a
b
intensity
(arbitrary units)
540
600
660
720
wavelength (nm)

FIGURE 21

U.V.-Visible spectra of $Rh_2(TMB)_4(TRF)_2$
during reductive electrolysis up to one equivalent

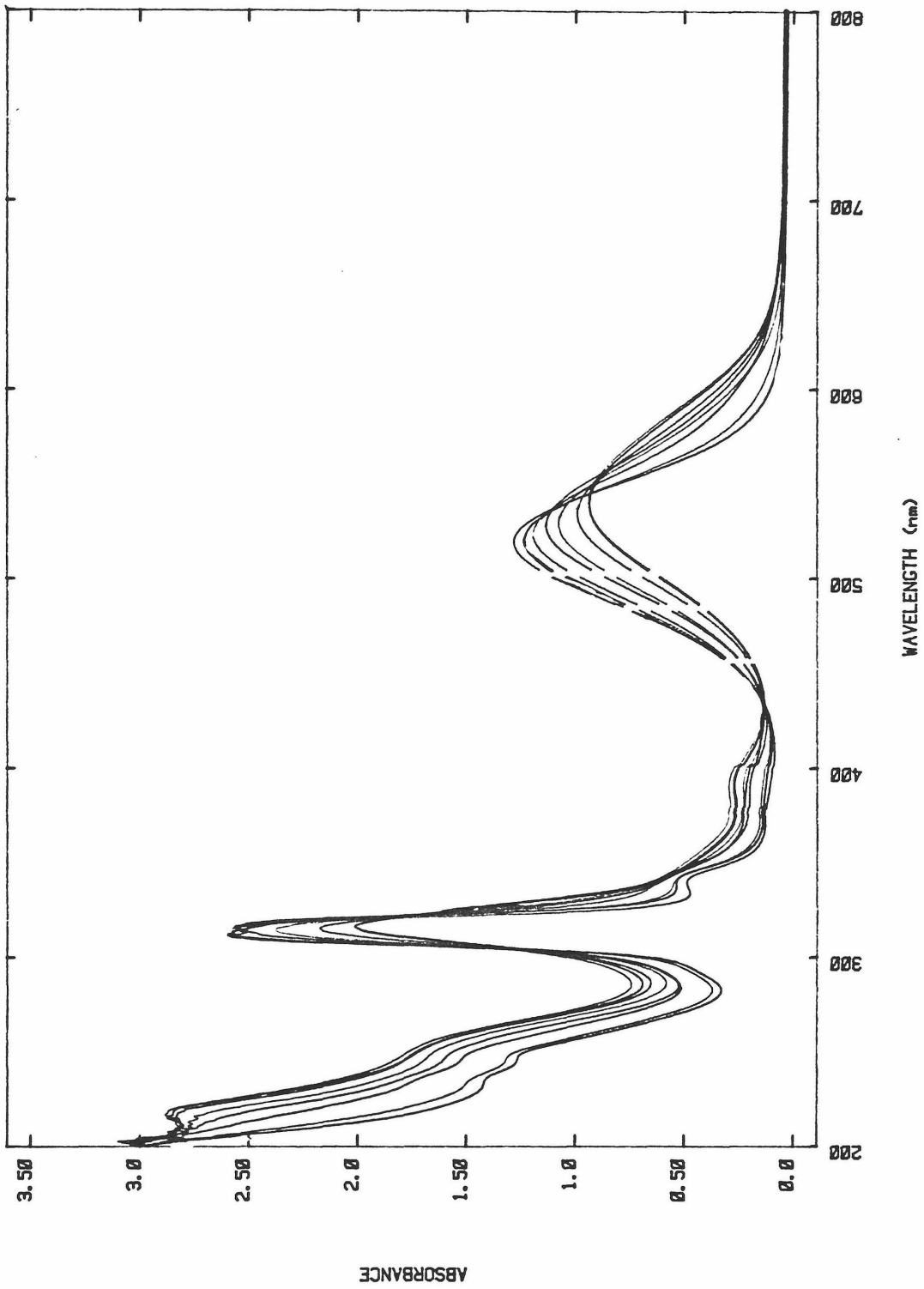
ABSORBANCE
3.50
3.0
2.50
2.0
1.50
1.0
0.50
0.0
200
300
400
500
600
700
800
WAVELENGTH (nm)

The electrochemical and spectrochemical data point towards the purple color corresponding to a distinct species in solution. Unfortunately this one electron reduced species defied all attempts at isolation and purification. Large quantities of the purple material were prepared electrochemically, but it was impossible to separate out the electrolyte. Infrared spectra prepared from the gross mixtures showed only one additional band: the CN stretch had broadened with shoulders on the low energy side of the original stretch indicating the material was more reduced. While attempting to separate the reduced species on the column it was discovered that the crude purple material reacted with neutral alumina, silica gel, dried Fluorosil, and dried reverse phase silica gel. Only on dried activated neutral alumina did the purple species remain purple; however, it proved impossible to remove it from the column.

A small amount of light blue material did come off the column. It was later isolated, purified and identified as the two-electron reduced species $Rh_2(TMB)_3$(3,3,6,6-tetramethylcyclohexylimine)TRF abbreviated as $Rh_2(TMB)_3$(TMI)TRF. The crystal structure of the molecule is discussed in the next chapter. The $Rh_2(TMB)_4(TMI)_2$ has an absorption at 582 nm producing the blue color. It was found that by continuing the electrolysis at -2.3 V for longer times, increased the amount of the blue material, even though no CV wave existed. If the solution was allowed to electrolyze for 2 equivalents of electrons the entire solution turned blue (582 nm). If the purple material was allowed to stand undisturbed for a similar length of time no changes occurred. Figure 22

FIGURE 22

Spectra $Rh_2(TMB)_4^{2+}$

electrolysis past one equivalent per Rh_2 unit

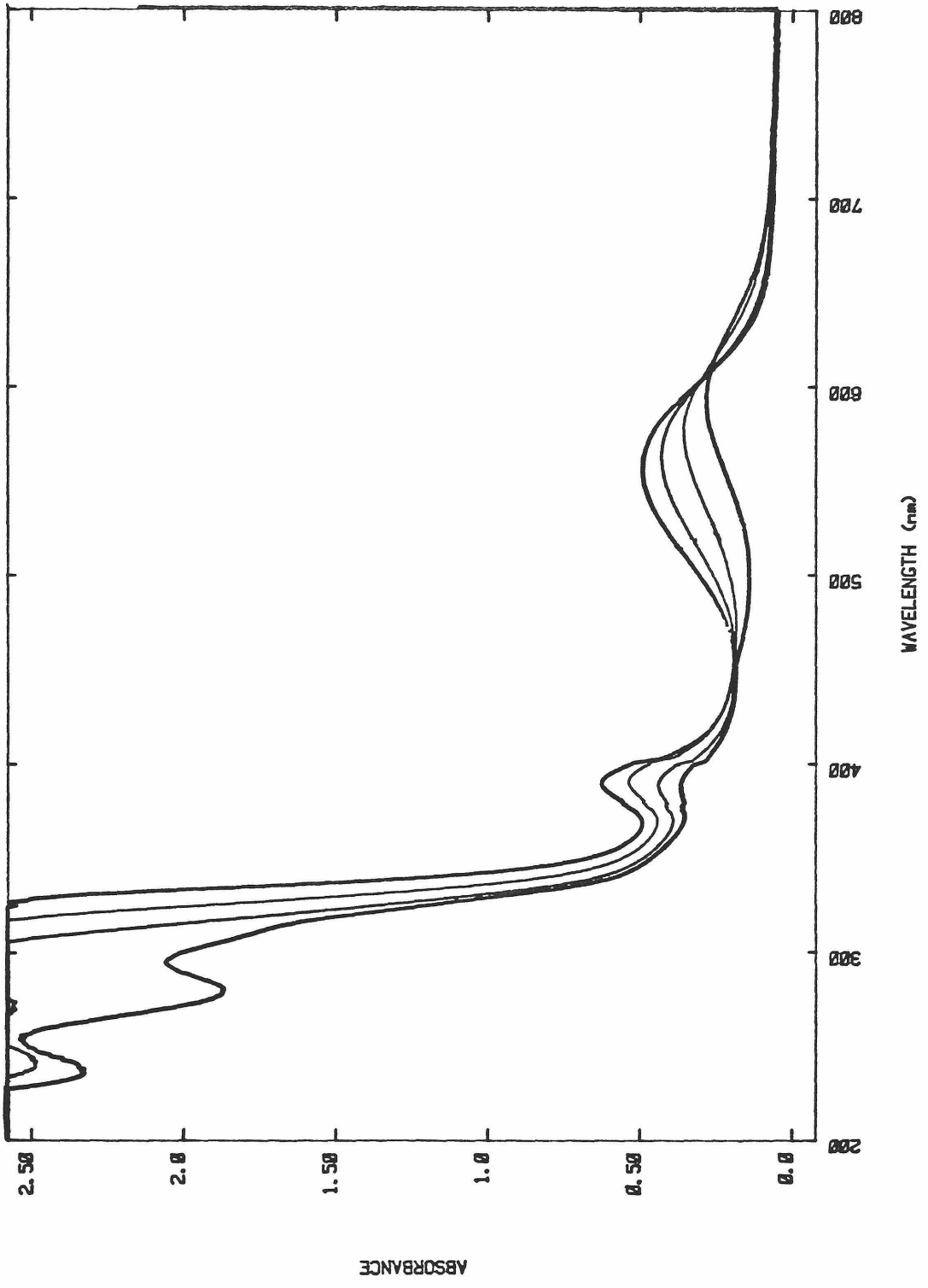
ABSORBANCE
2.50
2.0
1.50
1.0
0.50
0.0
200
300
400
500
600
700
800
WAVELENGTH (nm)

shows the resultant spectra for the reduction of 0.04 mM $Rh_2(TMB)_4^{2+}$ for a second equivalent of electrons per Rh_2 unit. In this instance the reduction was conducted totally in the spectroelectrochemical cell described previously (Figure 2). The upper curve is the spectrum of the intermediate purple one-electron reduced species. The lower curve is the spectrum of the final blue species. This final spectrum differs somewhat in the UV region from a spectrum obtained by dissolving purified $Rh_2(TMB)_3(TMI)TRF$ in acetonitrile. The electrolysized solutions have a strong band at wavelengths shorter than 275 nm which distort the peaks at wavelengths less than 275 nm. This large extra peak grows during the passage of the second equivalent.

Upon exposure to oxygen, the color of solutions of $Rh_2(TMB)_4(TMI)TRF$ slowly ($t_{1/2}$ = 5 min) faded to yellow but at no time did the solution turn pink. The infrared spectrum was very similar to that of the purple species; even the CN stretch was broad with shoulders on the low energy side. The only difference is an extra absorption at 1730 cm^{-1} which is presumably due to the imine stretch.

The bulk electrolysis and spectrochemical studies suggested that the one-electron reduced purple species was the precursor of the blue $Rh_2(TMB)_4(TMI)TRF$ but without knowing the exact nature of the purple species it was difficult to find a plausible mechanism for the two-atom expulsion and the ring closure. The fact that the purple species has been reduced one electron per two rhodium atoms, yet has no unpaired electrons can be accounted for by assuming some form of dimerization. The fact that CN^- loss did not occur is supported by the partial restor-

ation of the pink color upon exposure to oxygen and the lack of CN^- waves in the cyclic voltammogram. Although the exact nature of the CN^- wave in acetonitrile has not been studied the results obtained by experiments in anhydrous pyridine suggest that the wave should have occurred at +0.4 V on a platinum electrode (82).

E. DISCUSSION

The experimental results indicate that a complicated process occurs when $Rh_2(TMB)_4^{2+}$ is reduced. Initially a two electron reduction occurs followed by a chemical reaction. Cyclic voltammetric concentration results and bulk electrolysis results favor the formation of a tetranuclear species. Since the cyclic voltammograms show no additional waves the initially formed species must be an electroinactive moiety which later becomes the purple species. The spectral and bulk electrolysis evidence suggests that the purple species is a one-electron reduced molecule. The similarity of the optical spectrum of the purple species with that of the starting material and the two-electron reduced blue species suggests that the purple species has a Rh(I) - Rh(I) core with possibly a bound one-electron reduced ligand. The free ligand has no electrochemical response in the potential range available in acetonitrile. The lack of E.S.R. signal indicates that the added electron has been coupled. The ease with which the purple solution can be restored to a pink color (oxygen and electrochemical oxidation) indicates that the species is (partially at least) chemically reversible. Since the blue species cannot return to a pink color because of CN^- loss, the purple species must still contain these two atoms. This is supported by the lack of a CV CN^- wave for the purple solution. The final step of the process is the slow reduction of the purple species with concomitant loss of CN to the known blue species $[Rh_2(TMB)_4(TMI)(TRF)]$. There is very little previous work dealing with cyanide or isocyanide loss.

Saturated nitriles are very stable compounds (81).

At no time during the study was a spectrum obtained for any species which resembled the one-electron transient observed by Milder et al. (33). However the irreversible $Rh_2(TMB)_4^{2+}$ reduction results obtained in this study indicate that any process which depends on the reduction of rhodium isocyanide complexes should be avoided.

VIII. CRYSTAL STRUCTURE OF Rh_2(TM4-bridge)$_3$(3,3,6,6,-tetramethylcyclohexylimine)$^+$TRF$^-$

A. SYNTHESIS

It was found that 3% sodium-mercury amalgam could also be used to reduce $Rh_2(TMB)_4(TRF)_2$. The amalgam used contained several large pieces of solid amalgam to raise the sodium content and lower the tendency of the mercury to react with the rhodium complex. $Rh_2(TMB)_4(TRF)_2$ (0.1 g, 86 micromolar) was dissolved in acetonitrile (5 ml) and filtered into a flask. A large excess of Na/Hg amalgam was pipetted into the flask and allowed to react with vigorous stirring for 30 minutes. This blue-purple solution was placed on a column of activated alumina an inch in depth and one inch in diameter. The light blue band was eluted with acetonitrile (ca. 100 ml). This was then concentrated under vacuum to 5 ml again and placed on a new column of activated alumina. The light blue band was eluted again with acetonitrile (ca. 100 ml). The liquid was concentrated under vacuum to 2 ml, placed in a small vial and the volume was increased to 10 ml by the addition of dried toluene. Slow evaporation proceeded over several days to reduce the volume to ca. 2 ml

with the formation of dark blue needle-like crystals. An NMR spectrum recorded in CD_3CN was very complicated: 1.02δ, 1.16δ, 1.29δ, 1.34δ, 1.44δ, 1.48δ, 1.69 δ, 1.84δ, 1.29δ. This attests to the lack of symmetry in the molecule. The infrared spectrum was virtually identical to that found for $Rh_2(TMB)_4(TRF)_2$, except for the wide CN stretch and the band at 1730 cm^{-1} assumed to be the CN stretch. Anal calculated for $C_{40}H_{64}F_3N_7O_3Rh_2S$: [C, 48.76; N, 9.95; H, 6.54; S, 3.25; F, 5.78. Found: C, 46.06; N, 9.41; H, 6.44; S, 2.97; F, 4.96].

B. X-RAY DATA COLLECTION

Preliminary oscillation and Weissenburg photographs revealed monoclinic symmetry, and the systematic absences (0k0 for k odd and h01 for l odd) indicated the space group $P1_1/c$. Lattice constants were obtained from a least squares refinement of the orientation matrix using fifteen reflections in the range $7.5 < 2\theta < 19°$: a - 17.540(16), b = 8.582(15), c = 32.36(5) Å, B = 91.59(10)°, and V = 4869 Å^3. All data were collected at 160 ± 5 K on a locally-modified Syntex P1 diffractometer using monochromatized MoK_α radiation (λ = 0.71069 Å).

A total of 4407 unique reflections ($+h, +k, \pm l$) were collected to a maximum $\sin\theta/\lambda$ of 0.48 Å^{-1}. Intensities were measured by θ - 2θ scans with a constant scan speed of 2 deg/min, angular dispersion correction to a fixed scan width of 2.0° in 2θ, and stationary-counter stationary-crystal background counts. Intensities of three check reflections, measured after each block of 47 reflections, showed no decomposition. During one period of data collection a pulse of electronic noise was periodically introduced into the scalar. This increased the observed counting rates, but apparently did not affect the net intensities when the pulse lasted through the scan and background counting. Also, due to the length of the c-axis, and the use of MoK_α radiation, reflections with large l were examined. Reflections with unusual backgrounds (either due to electronic noise or overlap) were discarded.

The remaining (4281, 3903 with $F_o^2 > 0$) reflections were corrected for Lorentz and polarization effects, but not for absorption (μ = 7.6

cm^{-1}). Observational variances, $\sigma^2(F_o^2)$, were based on counting statistics plus a term $(0.02s)^2$, where s is the scan count.

C. STRUCTURE DETERMINATION

The rhodium atomic positions were derived from the Patterson map. A density map ("Fourier") based on these two atoms revealed all the other non-hydrogen atoms. Isotropic refinement was carried out by using atomic scattering factors from Cromer and Weber (72) for Rh, from reference 73 for C, N, O, F, and S, and from Stewart et al. (74) for H. The real part of the anomalous dispersion correction for Rh was applied to the form factors. Several cycles of full-matrix least-squares refinement (quantity minimized was $\Sigma w(F_o^2 - F_c^2/s^2)^2$, $w = \sigma^{-2}(F_o^2)$, s = scale factor) on all non-hydrogen atoms resulted in convergence at $R_f = \Sigma(|F_o| - |F_c|)/\Sigma|F_o| = 0.092$. At this point CN1 and CN6 had negative B's, and more electron density was introduced into each position by assuming that they were full nitrogen atoms and not carbon atoms. The refinement of partial populations as disordered C and N atoms indicated a 1:1 occupancy. The partial populations of CN1 and CN6 were thus fixed as 1/2C and 1/2N in all subsequent refinements.

Hydrogen atoms were introduced into the model at this stage, each corresponding to areas of positive electron density in a difference map, and placed at idealized positions (C-H = 0.95 Å). An isotropic Gaussian amplitude of 5.0 $Å^2$ was assigned to all hydrogen atoms. Further refinement was carried out by using anisotropic Gaussian amplitudes for all non-hydrogen atoms except CN1, CN6, C2, and C5. The matrix was blocked for economy into three blocks with all non-hydrogen atomic coordinates in the first block, Gaussian amplitudes of the anion in the second, and

the remaining Gaussian amplitudes and scale factor in the third. The refinement converged at R_f = 0.060 (R_f based on all data with $F_o^2 > 0$), goodness-of-fit = $[\Sigma\omega (F_o^2 - F_c^2)^2/(m - s)]^{1/2}$ (m = number of observations and s = number of parameters = 475) = 1.46, and R_f = 0.037 (R_f based on all data with $F_o^2 > 3\ F_o^2$). A final difference map showed no peaks larger than 0.6 $e^-/Å^3$. The final fractional atomic coordinates and Gaussian amplitudes and a list of observed and calculated structure factors are available as supplementary material.

E. SPECTROSCOPY

The UV-Visible spectrum displayed several features very similar to those found in $Rh_2(TMB)_4^{2+}$. This supports the notion that $Rh_2(TMB)_3(TMI)TRF$ contains two interacting rhodium(I) atoms. Figure 23 is the UV-Visible absorption spectrum of a 0.19 mM solution made by dissolving crystals in acetonitrile. Two prominent peaks are visible, one at 318 nm (ε 1.0 x 10^4) and one at 582 nm (ε 1.3 x 10^4). There is a shoulder at 340 nm and a small absorption at 390 nm. For $Rh_2(TMB)_4^+$ these absorptions occur at 313 nm (ε 4.3 x 10^4) and 515 nm (ε 1.2 x 10^4) with shoulders at 338 nm and 390 nm. For $Rh_2(bi)_4^{2+}$ they occur at 318 nm (ε 3.15 x 10^4) and 553 nm (ε 1.4 x 10^4) with shoulders at 334 (ε 0.55 x 10^4) and 380 nm (53). It is difficult to ascertain the reason for the shift of the low energy $^1A_{1g}$ - $^1A_{2u}$ band to longer wavelengths since the Rh-Rh bond distance, the torsional angle and one of the ligands have been changed. Unfortunately, since the molecule does not emit, it was not possible to compare the Stokes shift with the degree of ligand stagger in the ground state as was done with $Rh_2(TMB)_4^{2+}$ and $Rh_2(bi)_4^{2+}$.

FIGURE 23

U.V.-Visible spectrum of $Rh_2(TMB)_3(TMI)(TRF)$

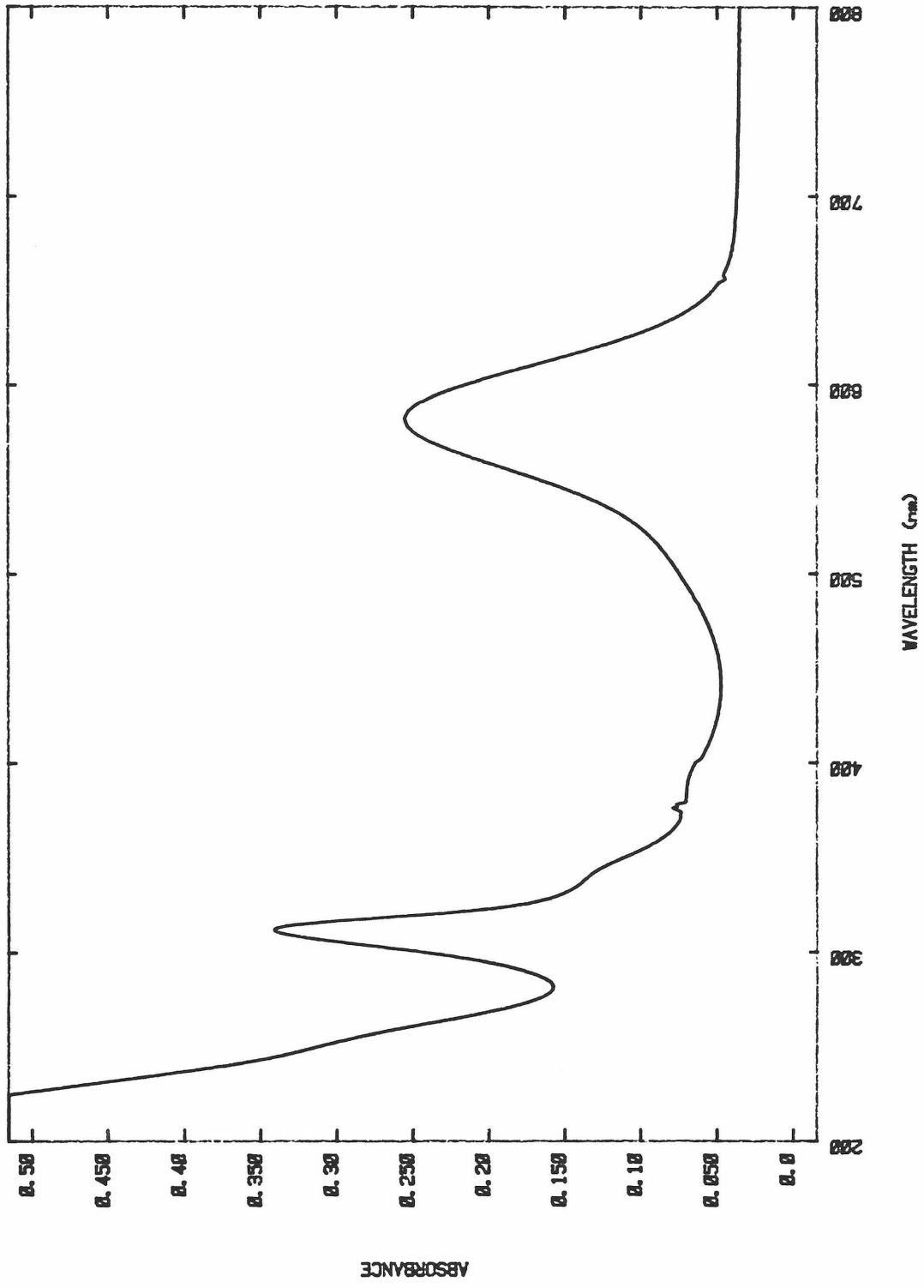
0.50
0.450
0.40
0.350
0.30
0.250
0.20
0.150
0.10
0.050
0.0
ABSORBANCE
200
300
400
500
600
700
800
WAVELENGTH (nm)

F. CRYSTAL STRUCTURE DESCRIPTION AND COMPARISON

The crystal consists of discrete cations and $CF_3SO_3^-$ anions separated by normal van der Waals distances. Figure 24 shows the atomic labelling scheme while Figure 25 depicts a stereo pair of the ion.

There is no crystallographically imposed symmetry on the binuclear molecule, nor is there any internal molecular symmetry. Selected interatomic distances may be found in Table 14, while Table 15 contains selected interatomic angles and selected interatomic torsion angles.

FIGURE 24

Labelled structure of $Rh_2(TMB)_3(TMI)(TRF)$

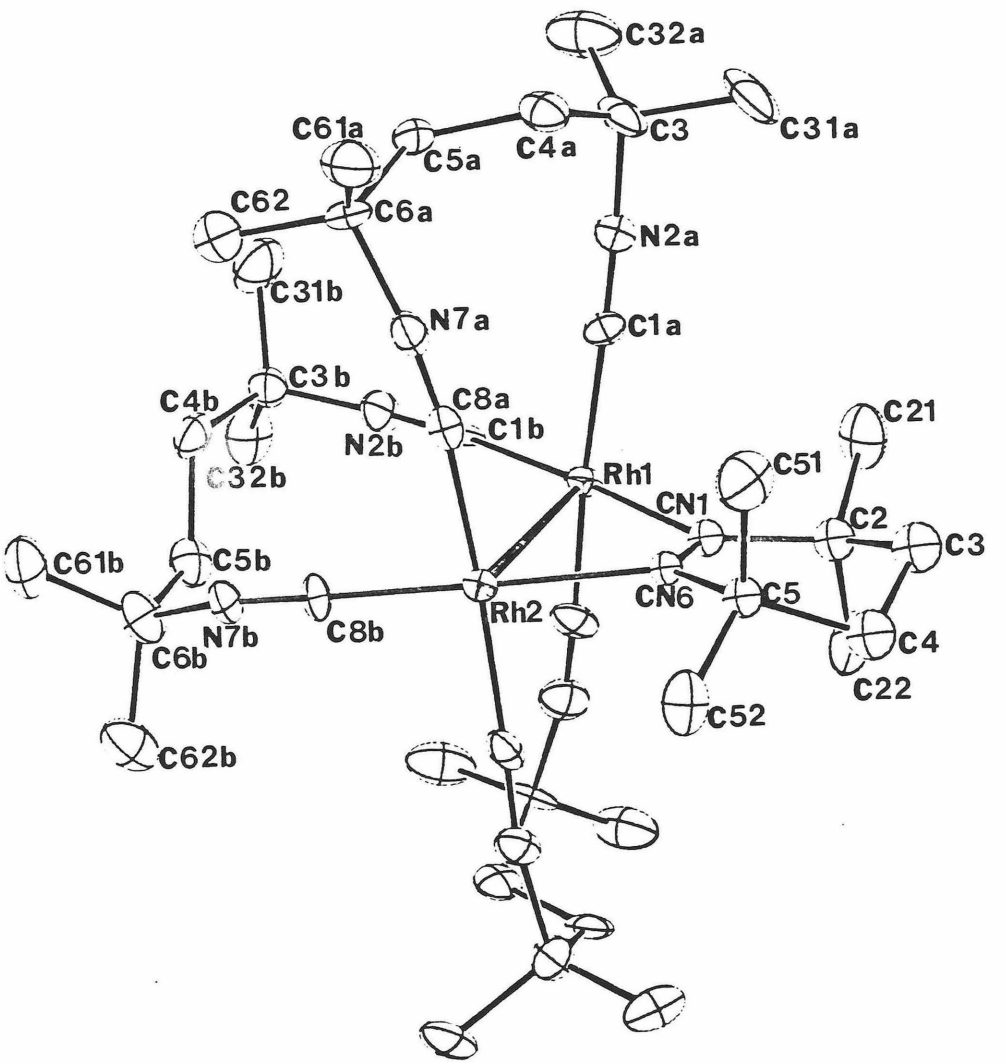
C32a
C61a
C5a
C4a
C3
C31a
C62
C6a
N2a
C31b
N7a
C1a
C3b
C4b
C8a
C21
N2b
C1b
C32b
Rh1
C51
CN1
C2
C3
C61b
C5b
CN6
C5
C8b
Rh2
N7b
C4
C6b
C22
C52
C62b

FIGURE 25

Stereoview of $Rh_2(TMB)_3(TMI)(TRF)$

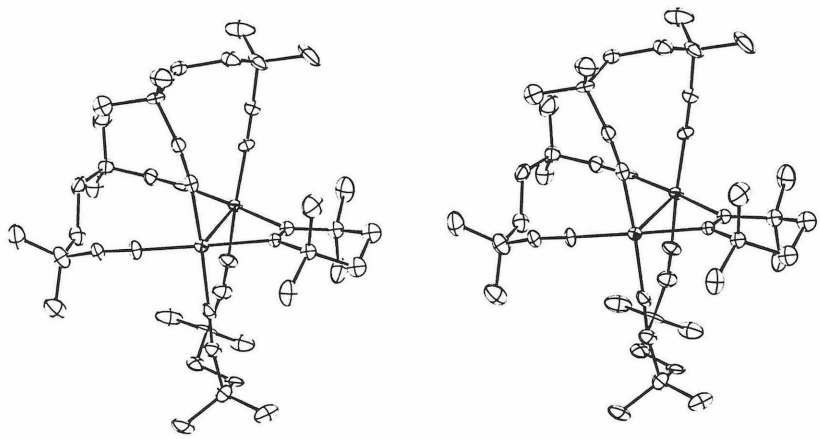

The anion has a normal isolated trifluoromethane sulfonate structure and is unexceptional. The cation consists of two rhodium ions mutually bridged by three TMB ligands and a tetramethyl cyclohexylimine ligand. The latter binds to the metals through the imine function which suffers from a two-fold disorder. The rhodium-rhodium distance is 2.969(1) Å. The geometry around each Rh is square planar with a slight tetrahedral distortion. The two planes are tipped toward each other 38.5(29) degrees (where zero degrees would be parallel), making the molecule resemble an A-frame complex. The TMB are not unexpectedly distorted, the Rh-C-N bond angle being close to 180 degrees and the CN bond length is 1.175 Å. The torsional blade angles are nearly equal for the two trans TMB [16.36(31)°, 16.62(31)°] and larger than that trans to the imine [12.03(31)°]. Except for the torsional blade angles the three TMB ligands have bond lengths and bond angles very similar to those found in the parent molecule (53). The imine itself shows a slight angle [5.25(26)°]. The imine CN1-CN2 distance is 1.24(24)Å. The rest of the carbons show normal C-C distances. The ring is not planar and shows some chair distortion. The Rh-C/N bonds to the imine are longer than the Rh - C isocyanide bonds (typically ca. 1.96Å).

The Rh-Rh distance (2.970(1)Å) found in $Rh_2(TMB)_2(TMB)^+$ is the shortest found for rhodium dimers with weakly interacting isocyanides. This is shorter than bond lengths observed in A-frame molecules with weakly interacting rhodiums 3.1520(8) and 3.155(4) for $[Rh_2(CO)_2(\mu\text{-}Cl)(DPM)_2]^+$ and $Rh_2(CO)_2(\mu\text{-}Cl)(DPM)_2$ respectively (85). The rhodium A-

frame molecules which contain formal Rh-Rh bonds however, have shorter interatomic distances of 2.617 - 2.8415 Å [(2.7566(9) Å for $Rh_2Br_2(CO)(DPM)_2$] (77). The oxidized rhodium isocyanide species $Rh_2(bi)_4Cl_2^{2+}$ with a formal Rh-Rh bond also contains a shorter bond (2.84 Å) (80).

Table 14

Selected Interatomic Distances (Å) and Esd's for $[Rh_2(TMB)_3(TMCI)]$ [TRF]

atoms	distance (Å)
A. Rhodium - Rhodium Distance	
Rh(1) - Rh(2)	2.970(1)
B. Distances from the Rhodium Atoms	
Rh(1) - C(1a)	1.959(7)
Rh(1) - C(1b)	1.932(8)
Rh(1) - C(1c)	1.939(7)
Rh(1) - CN(1)	2.102(6)
Rh(2) - C(8a)	1.937(8)
Rh(2) - C(8b)	1.974(7)
Rh(2) - C(8c)	1.939(7)
Rh(2) - CN(6)	2.107(6)
C. Isocyanide Carbon - Nitrogen Distances	
C(1a) - N(2a)	1.175(9)
C(8a) - N(7a)	1.172(9)
C(1b) - N(2a)	1.171(10)
C(8b) - N(7b)	1.157(9)
C(1c) - N(2c)	1.157(9)
C(8a) - N(7c)	1.153(9)
CN(1) - CN(6)	1.254(9)

Table 15

Selected Interatomic Bond Angles, Torsion Angles and Esd's for $[Rh_2(TMB)_3(TMI)]$ [TRF]

atoms	angle
D. Selected Bond Angles	
Rh(1) - Rh(2) - C(8a)	90.55(22)
Rh(1) - Rh(2) - C(8b)	97.59(21)
Rh(1) - Rh(2) - C(8c)	103.76(22)
Rh(1) - Rh(2) - CN(6)	65.69(16)
Rh(2) - Rh(1) - C(1a)	96.85(21)
Rh(2) - Rh(1) - C(1b)	90.77(23)
Rh(2) - Rh(1) - CN(1)	65.79(17)
Rh(1) - C(1a) - N(2a)	178.17(63)
Rh(1) - C(1b) - N(2b)	175.50(67)
Rh(1) - C(1c) - N(2c)	173.36(64)
Rh(1) - CN(1) - C(2)	172.00(44)
Rh(2) - C(8a) - N(7a)	171.65(65)
Rh(2) - C(8b) - N(7b)	176.54(64)
Rh(2) - C(8c) - N(7c)	171.91(65)
Rh(2) - CN(6) - C(5)	122.02(43)
E. Selected Torsional Angles	
C(1a) - Rh(1) - Rh(2) - C(8a)	16.62(31)
C(1b) - Rh(1) - Rh(2) - C(8b)	16.36(31)
C(1c) - Rh(1) - Rh(2) - C(8c)	12.03(32)
CN(1) Rh(1) - Rh(2) - CN(6)	5.26(26)
C(1a) - Rh(1) - Rh(2) - C(8c)	104.68(31)
C(1a) - Rh(1) - Rh(2) - CN(6)	-79.19(28)
C(1b) - Rh(1) - Rh(2) - C(1c)	88.24(32)
C(1b) - Rh(1) - Rh(2) - CN(6)	99.92(29)

APPENDIX

A. INTRODUCTION

Most of the common electrochemical methods for the determination of heterogeneous rate constants have been formulated on the assumption that very little adsorption of the electroactive species onto the surface of the electrode occurs. Chronocoulometry has been available for some time as a fairly easy method for the detection of specific adsorption (69). In order to test whether adsorption was occurring with the rhodium complexes a 0.08 mM solution of $Rh(DPE)_2ClO_4$ in acetonitrile with 0.2 M TBABF4 added was studied. The solution was vigorously degassed before the start of the experiment and was covered with a blanket of nitrogen during the experiment. In a typical run the computer control system extruded a new drop, allowed equilibration at the initial potential (-1.5 V) for 15 seconds, stepped to the intermediate potential (-2.0 V), collected data for 250 milliseconds (100 pts) and stepped back to the initial potential to collect data for another 250 milliseconds. The computer then calculated the Q vs. $t^{/12}$ plot and reported the intercept. The experiment included a repeat of the mea-

surements on an electrolyte solution with no depolarizer. The forward and reverse intercepts in the presence of the complex agreed fairly closely with those found in the absence of complex. This indicates very little adsorption.

B. FORMULATION

In the Butler-Volmer formulation of electrode kinetics the current (i) is given at any potential by

$$i = i_c - i_a = nFA[k_f C_o(0,t) - k_b C_R(0,t)]$$

where $k_f = k°e^{-\alpha nF(E-E°)/RT}$

and $k_b = k°e^{(1-\alpha)nF(E-E°)/RT}$

α is the transfer coefficient and k° is the standard rate constant. k° is related to the activation barrier to electron transfer and α is related to the reaction pathway. When a solution is in equilibrium no net current flows but an exchange current still exists and is given by

$$i_o = nFAk°C_o e^{-\alpha nF(Eeq - E°')}$$

Rearranging the first equation gives

$$i = i_o [C_o(0,t)e^{-\alpha nF(E - E°)/RT}/C_o - C_R(0,t)e^{(1-\alpha)nF(E-E°)/RT}/C_R]$$

This is the current-overpotential equation.

C. CYCLIC VOLTAMMETRY

In the cyclic voltammetric formulation of the reversible electron transfer case the Nernst equation is the boundary condition to the diffusion equation. In the quasi-reversible case the boundary condition is a form of the current-potential equation. The solution of the diffusion equation for the description of the current-potential is not straightforward. A closed-form solution is not possible but numerical methods have given excellent results. Randles (64) and Sevcik (65) initially worked on the reversible case and it was later reexamined by Nicholson and Shain (66). Matsuda and Agabe (48) evaluated the quasi-reversible case for a scan in one direction and Nicholson reevaluated the case for a full potential sweep forward and back (67). A characteristic finding for a quasi-reversible system caused by the slow electrode kinetics is that the peak splitting in a cyclic voltammogram varies as a function of scan rate. As the scan rate increases the peak splitting increases from the reversible ΔE_p at slow scan rates to higher values at faster scan rates. Nicholson defined a kinetic parameter Ψ, which was related to k° and v as follows:

$$\Psi = [(D_O/D_R)^{\alpha/2}k^\circ]/[D_O{}^{\pi}v(nF/RT)]^{1/2}$$

Nicholson also published a table that related the observed ΔE_p value to Ψ. This table has been reproduced as Table 12A. To use this tabulation effectively a large working curve was constructed. Cyclic voltammetric measurements constitute the simplest means of evaluating electron

transfer rate constants. The exact concentration is not needed, only the scan rate and the working curve. The problems lie in measuring the broad peak potentials accurately and compensating for the cell resistance which increases the peak splittings. In the present study care was taken to minimize uncompensated resistance as was discussed earlier.

The electrolyte concentration used was 0.20 M and a known reversible couple, p-benzoquinone was added. The extra peak splitting of 3 mV - 10 mV (depending on the particular scan) arising from the benzoquinone was subtracted from the rhodium splitting. The scan rates, peak splittings, Ψ and k° are tabulated in Table 12B. It can be seen that the values of k° range from 0.0082 cm/sec to 0.0108 cm/sec. At slow scan rates where the peak splittings were small, ΔE and hence Ψ were very sensitive to small peak potential error because of the steepness of the working curve. The average value of k° is 0.0092 cm/sec.

Table 12

A. Variation of E_p with kinetic parameter Ψ at 25° C
$\alpha = 0.5$

Ψ	$n(E_p^a - E_p^c)$ (mV)
20.00	61
7.00	63
6.00	64
5.00	65
4.00	66
3.00	68
2.00	72
1.00	84
0.75	92
0.50	105
0.35	121
0.25	141
0.10	212

B. Cyclic Voltammetric Data for 1.6 mM $Rh(DPE)_2ClO_4$ in 0.2 M $TBABF_4$

v (V/sec)	$\Sigma \Delta E$ (mV)	Ψ	K^o (cm/sec)
1.000	156	0.204	0.0082
0.750	144	0.240	0.0084
0.500	132	0.290	0.0082
0.350	114	0.410	0.0098
0.200	106	0.490	0.0088
0.150	100	0.580	0.0090
0.100	94	0.700	0.0089
0.075	84	1.000	0.0110
0.050	80	1.200	0.0108

(THIS PAGE IS BLANK, DUE TO ERROR IN PAGINATION)

D. CHRONOAMPEROMETRY

As described earlier the chronoamperometric technique involves stepping the potential rapidly and then monitoring the current. When the current-overpotential equation is combined with the boundary conditions and the diffusion equations the resulting current-time curve has been shown by Gerischer (68) to be:

$$i(t) = nFA(k_f C_O^* - k_b C_R^*)\exp(H^2 t)\mathrm{erfc}(Ht^{1/2})$$

where $H = k_f/D_O^{1/2} + k_b/D_R^{1/2}$

When only the oxidized material is present at the start of a step:

$$i(t) = nFAk_f C_O^* \exp(H^2 t)\mathrm{erfc}(Ht^{1/2})$$

At $t = 0$, $\exp(H^2 t)\mathrm{erfc}(Ht^{1/2}) = 1$

so $i(o) = nFAk_f C_O^* = i_o$

Thus if the current can be accurately extrapolated back to $t = 0$, then k_f can be obtained. Gerisher and Vielstich (68) were the first to successfully demonstrate the technique. At small values of $Ht^{1/2}$, i.e., short times, $\exp(Ht)\mathrm{erfc}(Ht)$ can be linearized to

$$1 - [2Ht^{1/2}/\pi^{1\,2}]$$

so that

$$i = nFAk_f C_O^*(1-2Ht^{1/2}/\pi^{1/2})$$

Gerischer and Vielstich showed that when the current was plotted against the square root of time at short times the curve approached a straight line and could be extrapolated to t = 0 to obtain i_o. Oldham and Osteryoung (70) examined the current behavior and indicated that over short time spans the full current equation does not itself differ significantly from linearity when compared to the $t^{1/2}$ approximation. They pointed out that if care is not taken it is possible to collect "k°" data when the $t^{1/2}$ approximation is not valid. By evaluating the deviation of $t^{1/2}$ from $\exp(H^2)\mathrm{erfc}(Ht^{1/2})$ they constructed a working curve for the estimation of i_o. By their modification current data are gathered from very short time spans where double layer charging dominates, to longer times where the $t^{1/2}$ approximation is definitely not valid. The current data are plotted versus $t^{1/2}$; tangents are drawn to the curve and extrapolated to the current axis. This extrapolated value of i_x along with the current value (i) at which the tangent was drawn can be applied to the working curve to obtain a factor by which i_x can be multiplied to give i_o.

In the present study a 1.28 mM solution of $Rh(DPE)_2ClO_4$ with 0.2 M TBABF4 was examined. A cyclic voltammogram was taken at slow scan rates which indicated that $E_{1/2}$ was -2.085 V. The potential was stepped in turn from -1.900 where only the oxidized species existed, to -2.020, -2.040, -2.060, -2.080 and -2.090 V. The current transient was collected for 1.8, 9, 45 and 180 milliseconds. A new drop was extruded for each measurement. The current was plotted vs. square root of time and a typical plot is shown in Figure 26. This is the plot for the step to

FIGURE 26

Chronoamperametry of $Rh(DPE)_2^+$ for k_s

i vs. $t^{1/2}$ plot

step from -1.900 V to -2.090 V

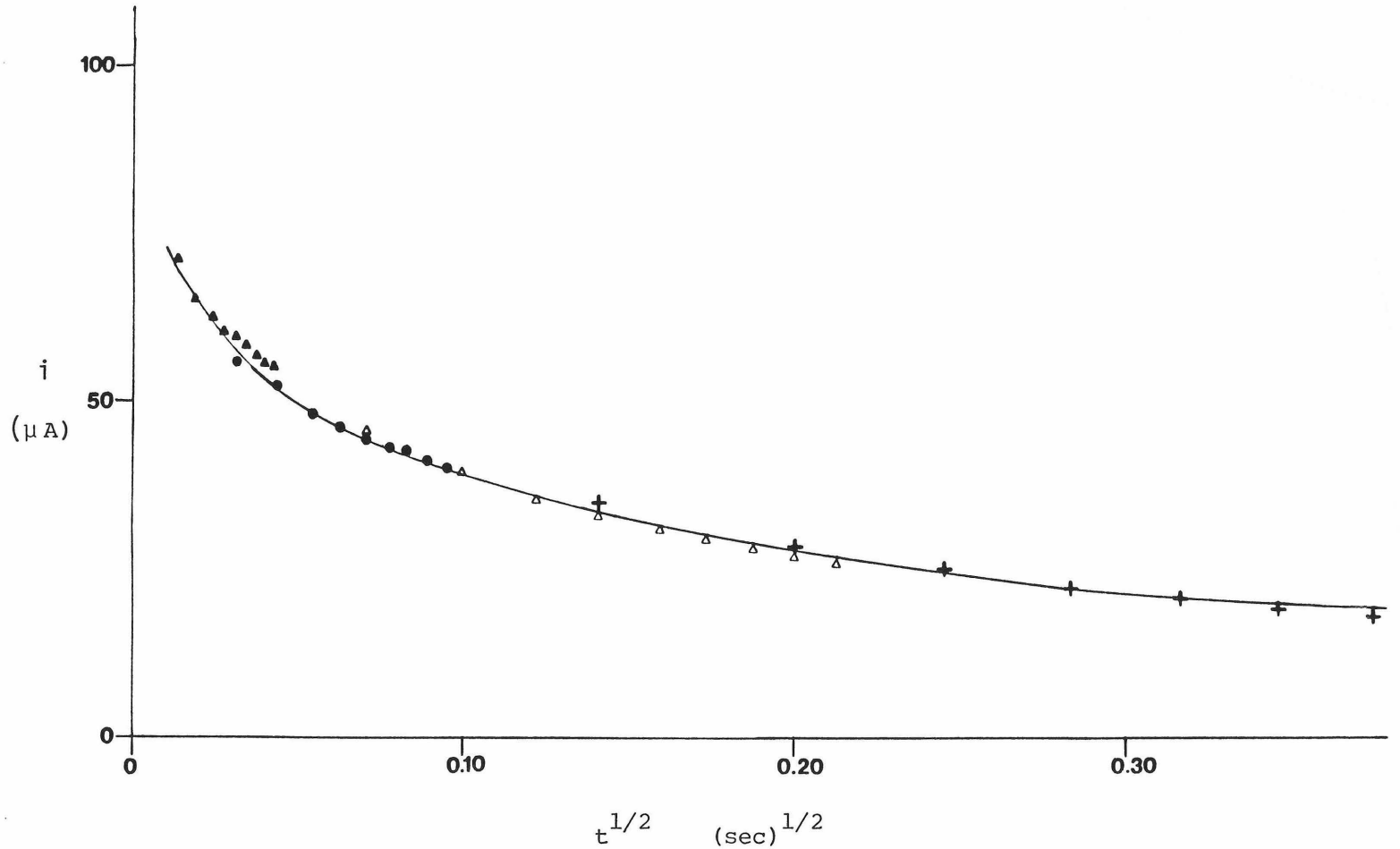
100
50
0
i
(μA)
0
0.10
0.20
0.30
t^1/2 (sec)^1/2

-1.090 V. Table 13 contains the tangent data drawn through several points on each curve. The average of the i_o values thus obtained was used to calculate k_f values by $k_f = i_o/nFAC_o$ where n = 2. Since

$$k_f = k^\circ e^{\alpha n_a F(E - E^\circ)/RT}$$

where n_a is the rate determining electron step, we have

$$\ln k_f = \alpha n_a F(E - E^\circ)/RT + \ln k^\circ$$

In Figure 27, $\ln k_f$ has been plotted against the overpotential; the result is a straight line. The k° value at zero overpotential is 0.0087(5) cm/sec. The slope of the line leads to a value for α of 0.65 if $n_a = 1$ and 0.32 if $n_a = 2$. Both values of α are not unrealistic. The value of k° by chronoamperametric measurements agrees within experimental limits with the cyclic voltammetric value.

Table 13

Tangents to i vs. $t^{1/2}$ curves for $Rh(DPE)_2ClO_4$

$E - E^{o}$ (V)	step to (V)	i (μA)	i_x (μA)	i_x/i_o	i_o/i_x	i_o (μA)
0.005	2.090	55	67.0	0.82	0.96	69.0
		50	65.0	0.76	0.92	66.0
		45	61.0	0.75	0.91	67.0
		40	56.0	0.71	0.87	64.0
		K_f = 0.011				68.0 avg.
-0.005	2.080	325	44.0	0.74	0.91	48.4
		300	41.0	0.73	0.90	45.5
		275	39.0	0.71	0.87	44.8
		250	36.0	0.69	0.85	42.3
		K_f = 0.0071				45.0 avg.
-0.025	2.060	16	22.5	0.71	0.88	25.0
		14	20.5	0.68	0.84	24.0
		12	18.0	0.66	0.81	23.0
		K_f = 0.0038				24.0 avg.
-0.045	2.040	10	15.0	0.66	0.81	18.6
		8	13.0	0.61	0.74	17.6
		6	10.5	0.57	0.59	17.7
		K_f = 0.0028				18.0 avg.
-0.065	2.020	6	9.5	0.63	0.79	12.0
		5	8.5	0.59	0.65	13.0
		4	6.9	0.58	0.60	11.5
		K_f = 0.0019				12.0 avg.

FIGURE 27

Plot of ln k_f vs. (E - E°) for $Rh(DPE)_2ClO_4$

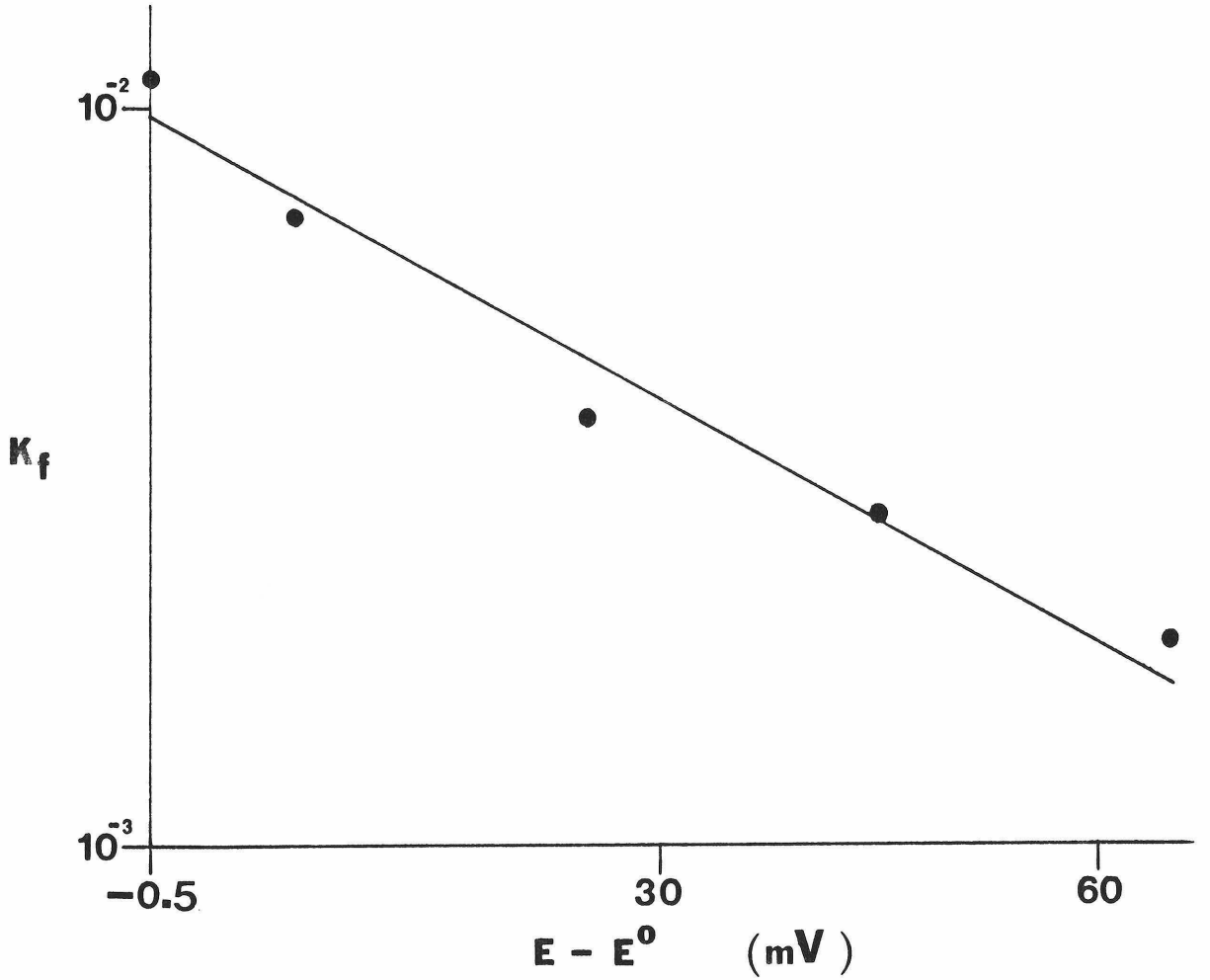
10^{-2}
10^{-3}
K_f
−0.5
30
60
E − E° (mV)

REFERENCES

(1) D. C. Olson and W. Keim Inorg. Chem., 8, 2028(1969).

(2) G. Pilloni, S. Valcher and M. Martelli J. Electroanal. Chem., 40, 63(1977).

(3) D. deMontauzon and R. Poilblanc. J. Organomet. Chem., 93, 379(1975).

(4) D. Evans, G. Yagupshi and G. Wilkinson J. Chem. Soc., A, 2260(1968).

(5) D. H. Geske J. Phys. Chem., 63, 1062(1959).

(6) S. Zecchin J. Orgamomet. Chem., 110, C45(1976).

(7) J. Tomes Collect. Czech. Chem. Comm., 9, 12(1937).

(8) G. Pilloni, E. Vecchi, and M. Martelli J. Electroanal. Chem., 45, 483(1973).

(9) G. Kew, K. DeArmond and K. Hanck J. Phys. Chem., 78, 727(1971).

(10) E. Makrlik, J. Hanzlik, A. Camus, G. Mestroni and G. Zassinovichy J. Organomet. Chem., 142, 95(1977).

(11) W. A. Fordyce, K. H. Pool and G. A. Crosby, submitted for publication.

(12) S. Rice, Ph.D. Thesis, California Institute of Technology, 1982.

(13) C. Amatore J. Electronal. Chem., 107, 59(1980).

(14) R. S. Nicholson and I. Shaw Anal. Chem., 37, 190(1965).

(15) J. A. Sofranko, R. Eisenberg and J. A. Kampmier J. Am. Chem. Soc., 101, 1042(1979).

(16) J. A. Sofranko, R. Eisenberg and J. A. Kampmier J. Am. Chem. Soc., 102, 1163(1980).

(17) J. M. Rao, M. C. Hughes and D. J. Macero Inorg. Chim. Acta., 35, L369(1979).

(18) G. Pilloni, G. Zotti, and M. Martelli Electroanal. Chem., 50, 295(1974).

(19) M. Martelli, G. Pilloni, G. Zotti and U. S. Daolio Inorg. Chem. Acta., 11, 155(1974).

(20) J. A. Sofranko, Ph.D. Thesis, University of Rochester (1979).

(21) T. Okybo, M. Hirota, Y. Umezawa and S. Fujiwara J. Inorg. Nucl. Chem., 37, 573(1975).

(22) V. M. Kiselleva, M. I Gelfman, V. V. Razumovskii and L. V. Rapport Russ. J. Inorg. Chem., 18, 564(1973).

(23) M. Martelli, G. Zotti, and G. Pilloni J. Electroanal. Chem., 63, 421(1975).

(24) G. Mazzochin, G. Bontempelli, U. Nicolini and B. Crociani Inorg. Chem. Acta., 18, 159(1976).

(25) P. Zanello, R. Seeber, B. Crociani and M. Nicolini Trans Met. Chem., 5, 45(1980).

(26) P. Zanello, R. Seeber, A. Cinquantini and B. Crociani Trans. Met. Chem., 5, 226(1980).

(27) C. N. Lai and A. T. Hubbard Inorg. Chem., 13, 1199(1974).

(28) C. N. Lai and A. T. Hubbard Inorg. Chem., 11, 2081(1972).

(29) R. F. Lame and A. T. Hubbard J. Phys. Chem., 84, 734(1977).

(30) M. Martelli, G. Pilloni, G. Zotti and S. Daolio Inorg. Chim. Acta, 11, 155(1974).

(31) P. Rechberger, G. Gritzner and V. Gutmann Monatsh. Chem, 108, 57(1977).

(32) G. L. Geoffroy, M. S. Wrighton, G. S. Hammond and H. B. Gray J. Am. Chem. Soc., 96, 3105(1974).

(33) S. J. Milder, R. A. Goldbeck, D. S. Klinger and H. B. Gray J. Am. Chem. Soc., 102, 6761(1980).

(34) B. Parkinson and K. R. Mann Inorg. Chem., 20, 1921(1981).

(35) J. R. Bolton Science, 202, 705(1978).

(36) A. Sacco and F. Gorieri Gazzetta, 93, 687(1963).

(37) A. J. Bard and L. R. Faulkner "Electrochemical Methods and Applications ; Wiley, New York, 1980.

(38) D. H. Evans "Encyclopedia of Electrochemistry of the Elements"; A. Bard, F. Lund, Eds.; Marcell Dekker Inc., 1975.

(39) S. Wawzonek, R. Berkey, E.W. Blaha and M. E. Runner J. Electrochem. Soc., 103, 456(1956).

(40) R. S. Nicholson and I. Shain Anal. Chem., 36, 706(1964).

(41) B. S. Jenson and V. D. Parker J. Chem. Soc., Chem. Comm., 367(1974).

(42) M. E. Peover in "Electroanalytical Chemistry"; A. J. Bard, Ed.; Marcel Dekker, Inc., New York, 1967, Vol. 2.

(43) E. R. Brown and R. F. Lange "Techniques of Chemistry, Vol. 1: Physical Methods of Chemistry, Part IIB: Electrochemical Methods"; A. Weissber, B. W. Rossiter, Eds.; Wiley-Interscience, New York, 1971, Chap. VI.

(44) R. S. Nicholson Anal. Chem., 38, 1406(1966).

(45) R. S. Nicholson Anal. Chem., 37, 667(1965).

(46) "Digital Coulometer Model 179 Instruction Manual"; Princeton Applied Research Corp., Princeton, N.J., 1973.

(47) M. L. Olmstead, R. G. Hamilton and R. S. Nicholson Anal. Chem., 41, 260(1969).

(48) H. Matsuda and Y. Agabe Z. Electrochem., 59, 494(1955).

(49) D. S. Polcyn and I. Shain Anal. Chem., 38, 370(1966).

(50) D. E. Richardson, H. Taube Inorg. Chem., 20, 1278(1981).

(51) E. P. Parry and R. A. Osteryoung Anal. Chem., 37, 163(1965).

(52) A. J. Bard and K. S. V. Santhanam Electroanal. Chem., 4, 215(1970).

(53) K. S. V. Santhanam and A. J. Bard J. Am. Chem. Soc., 88, 2269(1966).

(54) A. Sacco and R. Ugo J. Chem. Soc., 3274(1965).

(55) C. Brandstrom Acta. Chem. Scand., 3585(1969).

(56) K. R. Mann, J. A. Thich, R. A. Bell, C. L. Coyle and H. B. Gray Inorg. Chem., 19, 2462(1980).

(57) W. P. Weber, G. W.-Gobel and I. K. Ugi Angew. Chem., Int. Ed. Eng., 11, 530(1972).

(58) J. Chatt and L. M. Venanzi J. Chem Soc., 4735(1957).

(59) V. M. Miskowski, J. L. Robbings, G. S. Hammond and H. B. Gray J. Am. Chem. Soc., 98, 2477(1976).

(60) B. R. James and D. Mahajan Can. J. Chem., 57, 180(1979).

(61) C. P. Kubiak and R. Eisenberg Inorg. Chem., 19, 2726(1980).

(62) K. B. Oldham and E. P. Parry Anal. Chem., 42, 229(1970).

(63) D. F. Shriver, "The Manipulation of Air-Sensitive Compounds"; McGraw-Hill, Inc., New York, 1969.

(64) J. E. Randles Trans. Farad. Soc., 44, 327(1948).

(65) A. Sevcik Collect. Czech. Chem. Comm., 13, 349(1948).

(66) R. S. Nicholson and I. Shain Anal. Chem., 36, 706(1964).

(67) R. S. Nicholson Anal. Chem., 37, 1353(1965).

(68) H. Gerischer and W. Vielstich, Z. Physik. Chem., 3, 16(1955).

(69) F. C. Anson Anal. Chem., 38, 54(1966).

(70) K. B. Oldham and R. A. Osteryoung J. Electroanal. Chem., 11, 397(1966).

(71) G. L. Geoffroy, Ph.D. Thesis, California Institute of Technology, 1975.

(72) D. T. Cromer and J. T. Weber Acta Crystallogr., 18, 104(1965).

(73) International Tables for X-ray Crystallography. Kynoch Press: Birmingham, England, Vol. III, 1962.

(74) R. F. Stewart, E. R. Davidson, W. T. Simpson J. Chem. Phys., 42, 3175(1965).

(75) P.L. Goggin, R. J. Goodfellow, S. Haddock, B. F. Taylor, J. C. S. Dalton 459(1976).

(76) H. A. Tayimand and N. S. Akl, J. Inorg. Nucl. Chem., 36, 944(1974).

(77) R. G. Pearson, W. Louw, and J. Rajaram, Inorg. Chim. Acta, 9, 251(1974).

(78) C. Eaborn, A. Pidcock, and B. R. Stede, J. C. S. Dalton 767(1976).

(79) K. S. Santhanam and A. J. Bard, J. Am. Chem. Soc. 118(1968).

(80) K. R. Mann and H. B. Gray, Inorganic Compounds with Unusual Properties - II (R. B. King, ed.) Advances in Chemistry Series 173, 255(1979).

(81) M. M. Balzer, Organic Electrochemistry: An Introduction and a Guide, Marcel Dekker Inc., New York (1973).

(82) J. P. Randin Encyclopedia of Electrochemistry of the Elements Vol. 76, Marcel Dekker, Inc. (A. J. Bard, ed.), New York (1976).

(83) V. D. Parker and B. E. Gurgert Tet. Lett., 11, 627(1965).

(84) I. S. Sigal and H. B. Gray, J. Am. Chem. Soc., 103, 2220(1981).

(85) C. P. Kubiak and R. Eisenberg, J. Am. Chem. Soc., 99, 6129(1977).

(86) R. H. Wopschall and I. Shain, Anal. Chem., 39, 1514(1967).